

Computer simulations of
two-dimensional colloidal crystals
in confinement

Dissertation

zur Erlangung des Grades
"Doktor der Naturwissenschaften"
am Fachbereich Physik
der Johannes Gutenberg-Universität
in Mainz

vorgelegt von

Andrea Ricci

Juni 2006

Abstract

Monte Carlo simulations are used to study the effect of confinement on a crystal of point particles interacting with an inverse power law potential in $d = 2$ dimensions. This system can describe colloidal particles at the air-water interface, a model system for experimental study of two-dimensional melting. It is shown that the state of the system (a strip of width D) depends very sensitively on the precise boundary conditions at the two “walls” providing the confinement. If one uses a corrugated boundary commensurate with the order of the bulk triangular crystalline structure, both orientational order and positional order is enhanced, and such surface-induced order persists near the boundaries also at temperatures where the system in the bulk is in its fluid state. However, using smooth repulsive boundaries as walls providing the confinement, only the orientational order is enhanced, but positional (quasi-) long range order is destroyed: The mean-square displacement of two particles n lattice parameters apart in the y -direction along the walls then crosses over from the logarithmic increase (characteristic for $d = 2$) to a linear increase (characteristic for $d = 1$). The strip then exhibits a vanishing shear modulus. These results are interpreted in terms of a phenomenological harmonic theory. Also the effect of incommensurability of the strip width D with the triangular lattice structure is discussed, and a comparison with surface effects on phase transitions in simple Ising- and XY-models is made.

Contents

Introduction	4
1 Elasticity and thermodynamics	7
1.1 The strain and the stress tensor	7
1.2 Thermodynamic relations	8
1.3 Stress-strain relations and propagation of elastic waves	10
1.4 Notes on surface elasticity	13
2 Model of a confined colloidal crystal	16
2.1 Choice of a Model	16
2.2 First simulations with flat walls: choosing the parameter ϵ_{wall}	19
2.3 Evaluation of the elastic constants	22
2.4 Stress fluctuations	22
2.5 Strain fluctuations	25
2.5.1 How the method works: the block analysis	26
2.5.2 Strain fluctuations and elastic constants	29
3 Numerical results for the elastic constants	31
3.1 Details about the block analysis and the evaluation of the strain field	31
3.2 Block analysis: results for the bulk	33
3.3 Block analysis: results for the confined systems	34
3.4 Numerical values of the elastic constants: the two different methods and different wall distances	35
4 Fluctuations and dimensionality	40
4.1 Introduction	40
4.2 The structure factor in two and in one dimension	41

4.3	The structure factor measured in the confined systems	43
4.4	Displacement correlation function: the case of the harmonic lattice in the bulk	48
4.5	Results from the simulations and comparison with the theory	51
5	Confinement induced order	57
5.1	Order in a two-dimensional system	57
5.2	Ordering and surfaces	60
5.3	The case of the partially confined XY model as simpler theo- retical background	62
5.4	Order in two-dimensional confined crystals: numerical results	66
	Conclusions	83
	A Varying the distance between the walls	87
	Bibliography	95

Introduction

Over the last decades, colloidal suspensions have drawn much attention from researchers. The reasons for that are many, in fact colloidal particles can be used as readily available physical models for studying collective phenomena. Colloidal dispersions can be prepared and characterized to large extents in a controlled way, effective interactions can be changed by various means. The large size of the particles (up to $\sim 1 - 10\mu m$) allows innovative observation techniques like for example video microscopy and digital image processing which cannot be applied in the order-disorder phenomena of atomic systems so a deep insight into the static and dynamical processes going on such systems is possible. Also from the technological point of view in many fields from material science to nanotechnology and biology, the investigation of colloids is of great interest.

Particularly interesting is the possibility of creating confined colloidal crystals in $2d$ or even in $1d$ to test fascinating concepts on the statistical mechanics of low-dimensional systems. Consider for example the crystallization and melting in two dimensions: a classic problem since the KTHNY theory of melting has been formulated in the mid 70's of the last century.

In the present thesis we shall consider systems *in between these dimensionalities*, i.e. colloids confined in one dimensional strip of width D .

We will investigate these confined colloidal systems through computer simulations performed with the Monte Carlo method.

Generally speaking, when boundaries are introduced in a system, and in particular, like in our case starting from scratch this kind of investigation, in order to keep the problem fairly simple one wants to stay as near as possible to the bulk situation. We followed this method, but it should be remarked that, although in these conditions, dramatic changes in the behaviour of the confined system with respect to the bulk one can often appear. In this sense

the investigation of a confined system is always very interesting.

In this thesis we will study the elastic behaviour of model confined $2d$ colloids and the degree and kind of order present in these systems and induced by the walls.

The elastic constants are one of the key quantities in the characterization of crystal systems. In $2d$ they play a crucial role in the mechanism of melting so they were intensively studied in simulations for bulk systems, in particular in the case of hard disks in a triangular crystal. We want to somehow generalize those calculations to the confined geometry and try and evaluate the elastic constants also in this case.

On the contrary, boundaries induced ordering in strips and half planes have already been studied in the past for spin systems primarily in the context of surface critical phenomena where both suppression or enhancement of order near free boundaries have been observed, we want to try and describe the order induced by a wall on our systems.

This thesis has the following structure:

in the first part we will investigate the elastic properties for our systems, in chapter 1 useful concepts quantities and relations in elasticity theory will be shortly reviewed, in chapter 2 we will describe our model of confined colloidal crystals and discuss why this model is a suitable one for colloidal systems (and it is also useful in other fields), we will give the details of our simulations, discuss the methods used for the calculation of the elastic constants and in chapter 3 we will present and discuss the result we found for them.

In chapters 4 and 5 we will focus on the order present in the colloidal strips, in chapter 4 we will particularly investigate how the types of boundaries we choose affect the thermal fluctuations from the equilibrium lattice positions in the bulk, eventually we will show that in one case, in the direction parallel to the boundaries there is a strong reduction in the positional long range order. Also some theoretical calculations on such fluctuations for a harmonic crystal in the strip geometry will be presented. In chapter 5 we will present the problem of the order induced by a surface discussing the behaviour of confined spin systems, in particular we will discuss in some detail the case of spins with a XY symmetry where a surface is present, this can be considered a sort of simpler reference model for our strips. After we will discuss the positional and orientational order induced by the boundaries

on our systems.

Finally in appendix A we will present some interesting although incomplete results obtained varying the distance between the walls in the strip. We looked at the behaviour of the strips when the distance between the boundaries and the interparticle bulk distance are incommensurate i.e. not an integer number of lattice rows can be allocated between the walls.

Chapter 1

Elasticity and thermodynamics

1.1 The strain and the stress tensor

The elasticity theory deals with macroscopic bodies and their deformations from the point of view of the mechanics of continua, the description of these deformations arises from the definition of two key mechanical quantities the strain and the stress tensor η_{ij} and σ_{ij} respectively.

Let's consider macroscopic body in a reference "undeformed" configuration and a generic point of it at position \mathbf{R} . After a deformation which here we suppose homogeneous the point will be in \mathbf{r} . The Lagrangian strain tensor η_{ij} is defined through the relation between r and R :

$$r = \sqrt{(2\eta_{ij} + \delta_{ij})R_i R_j},$$

if the deformation is small and we consider $r_i = R_i + u_i$ then

$$r_i \simeq R_i + \sum_j \frac{\partial u_i}{\partial R_j} R_j, \quad r_i^2 \simeq R_i^2 + 2 \sum_j \frac{\partial u_i}{\partial R_j} R_i R_j + \sum_{jk} \frac{\partial u_i}{\partial R_j} \frac{\partial u_i}{\partial R_k} R_j R_k.$$

So we can write for the strain tensor (repeated indexes are implicitly summed)

$$\eta_{ij} = \frac{1}{2} \left(\frac{\partial u_i}{\partial R_j} + \frac{\partial u_j}{\partial R_i} \right) + \frac{\partial u_l}{\partial R_i} \frac{\partial u_l}{\partial R_j}. \quad (1.1)$$

this tensor describes how lengths and configurations modify under the deformation.

The forces which arise are obtained considering the stress tensor σ_{ij} . If we consider a surface Σ , the force on the surface in the deformed state can

be written as:

$$F_i = \int_{\Sigma} \sigma_{ik} n_k d\Sigma,$$

so $\sigma_{ik} n_k d\Sigma$ is the i component of the force on the infinitesimal surface $d\Sigma$ with normal \mathbf{n} . Those definition are the starting point of the elasticity i.e. the description of the elastic behavior of a material [1].

1.2 Thermodynamic relations

After the short mechanical definitions of the previous section let's consider the problem of deformations in a material from the thermodynamical point of view.

Let's take a material at the equilibrium whose state is a function of let's say the temperature T and the macroscopic configuration \mathbf{x} . Let's consider also elastic homogeneous deformations from a reference starting configuration \mathbf{X} the hypothesis about the elastic deformations ensures that state functions are single-valued function of the variables we choose. We suppose that the free energy is invariant with respect to an arbitrary rigid rotation of the material, this means that this quantity depends only on the relative positions of the material particles and these positions in \mathbf{x} are function of the initial positions in \mathbf{X} and the strain tensor η_{ij} . Under these assumptions the free energy per unit mass (It is convenient in elasticity theory to work with functions per unit mass because the mass is conserved while the volume itself is a function of the strain) $f(\mathbf{x}, T)$ can be written as a function of the reference undeformed state, the strain tensor, and T . That is if the deformation is small:

$$f(\mathbf{x}, T) = f(\mathbf{X}, \{\eta_{ij}\}, T) \approx f(\mathbf{X}, \{0\}, T) + \frac{\partial f}{\partial \eta_{ij}} \eta_{ij} + \frac{\partial^2 f}{\partial \eta_{ij} \partial \eta_{kl}} \eta_{ij} \eta_{kl} + \dots \quad (1.2)$$

It can be shown, starting from the first principle of the thermodynamics [1, 2] that for the stress in the reference configuration at \mathbf{X} holds,

$$\sigma_{ij} = \rho(\mathbf{X}) \frac{\partial f}{\partial \eta_{ij}}, \quad (1.3)$$

where $\rho(\mathbf{X})$ is the density in the reference state and the derivative is taken at $\eta_{ij} = 0$. If we consider the second derivative then we obtain a fourth rank

tensor:

$$C_{ijkl} = \rho(\mathbf{X}) \frac{\partial^2 f}{\partial \eta_{ij} \partial \eta_{kl}}, \quad (1.4)$$

where the C_{ijkl} are called the elastic constants of the material.

The formula 1.3 can be generalized to get the stress in the strained configuration \mathbf{x} :

$$\sigma_{ij}(\mathbf{x}) = \rho(\mathbf{x}) \alpha_{ik} \alpha_{jl} \frac{\partial f}{\partial \eta_{kl}}, \quad (1.5)$$

where the derivatives are taken at \mathbf{x} and the alphas are here the transformation coefficients defined as

$$\alpha_{ij} = \frac{\partial r_i}{\partial R_j}. \quad (1.6)$$

It is also interesting to write the equation of motion for the \mathbf{r} 's in absence of body force, it comes from Newton's second law of motion

$$\rho(\mathbf{x}) \ddot{r}_i = \frac{\partial \sigma_{ij}}{\partial r_j}, \quad (1.7)$$

and the relation between the density in the reference and strained configuration

$$\frac{\rho(\mathbf{X})}{\rho(\mathbf{x})} = J = \det[\alpha_{ij}]. \quad (1.8)$$

Here J is the Jacobian of the transformation from \mathbf{X} to \mathbf{x} and the eqn. 1.8 is a continuity equation expressing the conservation of the mass.

Both the strain and the stress tensor are symmetric

$$\eta_{ij} = \eta_{ji}, \quad \sigma_{ij} = \sigma_{ji}, \quad (1.9)$$

and also for the elastic constants we have

$$C_{ijkl} = C_{klij} = C_{jikl} = \dots \quad (1.10)$$

The symmetry in eqns. 1.9 and 1.10 is usually called the Voigt symmetry and allows the so called Voigt notation, that means we can replace couples of indexes with only one. In two dimensions we have:

$$xx \rightarrow 1, \quad yy \rightarrow 2, \quad xy \rightarrow 3.$$

We will use this notation throughout the text so we will write for example C_{xxxx} as C_{11} or C_{xyxy} as C_{33} and so on.

Among the possible changes of indexes in the elastic constants there is one which lead to a non trivial symmetry: when the two inner or outer indexes are exchanged so for example $C_{ijkl} = C_{ikjl}$ the symmetries are called the Cauchy relations and they are not straightforward consequences of the definitions usually for normal materials they experimentally don't hold [3]. In two dimensions we have only one Cauchy relation

$$C_{xxyy} = C_{xyxy},$$

or in the Voigt notation

$$C_{12} = C_{33}, \quad (1.11)$$

while in three dimensions we have for example 6. From the experimental point view it is known that for many materials the Cauchy relations in general don't hold, while on the other hand theoretically it is possible to show that it is sufficient to have a single species crystal with pairwise interactions and the harmonic approximation, for the eqn. 1.11 to be verified [3]. This will be the case also in this thesis (at least in the bulk case) since we will deal here with a two-body potential and a triangular crystal.

1.3 Stress-strain relations and propagation of elastic waves

We wish to derive the linear relation between the variation of the strain and the variation of the stress from the reference configuration (Hooke's law). From eqns. 1.2, 1.5 and 1.8 we can write

$$\sigma_{ij}(\mathbf{x}) = \frac{\rho(\mathbf{X})}{J} \alpha_{ik} \alpha_{jl} \frac{\partial f}{\partial \eta_{kl}} = J^{-1} \alpha_{ik} \alpha_{jl} [\sigma_{kl}(\mathbf{X}) + C_{klmn} \eta_{mn} + \dots]. \quad (1.12)$$

Let's consider infinitesimal displacement from the reference configuration, we want to evaluate

$$\left. \frac{\partial \sigma_{ij}}{\partial \eta_{kl}} \right|_{\{\eta=0\}}, \quad (1.13)$$

where here we consider in the definition eqn. 1.1 for η_{ij} only the linear part in the displacements. In order to evaluate the derivative in the eqn. 1.13 we need expressions for the derivative of the Jacobian and for $\frac{\partial \alpha_{ij}}{\partial \eta_{kl}}$. For the first

we can use Jacobi's identity

$$\frac{\partial J}{\partial \alpha_{rs}} = (\alpha^{-1})_{sr} J, \quad (1.14)$$

while for the second we can use the formula [2]

$$\frac{\partial \alpha_{ij}}{\partial \eta_{kl}} = \frac{1}{2} (\delta_{ik} \delta_{jl} + \delta_{jk} \delta_{il}). \quad (1.15)$$

Using the eqns. 1.14 and 1.15 in the derivative 1.13 and considering the reference configuration $\eta = \mathbf{0}$ we have

$$\left. \frac{\partial \sigma_{ij}}{\partial \eta_{kl}} \right|_{\eta=\mathbf{0}} = B_{ijkl} = \frac{1}{2} (\sigma_{ik} \delta_{jl} + \sigma_{il} \delta_{jk} + \sigma_{jk} \delta_{il} + \sigma_{jl} \delta_{ik} - 2\sigma_{ij} \delta_{kl}) + C_{ijkl}, \quad (1.16)$$

and Hooke's law in its more general form is

$$\sigma_{ij}(\mathbf{x}) = \sigma_{ij}(\mathbf{X}) + B_{ijkl} \eta_{kl}. \quad (1.17)$$

In similar way we can write the 1.7 as a wave equation, starting from the eqn. 1.12 and using the identity of Euler Piola and Jacobi [2, 4]

$$\frac{\partial}{\partial r_j} \frac{\alpha_{jl}}{J} = 0, \quad (1.18)$$

and the definition 1.6 we have

$$\frac{\partial \sigma_{ij}}{\partial r_j} = \frac{\rho(\mathbf{X})}{J} \frac{\partial r_j}{\partial R_l} \frac{\partial}{\partial r_j} \left[\alpha_{ik} \frac{\partial f}{\partial \eta_{kl}} \right] = \frac{\rho(\mathbf{X})}{J} \frac{\partial}{\partial R_l} \left[\alpha_{ik} \frac{\partial f}{\partial \eta_{kl}} \right], \quad (1.19)$$

now taking into account the second part of eqn. 1.12 we have

$$\frac{\partial \sigma_{ij}}{\partial r_j} = [\sigma_{jl}(\mathbf{X}) \delta_{ik} + C_{ijkl}] \frac{\partial^2 r_k}{\partial R_j \partial R_l}, \quad (1.20)$$

so the equation of motion 1.7 becomes

$$\rho(\mathbf{X}) \ddot{r}_i = S_{ijkl} \frac{\partial^2 r_k}{\partial R_j \partial R_l}, \quad (1.21)$$

with the coefficients S_{ijkl} which in the more general case have the form

$$S_{ijkl} = \sigma_{jl}(\mathbf{X}) \delta_{ik} + C_{ijkl}. \quad (1.22)$$

The meaning of eqns. 1.16 and 1.22 is that if the stress in the reference configuration is non zero, then the three thermoelastic coefficients we defined namely the elastic constants C , the elastic moduli B and the coefficients S are all different. However there are some simplifications if we consider as we will do for almost all the cases in this thesis, the case of an initial hydrostatic pressure

$$\sigma_{ij}(\mathbf{X}) = -P\delta_{ij}, \quad (1.23)$$

the eqn. 1.16 simplifies in

$$B_{ijkl} = -P(\delta_{jl}\delta_{ik} + \delta_{il}\delta_{jk} - \delta_{ij}\delta_{kl}) + C_{ijkl}, \quad (1.24)$$

and the eqn. 1.22 becomes

$$S_{ijkl} = -P\delta_{jl}\delta_{ik} + C_{ijkl}. \quad (1.25)$$

If we consider an isotropic material, usually the the stress-strain relations (in two dimensions) are written in the form [1]

$$\sigma_{ik} = K\eta_{ll}\delta_{ik} + 2\mu(\eta_{ik} - \frac{1}{2}\eta_{ll}\delta_{ik}), \quad (1.26)$$

where K is called the bulk modulus and μ the shear modulus. Comparing with 1.24 we can write these elastic moduli as combination of the C (in the case of hydrostatic pressure)

$$K = \frac{1}{2}(C_{11} + C_{12}), \quad \mu = \frac{1}{2}(C_{11} - C_{12}) - P = C_{33} - P, \quad (1.27)$$

and the Cauchy relation 1.11 can be written

$$\mu = \frac{K}{2} - P. \quad (1.28)$$

We will use in this thesis also these moduli since the triangular lattice we will consider can be regarded as an isotropic material. This is due to the high symmetry of the lattice and in general it's not true so for example if we would consider the hexagonal symmetry but in 3 dimensions we would have 5 independent elastic constants.

1.4 Notes on surface elasticity

Also in elasticity theory concepts of thermodynamics at interfaces can be used. A definition of interfacial excess quantity for the elastic energy is possible and from that a surface stress and a surface strain.

The interfacial elastic energy change δW^{interf} can be written as

$$\delta W^{\text{interf}} = \int_{x_A}^{x_B} \sigma_{ij}(x) \delta \eta_{ij}(x) dV - \sigma_{ij}^A \delta \eta_{ij}^A V^A - \sigma_{ij}^B \delta \eta_{ij}^B V^B, \quad (1.29)$$

where $\sigma_{ij}(x)$ and $\eta_{ij}(x)$ are the bulk stress and strain tensor profiles across the interface (perpendicular to the x direction). If conditions like mechanical equilibrium and absence of relative gliding between the two materials are fulfilled and splitting the strain and the stress tensors in a parallel and a perpendicular part with respect to the surface, the eqn. 1.29 has a simpler form

$$\delta W^{\text{interf}} = (\delta \eta_{ij}^{\parallel} s_{ij} + \sigma_{ij}^{\perp} \delta e_{ij}) S_{AB}, \quad (1.30)$$

where

$$s_{ij} = \frac{1}{S_{AB}} \left[\int_{x_A}^{x_B} \sigma_{ij}^{\parallel}(x) dV - \sigma_{ij}^{\parallel A} V^A - \sigma_{ij}^{\parallel B} V^B \right], \quad (1.31)$$

$$e_{ij} = \frac{1}{S_{AB}} \left[\int_{x_A}^{x_B} \epsilon_{ij}^{\perp}(x) dV - \epsilon_{ij}^{\perp A} V^A - \epsilon_{ij}^{\perp B} V^B \right]. \quad (1.32)$$

The relations 1.31 and 1.32 define s_{ij} as the interfacial excess quantity (per unit area) of the parallel components of the bulk stress tensor and e_{ij} as the interfacial excess quantity of the perpendicular components of the bulk strain tensor. The two conditions used have the following meaning: the non gliding condition tells that the infinitesimal change of the strain tensor parallel to the interface must be the same in the whole material i.e. $\delta \eta_{ij}^{\parallel}(z) = \delta \eta_{ij}^{\parallel A} = \delta \eta_{ij}^{\parallel B}$, while the mechanical equilibrium condition ensures that the normal components of the stress tensor are homogeneous in the whole material $\sigma_{ij}^{\perp}(z) = \sigma_{ij}^{\perp A} = \sigma_{ij}^{\perp B}$ so if one phase (for instance B) is the vacuum, mechanical equilibrium means zero perpendicular stress.

The surface stress and strain tensor are important for describing elastic effects on the thermodynamics of a solid/solid interface. If we consider two solid phases separated by an interface and a reversible transformation in which heat, stress and particle number can be changed, the interfacial excess

part in the (for example) internal energy can be written using the eqn. 1.30 and has the form

$$dU^{\text{interf}} = TdS^{\text{interf}} + (\delta\eta_{ij}^{\parallel}s_{ij} + \sigma_{ij}^{\perp}\delta e_{ij})A + \mu_i dN_i^{\text{interf}}. \quad (1.33)$$

The similar expression in the case of fluid/fluid interface would involve the surface tension γ

$$dU^{\text{interf}} = TdS^{\text{interf}} + \gamma dA + \mu_i dN_i^{\text{interf}}. \quad (1.34)$$

Actually in the most general case we can have a reversible transformation in which at the same time there is deformation and creation of the surface, that is instead of the eqn. 1.33 we should consider

$$dU^{\text{interf}} = TdS^{\text{interf}} + \gamma dA^{\text{cre}} + (\delta\eta_{ij}^{\parallel}s_{ij} + \sigma_{ij}^{\perp}\delta e_{ij})A + \mu_i dN_i^{\text{interf}}. \quad (1.35)$$

This expression together with the fact that the excess internal energy U^{interf} is always a function only of the entropy, the interface area, and the number of particles can be used to derive thermodynamical relations involving the surface quantities of eqn. 1.35 particularly the Shuttleworth equation connecting the interface stress s_{ij} to the interface energy γ [5, 6].

It is also possible to define surface elastic constants and also to write an Hook's law for the surface stress. For a system with a free surface the energy upon a deformation of a given part of the system of volume V_0 and surface of area A_0 can be written as

$$E = E_0 + A_0\gamma_0 + A_0s_{0,ij}\eta_{ij} + \frac{1}{2}V_0C_{ijkl}\eta_{ij}\eta_{kl} + \dots, \quad (1.36)$$

where γ_0 and $s_{0,ij}$ are the surface energy and surface stress of the undeformed system. On the other hand for the bulk system we can write

$$E^{\text{bulk}} = E_0 + \frac{1}{2}C_{ijkl}^{\text{bulk}}\eta_{ij}\eta_{kl} + \dots. \quad (1.37)$$

Expanding the excess energy $E - E^{\text{bulk}}$ one has

$$\begin{aligned}
 A_0 \gamma_0 &= [E - E^{\text{bulk}}]_{\eta=\mathbf{0}}, & A_0 s_{0,ij} &= \left[\frac{\partial E}{\partial \eta_{ij}} - \frac{\partial E^{\text{bulk}}}{\partial \eta_{ij}} \right]_{\eta=\mathbf{0}}, \\
 A_0 C_{ijkl}^{\text{surf}} &= \left[\frac{\partial^2 E}{\partial \eta_{ij} \partial \eta_{kl}} - \frac{\partial^2 E^{\text{bulk}}}{\partial \eta_{ij} \partial \eta_{kl}} \right]_{\eta=\mathbf{0}}.
 \end{aligned}$$

>From these definitions it is also possible to calculate the dependence of the surface energy and the surface stress with the deformation.

However although in this thesis we will deal (among other things) with the elastic behaviour of a confined system i.e. surfaces will be present we will not use the quantities which appear here. This section has to be intended more as an overview on the problem of elasticity in presence of surfaces.

For a comprehensive description of this subject (in 3 dimensions) and the rich phenomenology stemming from it see [7].

Chapter 2

Model of a confined colloidal crystal

2.1 Choice of a Model

As it is well-known, one can prepare systems of spherical colloidal particles with various types of interactions: neutral particles coated with polymer brushes that have a short range entropic repulsion due to the excluded volume interaction between polymers provide a model for approximate hard spheres [11, 12, 13, 14]. Charged colloids (with counterions in the solution) interact with the DeJaguin-Landau-Vervey-Overbeek (DLVO) potential [15, 16], a screened (Yukawa-type) Coulomb interaction.

However of particular interest, in our context are particles containing a superparamagnetic core: if such particles are held at the water-air interface of a water film underneath a glass plate and one applies a magnetic field oriented perpendicular to the glass plate, one creates a $2d$ system of colloidal particles interacting with a uniformly repulsive r^{-3} interaction [8, 9]. Using laser fields based devices (optical tweezers) it is even possible to confine single rows of particles and the ordering of the particles can be directly observed in real space by video microscopy.

However experiments can infer the precise form of the interparticle potential at best indirectly, if at all, so it is important, as a sort of guide line for the experiments to perform computer simulations of suitable model systems.

So the interaction among colloidal particles may be conveniently param-

eterized by

$$V(r) = \epsilon \left(\frac{\sigma}{r} \right)^n, \quad (2.1)$$

where the exponent may vary from $n = \infty$ [11, 12, 13, 14] in the case of hard sphere colloids to $n = 3$ for superparamagnetic dipolar colloids [8, 9, 10]. We have chosen a potential with $n = 12$ and with a cutoff at $r_c = 5\sigma$, at a temperature $k_B T / \epsilon = 1$ (k_B is the Boltzmann constant) and density (choosing units such that $\sigma = 1$) $\rho = 1.05$. This choice retains the advantage of a smooth potential which is also sufficient short ranged for computational convenience.

At the chosen density and temperature the bulk $2d$ system is deep in the crystalline phase since for the chosen density melting occurs at $T \approx 1.35$ [17]. Note that the homogeneity of the potential, eqn. 2.1, implies that (in $d = 2$ dimensions) excess thermodynamic properties (relative to the ideal contribution) and the scaled pair distribution function $g(r/\sigma)$ depend on a single parameter

$$x = \rho \sigma^2 (\epsilon / k_B T)^{2/n}, \quad (2.2)$$

rather than ρ and T separately [43].

Next we discuss how to represent the confining walls. We have considered two types of boundary potential which provides the confinement in a strip with the walls oriented parallel to lattice axes of the triangular lattice:

1. The first choice is a so called “flat wall” and it is given by an integration of the repulsive part of the Lennard-Jones potential:

$$V_{\text{wall}} = \epsilon_{\text{wall}} \left(\frac{\sigma}{|x - x_{\text{wall}}|} \right)^{10}, \quad (2.3)$$

for a particle at position $\mathbf{r} = (x, y)$, where the x -direction is chosen perpendicular to the boundaries, while y runs along the boundaries.

2. Structured walls causing a periodic corrugation of the potential. They are created by choosing two rows of particles (running in the y -direction) fixed in the positions of this ideal triangular lattice. These fixed particles interact with the mobile particles with the same potential $V(r)$ of eqn 2.1. Summing up these potentials due to the fixed particles defines the corrugation potential V_{struc} of such structured boundaries.

The position x_{wall} of the two walls are a distance D apart with D in the

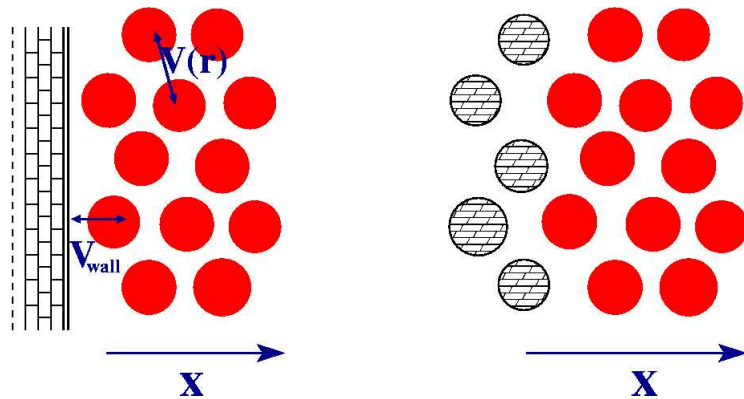


Figure 2.1: Sketch of the two kinds of wall considered: left the case 1 the “flat wall”, right the case 2 the “structured wall”

form:

$$D = na \frac{\sqrt{3}}{2}, \quad (2.4)$$

with n being an integer and a being the lattice spacing of the ideal triangular lattice compatible with the chosen density (see fig. 5.1, pag. 67, where the lattice spacing is denoted there with the symbol a_0)

$$a^2 \cdot \frac{\sqrt{3}}{2} = \frac{1}{\rho}, \quad (2.5)$$

so with $\rho = 1.05$ this means $a \approx 1.049$.

This choice was made in order to start considering the confined case in a situation as near as possible to the bulk case.

Finally we mention that looking at the effect of confinement on colloidal suspension can be of interest also for a wide variety of systems: e.g. electrons at the surface of liquid helium that is confined in a quasi-one-dimensional channel [18] provide an example for a confined Wigner crystal [44]; another such system where particles under geometric confinement are “dusty plasmas” [19] (e.g. negatively charged SiO_2 fine particles with $10 \mu\text{m}$ diameter are suspended in weakly ionized rf Ar discharges [20]; magnetorheological (MR) colloids under confinement [21, 22] are of great interest for various microfluidic applications.

2.2 First simulations with flat walls: choosing the parameter ϵ_{wall}

As we said we wanted to simulate a situation very near to the bulk case and this was true not only for the wall distance but also for the value of ϵ_{wall} in eqn. 2.3. In order to do so we tried different values of ϵ_{wall} (and also different distances among the walls) to see which changes occur to the lattice due to the potential 2.3 .

We performed Monte-Carlo simulations with the canonical Metropolis algorithm, the simulations were done in a “stripe geometry” we considered simulation boxes with angle among the x and y –direction of 60 degrees instead of the usual 90 degrees, this was done to simulate better the triangular geometry of the system. The dimensions of the boxes were (in unit of a) 30×30 and 20×60 . The averages were done over runs of 10^6 MC cycles after an equilibration of as many MC-cycles as in the production run

We considered in particular the angle α among the lattice planes (figure 2.2)

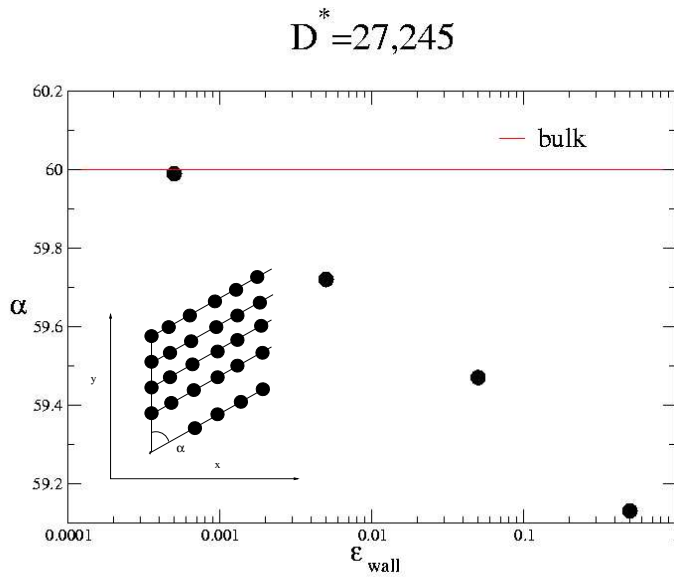


Figure 2.2: Angle α between lattice planes. Inset: schematic picture. Main plot: numerical values according to our simulations, the value of α for hard walls is $\alpha_{\text{hard walls}} = 60.68$.

In the figure 2.2 the distance is chosen in a way that at the density

$\rho = 1.05$, 30 layers can be allocated exactly as in the bulk. In the ideal (bulk) case the distance first layer-left wall ($x = 0$) and the distance last layer-right wall ($x = D^*$) are the same,

$$x_{1^{st}layer} = \frac{1}{2} \cdot \frac{\sqrt{3}}{2} a = D^* - x_{30^{th}layer}.$$

We considered in figure 2.3 this distance of the different layers (parallel to the wall direction) and the left wall, for different ϵ_{wall} and also for two different values of distances corresponding to considering 30 layers (up) and 20 layers (down) .

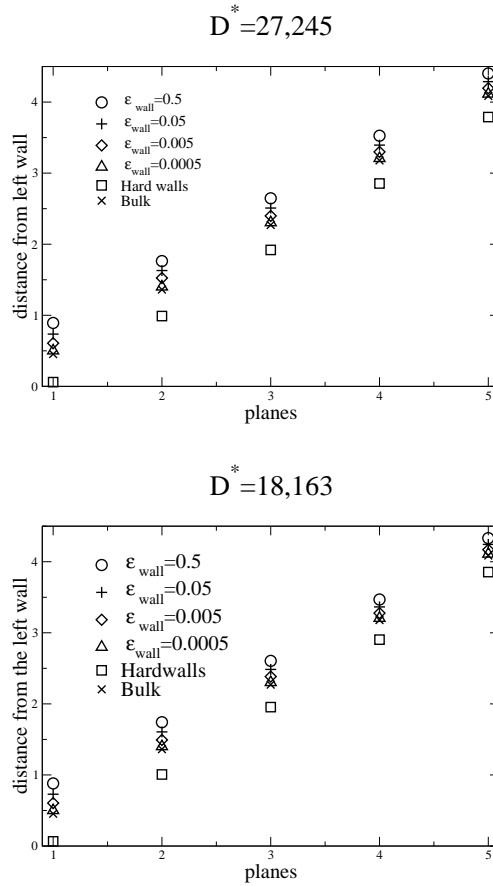


Figure 2.3: Distance between the first five crystal layers (planes) parallel to the wall direction and the left wall for different ϵ_{wall} , the bulk and the hard walls case

We see that the situation passing from 30 to 20 layers doesn't change much while on the other hand, looking at the figures 2.2 and 2.3, we see how much the value ϵ_{wall} is important in deforming the crystal. The value of ϵ_{wall} which minimize the deformations in the lattice structure is

$$\epsilon_{\text{wall}} = 0.0005.$$

This will be the value we will consider throughout this thesis for the simulations with the flat walls.

We considered also the case of hard walls in which the interaction potential is

$$V_{\text{wall}} = \begin{cases} 0 & 0 < x < D^*, \\ \infty & \text{elsewhere.} \end{cases} \quad (2.6)$$

In this case actually the system is not a crystal anymore as we can see in figure 2.4. However we performed some simulations imposing the crystal to remain dislocation free, that is, we rejected all the moves which bring a change in the nearest neighbours of any particle (cfr. following sections). Any system with this constraint will never melt so we could find also the lattice deformation values for the hard wall case.

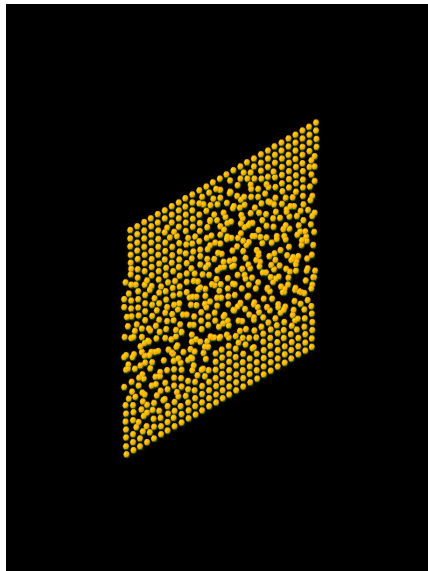


Figure 2.4: Configuration with hard potential 2.6 the walls run along the tilted sides

2.3 Evaluation of the elastic constants

Calculations of elastic constants from simulations fall into two categories, i.e. they are obtained either from thermal averages of fluctuations of the stress or the strain, the so called “fluctuation” methods [23], or from the stress-strain curve as computed from a series of simulations [24]. Fluctuation methods, though requiring longer runs for accumulating statistically significant data, are often preferred because the entire matrix of the elastic constants can be evaluated in a single run, while in the second method for every elastic constant an appropriate strain (or stress) has to be applied.

We applied two fluctuation methods in our simulations. In order to evaluate the elastic constants we monitor both the stress and the strain tensor during the simulations and evaluate their fluctuations, according to the eqns.1.2 and 1.4, can we then calculate the elastic constants.

All the simulations were done in the NVT ensemble so number of particle, volume and temperature are constant throughout the simulation. Both methods have advantages and disadvantages.

1. Sampling the stress tensor and its fluctuations keeping the volume constant means small finite size effect, but on the other hand it requires potentials which are everywhere differentiable. A generalization of this method, that can be used with non analytic potentials as well, exists but it is more difficult [25].
2. In the sampling of the strain tensor and its fluctuations the form of the potential is not so important but since the volume (and hence the total strain) are constant, a finite size analysis is required in order to get meaningful thermodynamical quantities, moreover as final result of this analysis we obtain the so called compliance matrix that then has to be linked to the elastic constants.

2.4 Stress fluctuations

The idea here is to evaluate the stress tensor from the virial formula and then to consider its fluctuations. For the bulk case the formulae for the canonical ensemble were given for the first time in [24]. For the stress tensor it reads:

$$\sigma_{ij} = \frac{1}{V} \left\langle \sum_{\langle \alpha\beta \rangle} V'(R^{\alpha\beta}) \frac{R_i^{\alpha\beta} R_j^{\alpha\beta}}{R^{\alpha\beta}} \right\rangle - \frac{NkT\delta_{ij}}{V}, \quad (2.7)$$

where the summation is over all distinct pairs of particles, $R_i^{\alpha\beta} = (\mathbf{R}^\alpha - \mathbf{R}^\beta)_i$, $R^{\alpha\beta} = |\mathbf{R}^\alpha - \mathbf{R}^\beta|$ and $V'(r) = \frac{dV}{dr}$.

For the elastic constants we have

$$\begin{aligned} C_{ijkl} &= \frac{1}{VkT} \left\{ \left\langle \sum_{\langle \alpha\beta \rangle} V'(R^{\alpha\beta}) \frac{R_i^{\alpha\beta} R_j^{\alpha\beta}}{R^{\alpha\beta}} \right\rangle \cdot \left\langle \sum_{\langle \alpha\beta \rangle} V'(R^{\alpha\beta}) \frac{R_k^{\alpha\beta} R_l^{\alpha\beta}}{R^{\alpha\beta}} \right\rangle - \right. \\ &- \left. \left\langle \left[\sum_{\langle \alpha\beta \rangle} V'(R^{\alpha\beta}) \frac{R_i^{\alpha\beta} R_j^{\alpha\beta}}{R^{\alpha\beta}} \right] \cdot \left[\sum_{\langle \alpha\beta \rangle} V'(R^{\alpha\beta}) \frac{R_k^{\alpha\beta} R_l^{\alpha\beta}}{R^{\alpha\beta}} \right] \right\rangle \right\} + \\ &+ \frac{1}{V} \left\langle \sum_{\langle \alpha\beta \rangle} V''(R^{\alpha\beta}) \frac{R_i^{\alpha\beta} R_j^{\alpha\beta} R_k^{\alpha\beta} R_l^{\alpha\beta}}{(R^{\alpha\beta})^2} \right\rangle - \frac{1}{V} \left\langle \sum_{\langle \alpha\beta \rangle} V'(R^{\alpha\beta}) \frac{R_i^{\alpha\beta} R_j^{\alpha\beta} R_k^{\alpha\beta} R_l^{\alpha\beta}}{(R^{\alpha\beta})^3} \right\rangle + \\ &+ \frac{2NkT\delta_{il}\delta_{jk}}{V}. \end{aligned} \quad (2.8)$$

For a confined system, we have to consider the contribution of the walls as well, we computed it in the following way:

In the case of structured walls we used the formulae 2.7 and 2.8 counting in them the contribution from the pairwise interactions between the moving particles and the particle forming the walls.

In the case of the flat walls given by the wall potential 2.3, we followed the suggestion in [26] where in a different but similar context (the evaluation of the local stress tensor in a confined system) each wall was treated as an additional particle of infinite mass which due to symmetry reasons, gives contributions only in the direction normal to the walls. So we considered for

this system the formulae

$$\begin{aligned}
\sigma_{ij} &= \frac{1}{V} \left\langle \sum_{\langle \alpha\beta \rangle} V'(R^{\alpha\beta}) \frac{R_i^{\alpha\beta} R_j^{\alpha\beta}}{R^{\alpha\beta}} \right\rangle - \frac{NkT\delta_{ij}}{V} \\
&+ \frac{1}{V} \left\langle \sum_{h=1}^N V'_{\text{wall}}[x_h - x_{\text{leftwall}}] \cdot (x_h - x_{\text{leftwall}}) \right\rangle \delta_{ix} \delta_{jx} \\
&- \frac{1}{V} \left\langle \sum_{h=1}^N V'_{\text{wall}}[x_{\text{rightwall}} - x_h] \cdot (x_{\text{rightwall}} - x_h) \right\rangle \delta_{ix} \delta_{jx}, \quad (2.9)
\end{aligned}$$

for the stress tensor while for the elastic constants we used

$$\begin{aligned}
C_{ijkl} &= \frac{1}{VkT} \left\{ \left\langle \sum_{\langle \alpha\beta \rangle} V'(R^{\alpha\beta}) \frac{R_i^{\alpha\beta} R_j^{\alpha\beta}}{R^{\alpha\beta}} + \text{wco} \right\rangle \cdot \left\langle \sum_{\langle \alpha\beta \rangle} V'(R^{\alpha\beta}) \frac{R_k^{\alpha\beta} R_l^{\alpha\beta}}{R^{\alpha\beta}} + \text{wco} \right\rangle - \right. \\
&- \left. \left\langle \left[\sum_{\langle \alpha\beta \rangle} V'(R^{\alpha\beta}) \frac{R_i^{\alpha\beta} R_j^{\alpha\beta}}{R^{\alpha\beta}} + \text{wco} \right] \cdot \left[\sum_{\langle \alpha\beta \rangle} V'(R^{\alpha\beta}) \frac{R_k^{\alpha\beta} R_l^{\alpha\beta}}{R^{\alpha\beta}} + \text{wco} \right] \right\rangle + \right. \\
&+ \frac{1}{V} \left\langle \sum_{\langle \alpha\beta \rangle} V''(R^{\alpha\beta}) \frac{R_i^{\alpha\beta} R_j^{\alpha\beta} R_k^{\alpha\beta} R_l^{\alpha\beta}}{(R^{\alpha\beta})^2} \right\rangle - \frac{1}{V} \left\langle \sum_{\langle \alpha\beta \rangle} V'(R^{\alpha\beta}) \frac{R_i^{\alpha\beta} R_j^{\alpha\beta} R_k^{\alpha\beta} R_l^{\alpha\beta}}{(R^{\alpha\beta})^3} \right\rangle + \\
&+ \frac{2NkT\delta_{il}\delta_{jk}}{V} + \frac{\delta_{ix}\delta_{jx}\delta_{kx}\delta_{lx}}{V} \left\langle \sum_{h=1}^N V''_{\text{w}}[x_h - x_{\text{lw}}] \cdot (x_h - x_{\text{lw}})^2 \right\rangle - \\
&- \frac{\delta_{ix}\delta_{jx}\delta_{kx}\delta_{lx}}{V} \left\langle \sum_{h=1}^N V''_{\text{w}}[x_{\text{rw}} - x_h] \cdot (x_{\text{rw}} - x_h)^2 \right\rangle - \\
&- \frac{\delta_{ix}\delta_{jx}\delta_{kx}\delta_{lx}}{V} \left(\left\langle \sum_{h=1}^N V'_{\text{w}}[x_h - x_{\text{lw}}] \cdot (x_h - x_{\text{lw}}) \right\rangle - \right. \\
&- \left. \left\langle \sum_{h=1}^N V'_{\text{w}}[x_{\text{rw}} - x_h] \cdot (x_{\text{rw}} - x_h) \right\rangle \right), \quad (2.10)
\end{aligned}$$

where the term “wco” indicates the wall contribution to the virial in eqn. 2.9 that is,

$$\begin{aligned}
\text{”wco”} &= \frac{1}{V} \sum_{h=1}^N V'_{\text{wall}}[x_h - x_{\text{leftwall}}] \cdot (x_h - x_{\text{leftwall}}) \delta_{ix} \delta_{jx} \\
&- \frac{1}{V} \sum_{h=1}^N V'_{\text{wall}}[x_{\text{rightwall}} - x_h] \cdot (x_{\text{rightwall}} - x_h) \delta_{ix} \delta_{jx}. \quad (2.11)
\end{aligned}$$

2.5 Strain fluctuations

We use here the method proposed by Sengupta et al. in [27]. One can apply it only in simulations of crystals, that is, when it is possible to have an underlying reference lattice and it is based on the sampling of an instantaneous microscopic strain “field” that is defined in every lattice point via the eqn.1.1, here the set $\{\mathbf{u}\}$ represents the displacements from the lattice equilibrium positions given by the set $\{\mathbf{R}\}$. The derivatives are evaluated numerically through finite differences and for the sake of simplicity, only the linear part in eqn. 1.1 is taken into account.

In order for this method to work as it is without modifications it is necessary not only to have a lattice but also that this lattice stays defect free in the simulations, that is all the Monte Carlo moves introducing dislocations are rejected so during the simulations the nearest neighbours of every particle cannot be changed. In this sense it is not even necessary to perform a Voronoi construction after every move to determine the new nearest neighbours of the moved particle, but it is sufficient to control that the nearest neighbours of the particle, listed at the beginning of the simulation, stayed unchanged, an example of such rejected moves are given in the figure below

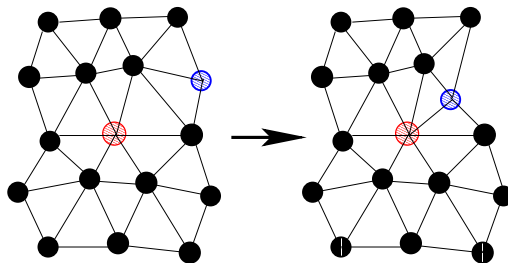


Figure 2.5: The blue particle is moved and after that the red one has now 7 nearest neighbours and not the canonical 6. One can show that this is equivalent to a dislocation-antidislocation pair separated by one lattice constant.

In addition the number of moves p which are rejected because of this constraint are stored in order to check how relevant this constraint is, but we expect that if the system is far enough from the melting point the fraction of moves rejected in this way will be anyway very low. On the other hand going nearer and nearer to the transition point this number should more and more increase, one can use this to estimate the dislocation pair formation

probability and from that discuss the two dimensional melting scenario [28].

2.5.1 How the method works: the block analysis

The block analysis method has been used for example to calculate the compressibility of the Ising lattice gas [30] and the two dimensional Lennard-Jones fluid [31, 32]. Here we describe a version of this method which allows us to explicitly and systematically incorporate the finite size effects arising from a non zero correlation length as well as special constraints due to the nature of the ensemble used.

Let's consider a two-dimensional system described by a scalar order parameter $\psi(\mathbf{r})$. We are interested in the properties of this system in the disordered phase. It is therefore sufficient to use the following quadratic free energy functional, $F[\{\psi\}]$,

$$F = k_B T \int \left(\frac{1}{2} r \psi^2 + \frac{1}{2} c \{ \nabla \psi(\mathbf{r}) \}^2 \right) d\mathbf{r}. \quad (2.12)$$

This method consists in measuring, during the simulation, ψ and its fluctuations averaged within some sub boxes of size $L_b < L$ that is,

$$\bar{\psi} = \frac{1}{L_b} \int^{L_b} \psi(\mathbf{r}) d\mathbf{r}, \quad (2.13)$$

$$\langle \bar{\psi}^2 \rangle = \frac{1}{L_b^2 \cdot L_b^2} \int^{L_b} \int^{L_b} \langle \psi(\mathbf{r}) \psi(\mathbf{r}') \rangle d\mathbf{r} d\mathbf{r}'. \quad (2.14)$$

We can determine the form of the eqn. 2.14 starting from the Ornstein-Zernick expression for the correlation function in the Fourier space [34]

$$\beta G_{\psi\psi}(\mathbf{q}) = \langle \psi_{\mathbf{q}} \psi_{-\mathbf{q}} \rangle = \chi_{\psi\psi}^{\infty} \frac{1}{1 + q^2 \xi_{\psi\psi}^2}, \quad (2.15)$$

where $\xi_{\psi\psi}$ is the correlation length, $\chi_{\psi\psi}^{\infty}$ is the susceptibility in the infinite system for the variable ψ , $\chi_{\psi\psi}^{\infty} = \langle \psi^2 \rangle = \lim_{q \rightarrow 0} \beta G_{\psi\psi}(q)$.

Note that eqs. 2.12 and 2.15 are appropriate for the long wavelength limit only and assume that correlations in this limit are isotropic. This assumption restricts the validity of the approach that is outlined below and should be kept in mind.

In the homogeneous case the eqn. 2.14 becomes

$$\langle \overline{\psi^2} \rangle = \frac{1}{L_b^2} \int^{L_b} \langle \psi(\mathbf{r})\psi(\mathbf{0}) \rangle d\mathbf{r} = \frac{1}{L_b^2} \int^{L_b} \beta G_{\psi\psi}(\mathbf{r}) d\mathbf{r} \equiv \frac{1}{L_b^2} \chi_{\psi\psi}^{L_b}, \quad (2.16)$$

where $G_{\psi\psi}(\mathbf{r})$ is the two-dimensional Fourier transformation of the 2.15. We have

$$G_{\psi\psi}(r) = \frac{1}{\xi^2} \chi_{\psi\psi}^\infty Y(r/\xi_{\psi\psi}), \quad (2.17)$$

where

$$Y(\eta) = \frac{1}{(2\pi)^2} \int_0^\infty z dz \int_0^{2\pi} \frac{e^{iz\cos\theta}}{[z^2 + \eta^2]} d\theta. \quad (2.18)$$

One expects that when the simulation box is sufficiently large the block susceptibility recovers its infinite value $\chi_{\psi\psi}^{L_b} \rightarrow \chi_{\psi\psi}^\infty$ as $L_b \rightarrow L$. However the behaviour of the block susceptibility is strongly dependent on the ensemble in which the simulation is carried out [33]. For example, using the lattice gas language [34], in a grand canonical ensemble where the chemical composition ψ of the lattice gas is allowed to fluctuate while the chemical potential difference is being kept constant, the block susceptibility approaches $\chi_{\psi\psi}^\infty$ for large L_b . However this is no longer true in a canonical ensemble since the average of ψ in the entire system is constrained to vanish. This means that when $L_b \rightarrow L$, $\chi_{\psi\psi}^{L_b}$ vanishes also. So in such a case the behaviour of $\chi_{\psi\psi}^{L_b}$ is more complicated but, although in the “wrong” ensemble, is still possible, performing the block analysis, to have informations on $\chi_{\psi\psi}^\infty$.

It can be shown [27] that the analysis done before can be repeated but one has to replace $G(r)$ with

$$G'(r) = G(r) - \Delta_L, \quad (2.19)$$

with

$$\Delta_L = \frac{1}{L^2} \int^L G(\mathbf{r}) d\mathbf{r}. \quad (2.20)$$

As for the $G(r)$ the integral 2.18 cannot be evaluated explicitly but it can be written in term of a Bessel function (cfr eqns. 3.915.2 and 6.532.4 in [35])

$$G(r) = \frac{2}{\pi} \xi^{-2} \chi_{\psi\psi}^\infty K_0(r/\xi), \quad (2.21)$$

where from now on we omit the subscripts in G , χ , ξ for simplicity. We have

therefore

$$\Delta_L = \frac{1}{L^2} \chi^\infty \Phi(L/\xi), \quad (2.22)$$

with the function $\Phi(\alpha)$ being defined as

$$\Phi(\alpha) = \frac{2}{\pi} \alpha^2 \int_0^1 \int_0^1 K_0 \left(\alpha \sqrt{x^2 + y^2} \right) dx dy. \quad (2.23)$$

It can be easily verified that for large α , $\Phi(\alpha)$ goes to 1 within a range $\mathcal{O}(1)$. Using the expressions above, we can write for the block susceptibility

$$\chi^{L_b} = \chi^\infty [\Phi(xL/\xi) - x^2 \Phi(L/\xi)], \quad x = \frac{L_b}{L}. \quad (2.24)$$

Note that the eqn. 2.24 gives $\chi^{L_b} \rightarrow 0$ as $L_b \rightarrow L$ as we expected. In general

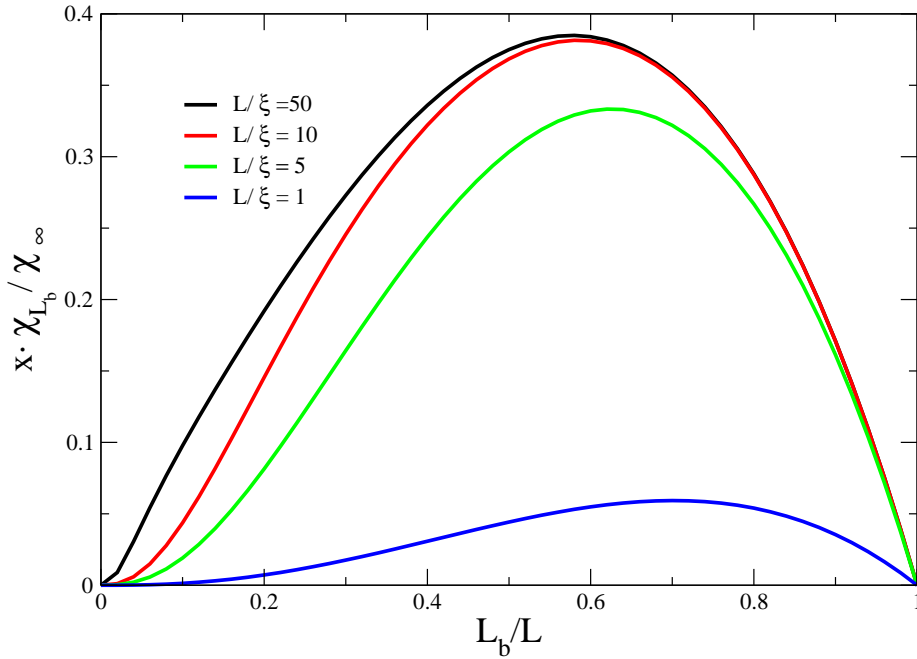


Figure 2.6: $\chi \cdot x$ taken from the eqn. 2.24 plotted versus $x = \frac{L_b}{L}$, for different values of $\frac{L}{\xi}$.

In the figure 2.6 we plotted $\chi^{L_b} \cdot x$ against x for various values of L/ξ . We can see that as $L/\xi \rightarrow \infty$ then $\Phi(\alpha) \rightarrow 1$, so the eqn. 2.24 goes over the

simple asymptotic form

$$\chi^{L_b} \cdot x = \chi^\infty (x - x^3). \quad (2.25)$$

We can then extract χ^∞ from the slope of the linear region in the eqn. 2.25. Of course when $L \sim \xi$ this procedure is not so well defined and finding the linear region is not so straightforward. Nevertheless by fitting the full data to the form in eqn. 2.24 we can still evaluate χ^∞ .

2.5.2 Strain fluctuations and elastic constants

We apply now the method of the previous subsection to our problem. In this case ψ represents suitable linear combinations of components of the strain tensor $\eta_{ij}(\mathbf{R})$. The susceptibilities χ then will give the compliance matrix. From that we can then evaluate the elastic constants. Let's point out first that we can use the analysis exposed before. In fact all the simulations are made in the canonical ensemble, that is, the volume and the shape of the box as well are constant. The overall strain of the whole simulation box is fixed (= 0 clearly). This means that the strain fluctuations go to zero when $L_b \rightarrow L$ so we expect a behaviour like the one in fig.2.6 ¹

Consider a triangular lattice far away from any phase transitions under an hydrostatic pressure P. The elastic free energy can be written, given the symmetries in the bulk case, in the quadratic form

$$F = \int \left[\frac{K}{2} \eta_+^2 + \frac{\mu + P}{2} (\eta_-^2 + 4\eta_{xy}^2) - P\eta_+ \right] d\mathbf{r}, \quad (2.26)$$

where η_+ and η_- are linear combinations of the diagonal components of the strain tensor

$$\eta_+ = \eta_{xx} + \eta_{yy}, \quad \eta_- = \eta_{xx} - \eta_{yy}.$$

In eqn. 2.26 K is the bulk modulus and μ the shear modulus (see sec. 1.3 and eqns. 1.27).

¹actually since we are considering here a lattice and not a field when $L_b = L$ there could be in the susceptibility a small offset $\mathcal{O}(a/L)^2$, where a is the lattice parameter i.e. $\chi^L = C \cdot (a/L)^2 \neq 0$.

The susceptibilities to consider in this case are:

$$S_{++} = \langle \eta_{++} \eta_{++} \rangle, \quad (2.27)$$

$$S_{--} = \langle \eta_{--} \eta_{--} \rangle, \quad (2.28)$$

$$S_{33} = 4 \langle \eta_{xy} \eta_{xy} \rangle. \quad (2.29)$$

We expect now for the three of them the form of eqn.2.24, so that equation can be used to obtain the system size independent quantities $S_{\gamma\gamma}^{\infty}$. Once these compliances are obtained the bulk and the shear modulus are given by the formulae [27]

$$\beta K = \frac{1}{2S_{++}}, \quad (2.30)$$

$$\beta\mu = \frac{1}{2S_{--}} - \beta P, \quad (2.31)$$

$$\beta\mu = \frac{1}{2S_{33}} - \beta P. \quad (2.32)$$

Following the same scheme if we consider now the triangular lattice in the confined case the elastic part of the free energy will have a lower symmetry. We considered instead of eqn. 2.26 a more general expression

$$F = \int d\mathbf{r} \left\{ \frac{1}{2} \begin{pmatrix} \eta_1 & \eta_2 & \eta_3 \end{pmatrix} \begin{pmatrix} C_{11} & C_{12} & 0 \\ C_{12} & C_{22} & 0 \\ 0 & 0 & 4C_{33} \end{pmatrix} \begin{pmatrix} \eta_1 \\ \eta_2 \\ \eta_3 \end{pmatrix} - P_t \eta_1 - P_l \eta_2 \right\}, \quad (2.33)$$

where here we used again the Voigt notation, in the bulk case of course we have $C_{11} = C_{22}$ and $C_{12} = C_{33}$, and the eqn. 2.33 is equivalent to eqn 2.26 (see also eqns. 1.27 for the relation between the C and the moduli K and μ). Again looking at the fluctuations of the different parts of the strain tensor we can calculate the compliance matrix \mathbf{S} and from that the elastic constants matrix \mathbf{C}

$$\beta\mathbf{C} = \frac{1}{2}\mathbf{S}^{-1}. \quad (2.34)$$

Chapter 3

Numerical results for the elastic constants

3.1 Details about the block analysis and the evaluation of the strain field

In this chapter we want to expose the results we found for the elastic constants. However we first start with some details about how the block analysis was performed and how we evaluate the derivatives needed for $\eta_{ij}(\mathbf{R})$ according to the 1.1.

We considered different wall distances and so different system sizes. Typical runs were performed for system containing between 20×20 and 80×80 particles performing 10^6 Monte-Carlo steps per particle for every run. We used standard Monte-Carlo methods where single particles are selected at random to attempt a small random displacement in a square of linear dimension $k = 0.206$ centered at the old position of the particle. In the direction parallel to the walls, periodic boundary conditions are used.

The block analysis is performed every 10 Monte-Carlo steps and it is done choosing L_b in the form

$$L_b = \frac{n}{100}L, \quad n = 1, 2, \dots, 100.$$

The sub box of size L_b is placed randomly 100 times in the simulation box. Every time the average values of the components of the strain tensor in the sub box are computed, and after that the needed correlations, according

to the eqn. 2.26 or the eqn. 2.33, times the number of points in the sub box (according to eqn.2.16). Then the average values over the 100 tries are considered and these will be the sampled block averages. To make an explicit example, let's take η_{++} in the bulk case: every time we consider a sub box with a given L_b/L , we evaluate

$$\overline{\eta_{++}} = \frac{1}{n(L_b)} \sum_{i=1}^{n(L_b)} \eta_{++}^i, \quad (3.1)$$

where the sum is over the $n(L_b)$ lattice sites inside the sub box. We then consider the square of eqn. 3.1 times $n(L_b)$. After averaging over 100 tries, we take this average, according to the eqn. 2.16 as the sampled value for

$$\overline{\eta_{++}}^2 \cdot L_b^2 = \chi_{L_b}^{\eta_{++}} \quad (3.2)$$

The strain field is evaluated as follows: we consider for every lattice point the instantaneous displacement from the average position

$$\mathbf{u}_{\mathbf{R}}(t) = \mathbf{R}(t) - \mathbf{R}, \quad (3.3)$$

where the average lattice $\{\mathbf{R}\}$ is updated every 10^5 Monte-Carlo steps. In order to get the strains we need the derivatives to the 2 components of $\mathbf{u}_{\mathbf{R}}$ with respect to x and y . The derivatives are calculated using the 6 nearest neighbours of every lattice site. We consider all the triplets made by the central lattice point plus two consecutive nearest neighbours (for example the points $\{0, 1, 2\}$ see figure below)

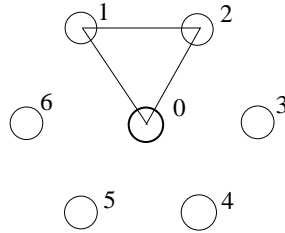


Figure 3.1: Lattice site and its nearest neighbours in a triangular crystal

Starting from these 3 points then we consider the 3 column vectors

$$\begin{pmatrix} u_i^0 \\ X^0 \\ Y^0 \end{pmatrix}, \quad \begin{pmatrix} u_i^1 \\ X^1 \\ Y^1 \end{pmatrix}, \quad \begin{pmatrix} u_i^2 \\ X^2 \\ Y^2 \end{pmatrix},$$

where u_i^α are the i -th component of the displacement from the equilibrium position for the α particle while $(X^\alpha; Y^\alpha)$ are the coordinates of its reference lattice point. Then we calculate the plane passing for the 3 points in the u_i, x, y space which will have the linear form

$$u_i = ax + by + c, \tag{3.4}$$

and we take $a = \frac{\partial u_i}{\partial x}$ and $b = \frac{\partial u_i}{\partial y}$. We repeat these calculations for all the 6 triplets possible and then take the average as the final result for the derivatives which are used in the linear part of eqn. 1.1 for η .

We conclude this section mentioning that, although in a modified version for the evaluation of the susceptibilities, this method was used not only in simulations but also in experiments where, with video microscopy techniques, one can monitor the fluctuations of the particles from their average positions and from that compute the elastic constants [10].

3.2 Block analysis: results for the bulk

We report here our results regarding the block analysis method which was considered in the previous chapter

We considered first the easiest case: the bulk, that is, soft disks with the interaction potential 2.1 with periodic boundary conditions in all directions. Here we want to find the block susceptibilities according to the scheme of eqn. 2.24 and fig. 2.6

Some results are shown in figs 3.2 and 3.3. The behaviours we found are the one we expect from the theory of the previous chapter and are in agreement with [27] as well.

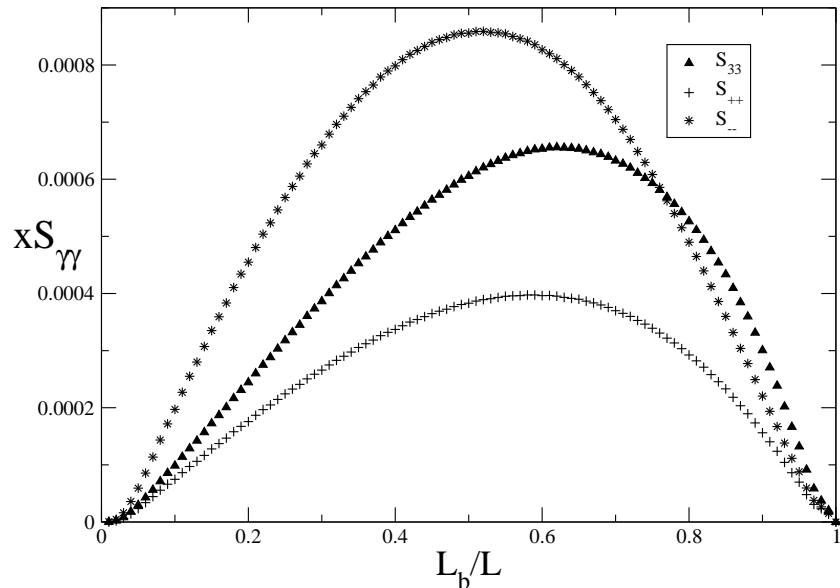


Figure 3.2: Compliances curves in the bulk case: system size 900 particles

3.3 Block analysis: results for the confined systems

We report here the results we found for the confined systems, that is, soft disks with interaction potential 2.1 plus the two types of walls we considered according to the secs. 2.1 and 2.2.

As already pointed out in subsec. 2.5.2, due to the lower symmetry of the problem instead of the 3 compliances S_{++} , S_{--} , and S_{33} we considered S_{11} , S_{22} , S_{12} and S_{33} . For the first 3 of them, in fig. 3.4, the results we found are the one we indeed expected

However for S_{33} we found an unexpected behaviour for the case of the flat walls, while in the case of the structured walls this does not happen, the curves are plotted in figs. 3.5 and 3.6 respectively. The curve in fig. 3.5 shows that for that case the block analysis scheme as we derived in subsec. 2.5.1 cannot be applied here, in particular we cannot here assume that the fluctuation of η_{xy} in the whole box is equal to 0 or very small. A reliable analysis for this case was not possible and this made it impossible for us to extract the C_{33} from this curve with the method of subsec. 2.5.2. The reason for the shear fluctuations to be so large, in the case of the flat walls, will be explained in the following chapters. Here we just say that it is clearly a

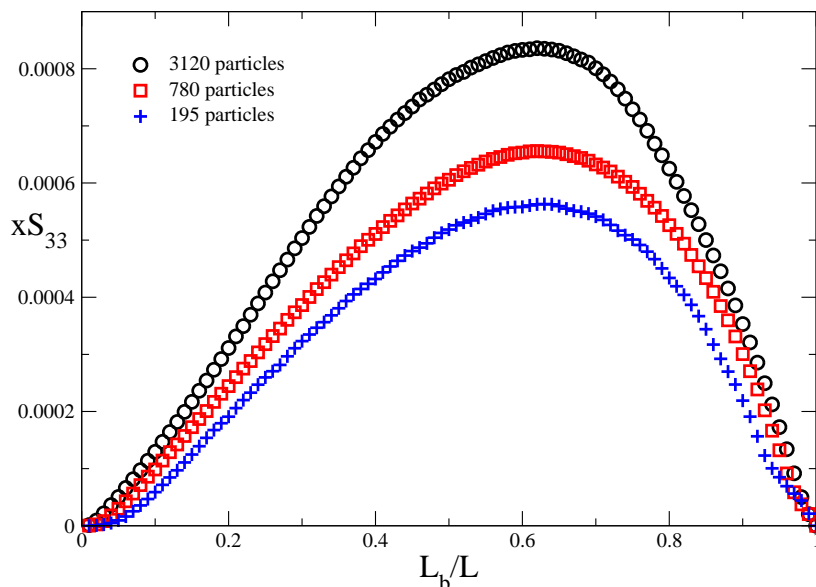


Figure 3.3: S_{33} in the bulk case for different system sizes, as the system size increases we go toward the limit 2.25. Look also at fig.2.6.

wall induced effect which shows that the system is loosing some "order" in the direction y parallel to the walls

3.4 Numerical values of the elastic constants: the two different methods and different wall distances

Here we give finally the values of the elastic constants for the systems we simulated. In the two tables 3.1 and 3.2 the results obtained with the two different methods, in the case of distance between the walls $D = 30\frac{\sqrt{3}}{2}a$ (sec. 2.1) are written. We found with the two methods, within the errors, the same results.

In the figs. 3.7 we consider the elastic constants for different distances of the walls. In both cases we see that the values of these constants don't change much with the distance. This is due to the fact that elastic deformations are long range, and so are the effects induced by the walls.

In order to have different behaviours with D one should vary it to much larger values, well beyond the possibilities of our computing power.

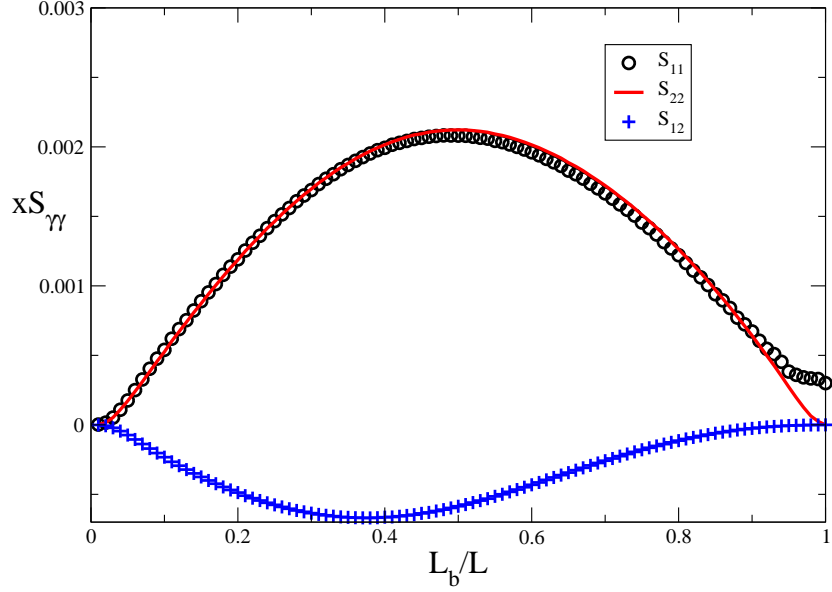


Figure 3.4: S_{11} , S_{22} , S_{12} for the system with flat wall, in the structured case the curves look similar

Another aspect of those results to point out is the value found for C_{33} in the case of flat walls, tab. 3.1 last row and fig. 3.7 (a). These values are quite different from the bulk ones, the Cauchy relation does not hold anymore. Approximately we have

$$2C_{33}(n) = C_{33}(\text{bulk}),$$

and since $C_{33}(n) \sim P$, where P is the pressure, this means that the shear modulus associated to C_{33} vanishes, see eqns. 1.16 and 1.24. In this kind of conditions it becomes very easy to shear the system. This is consistent also with the curve in fig. 3.5, where we point out again that the overall shear fluctuations in the whole box become exceptionally large although periodic boundary conditions in one direction are present.

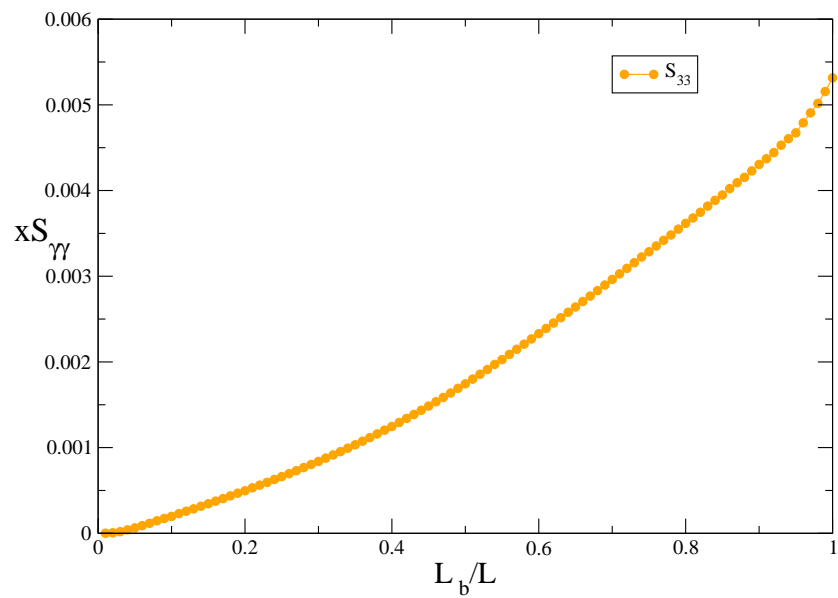


Figure 3.5: S_{33} : flat walls

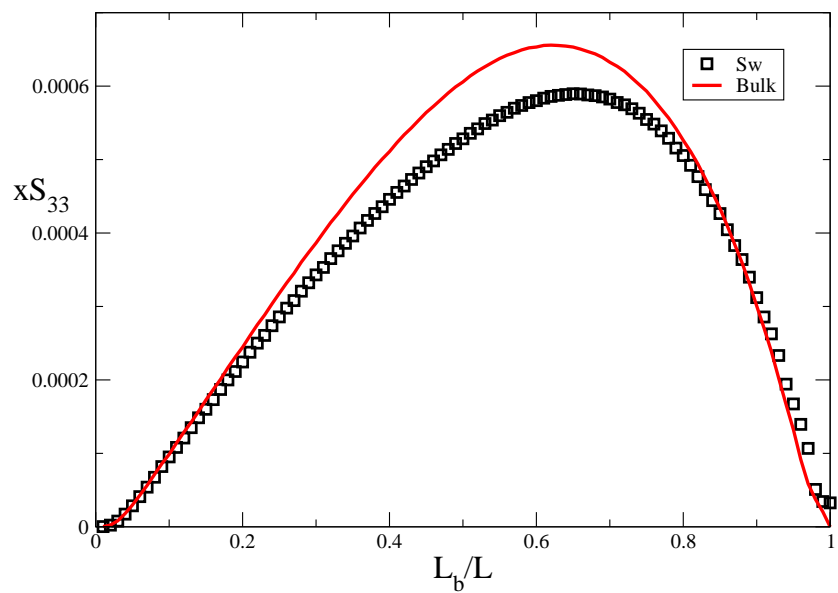


Figure 3.6: S_{33} : structured walls and bulk

Elastic Constants	Stress Fluct. Formula	Strain Fluct. Formula	Bulk
C_{11}	123	121	127.5
C_{22}	127	121	127.5
C_{12}	41	45	43
C_{33}	15	–	43

Table 3.1: Numerical value for the elastic constants in units of $k_B T / \sigma^2$ in the case of flat walls. Here we considered a 30×30 system, i.e. we considered 30 layers in the x direction, perpendicular to the confining walls and 30 layers in the y direction, in which periodic boundary conditions are applied, $\epsilon_{\text{wall}} = 0.0005$. Relative errors of the results are about 3%

Elastic Constants	Stress Fluct. Formula	Strain Fluct. Formula	Bulk
C_{11}	122	122	127.5
C_{22}	125	122	127.5
C_{12}	41	44	43
C_{33}	40	44	43

Table 3.2: Numerical values for the elastic constants in units of $k_B T / \sigma^2$ in the case of the flat walls, again we considered here a 30×30 system. Relative errors of the results are again about 3%

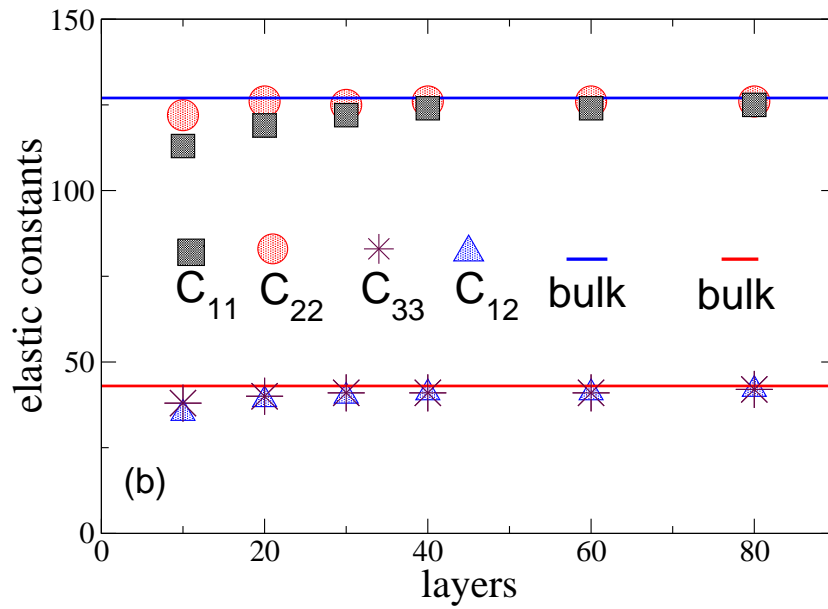
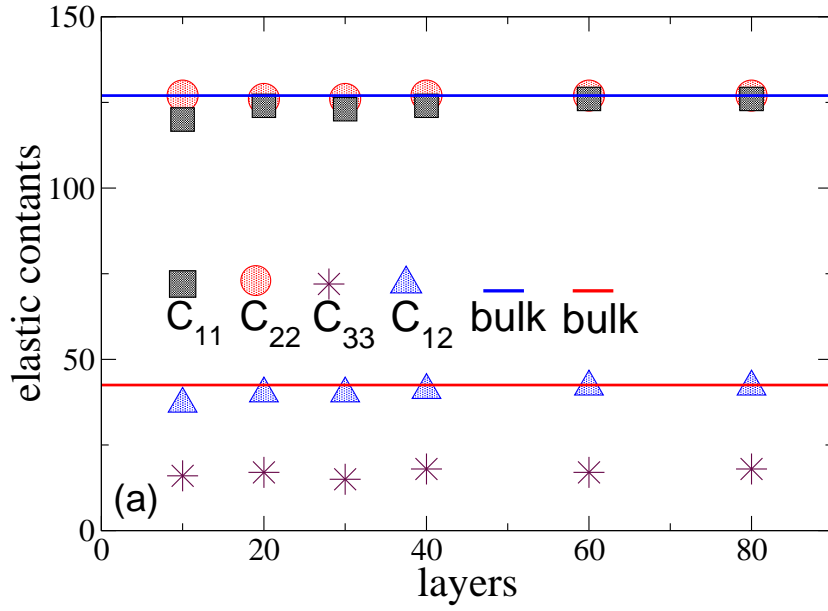


Figure 3.7: Elastic constants in units of $k_B T / \sigma^2$ for flat walls (a) and structured walls (b) plotted vs. the number of rows between the walls. Horizontal straight lines show the bulk values of the corresponding triangular crystal, for which the symmetries $C_{11} = C_{22}$ and $C_{12} = C_{33}$ hold

Chapter 4

Fluctuations and dimensionality

4.1 Introduction

In this chapter, we turn our attention mainly on the fluctuations from the equilibrium lattice positions for the confined systems we are considering.

Our aim is to link to the findings of the previous chapter to the behaviour of such fluctuations. Clearly due to the low dimensionality and the geometrical constraints of the problem (a $2d$ system confined in one direction) we expect these fluctuations to play an important role, and to help us in clarifying what is the effect of the confinement on such crystals.

In order to have a more quantitative analysis we discuss also, in the frame of the harmonic theory, the fluctuations of the particles from their lattice points with periodic boundary conditions.

However in order to have a situation more resembling the one of a confined system (for which we didn't try any analytical calculation) we consider the x direction independently from the y direction, that is, we vary the extension D over which we consider the periodic boundary conditions in x , while L , the extension in the y direction is kept constant. We expect to see a crossover between a $1d$ type behaviour, typical of $D \ll L$ to a $2d$ type behaviour as $D \sim L$.

We will then discuss when the crossover takes place and compare the analytical results with the simulations both with periodic boundary conditions and in the confined case of interest.

4.2 The structure factor in two and in one dimension

In describing the positional order in a system an important quantity is the static structure factor

$$S(\mathbf{q}) = \frac{1}{N} \sum_{l,l'} \langle \exp [i\mathbf{q} \cdot (\mathbf{R}_l - \mathbf{R}_{l'})] \rangle, \quad (4.1)$$

where $\{\mathbf{R}_l\}$ are the positions of the particles.

If we consider as $\{\mathbf{R}_l\}$ a set of points of a lattice we have, in the thermodynamic limit

$$S(\mathbf{q}) \propto \delta(\mathbf{q} - \mathbf{G}), \quad (4.2)$$

where \mathbf{G} is a vector in the reciprocal lattice. Of course in a crystal, the fluctuations from the equilibrium position have to be taken into account.

Let's consider an harmonic crystal we can write for the structure factor [36]:

$$S(\mathbf{q}) = \frac{1}{N} \sum_{l,l'} \exp [i\mathbf{q} \cdot (\mathbf{R}_l^0 - \mathbf{R}_{l'}^0)] \exp \left[-\frac{1}{2} \langle [\mathbf{q} \cdot (\mathbf{u}_l - \mathbf{u}_{l'})]^2 \rangle \right], \quad (4.3)$$

where \mathbf{R}_l^0 is the lattice equilibrium position and \mathbf{u}_l is the displacement of the l -th particle.

Considering again a reciprocal lattice vector for \mathbf{q} , and taking into account the homogeneity of the system eqn. 4.3 becomes

$$S(\mathbf{q}) = \sum_l \exp \left[-\frac{1}{2} \langle [\mathbf{q} \cdot (\mathbf{u}_0 - \mathbf{u}_l)]^2 \rangle \right]. \quad (4.4)$$

We will discuss in detail in sec. 4.4 how to evaluate rigorously the exponent in eqn. 4.4. Here we just say that for small q , the main contribution is given by a term like

$$\int \frac{d\mathbf{k}}{\omega_{\mathbf{k}}^2} = \frac{1}{c^2} \int \frac{d\mathbf{k}}{k^2}, \quad (4.5)$$

where $\omega(\mathbf{k})$ are the phonon frequencies which in the low wave vector limit are linear, $\omega(\mathbf{k}) = c\mathbf{k}$, with c being the sound velocity. The term in eqn. 4.5 gives a contribution which will depend on the dimension of the crystal we are considering. In two and in one dimension this contribution will diverge

respectively logarithmically and linearly with l . That is

$$\langle [\mathbf{q} \cdot (\mathbf{u}_0 - \mathbf{u}_l)]^2 \rangle \sim \log l \quad 2d, \quad (4.6)$$

$$\langle [\mathbf{q} \cdot (\mathbf{u}_0 - \mathbf{u}_l)]^2 \rangle \sim l \quad 1d. \quad (4.7)$$

These divergencies and their effects especially in the two dimensional case have been extensively studied and discussed in many papers [37, 38, 39, 40, 41]. Due to them in $d = 2$ and $d = 1$ it is possible to have a crystal only at $T = 0$.

Let's consider now more in detail the one-dimensional case, again in the harmonic case i.e we take an Hamiltonian of an harmonic chain [41]

$$\mathcal{H} = \frac{1}{2} \sum_l \left[\frac{\pi_l^2}{m} + mc^2 \frac{(y_{l+1} - y_l - a)^2}{a^2} \right], \quad (4.8)$$

where point particles of mass m have positions y_l and conjugate momenta π_l . In the classical ground state one has $y_n = y_0 + na$, $n = 1, 2, \dots, N \rightarrow \infty$, a being the lattice spacing of the one-dimensional periodic lattice. The parameter c plays the role of a sound velocity when one determines the eigenfrequency of \mathcal{H} . From eqn. 4.8 it is straightforward to calculate the correlation function of the main square displacements $u_n = y_n - na$ as

$$\langle (u_n - u_0)^2 \rangle = n \frac{a^2 k_B T}{mc^2} = n\delta^2. \quad (4.9)$$

Here δ characterizes the local displacements. The eqn. 4.9 is clearly the same as eqn. 4.7 only written in more precise way and its interpretation is that the relative displacements $u_l - u_{l-1}$ at each index l of the $1d$ lattice add up in a random walk-like fashion.

Using eqn. 4.9 the structure factor in eqn. 4.3 can be written in the form

$$S(q) = \frac{\sinh\left(\frac{q^2 \delta^2}{2}\right)}{\left[\cosh\left(\frac{q^2 \delta^2}{2}\right) - \cos(qa)\right]}. \quad (4.10)$$

Since $\cos(qa) = 1$ for the Bragg peaks positions $qa = 2\pi\nu$, $\nu = 0, \pm 1, \pm 2, \dots$, one recognizes that for small δ the structure factor has a series of rather sharp peaks at the Bragg positions, which smoothly develop toward a series of delta functions $\delta(q - q_\nu)$ as $\delta \rightarrow 0$ (which means $T = 0$, cfr. eqn. 4.9). For T

small but nonzero, on the other hand, the structure factor resembles a series of Lorentzian peaks

$$S(q \approx q_\nu) \approx \frac{q_\nu^2 \delta^2}{\left[q_\nu^4 \delta^4 / 4 + (q - q_\nu)^2 a^2 \right]} = \frac{4}{q^2 \delta^2} \frac{1}{\left[1 + (q - q_\nu)^2 \nu^{-4} \xi^2 \right]}, \quad (4.11)$$

$$\nu = 1, 2, 3, \dots, \quad \xi = amc^2 / (2\pi^2 k_B T). \quad (4.12)$$

The length ξ describing the width of the first pseudo-Bragg peak can be interpreted as the correlation length of the positional order in the $1d$ chain. From eqn. 4.9 we see that this corresponds to a distance na along the chain for which the mean square displacements has grown to a value $\frac{a^2}{2\pi^2}$, which hence is an analogue to the ‘‘Lindemann criterion’’ of melting familiar from crystals in $d = 3$ [34]. Note that Piacente et al. [44] suggested to generalize the ‘‘Lindemann criterion’’ to estimate the melting temperature of a crystal to low-dimensional system by requiring for the ‘‘Lindemann parameter’’ L_p

$$L_p = \frac{\langle (u_1 - u_0)^2 \rangle}{a^2} = 0.1. \quad (4.13)$$

Such a notion would imply that even a crystal in $d = 1$ has a nonzero melting temperature $T_m > 0$.

As is well known, eqns. 4.10 and 4.11 do provide a realistic description of materials such as the mercury chain compound $Hg_{3-\delta}AsFe_6$ [41, 42].

4.3 The structure factor measured in the confined systems

While a general discussion on the ‘‘orders’’ present in the systems and how these orders are changed by the presence and the nature of the walls will be carried out in the next chapter, in this chapter we are interested specifically only in the positional long range order (LRO) along the wall direction and see how it is affected by the confinement. So we consider and measure in the simulations, for our confined systems, for every layer a $1d$ -like structure factor per layer with q is directed along y . We take a definition like the one eqn. 4.1 but with the particles considered only in a single layer parallel to

the wall and with only the y coordinates, so for the generic n^{th} layer this means

$$S(q) = \frac{1}{N_{\text{layer}}} \sum_{l' \in n^{\text{th}} \text{layer}} \langle \exp [iq (y_l - y_{l'})] \rangle. \quad (4.14)$$

In the fig. 4.1 the results are shown for the case of the flat walls (plot a) and for the one of the structured walls (plot b). We clearly see a dramatic difference in the behaviour of $S(q)$ for the two cases. For the structureless repulsive wall, we have a typical fluid-like structure factor, but with heights of the first two peaks which are much larger than for typical fluids (remember that in three dimensional fluids at the melting temperature the first peak of $S(q)$ reaches a height of about 3 [43]). In fact this structure factor is almost in a quantitative agreement with a fit to the $S(q)$ for the $1d$ harmonic chain of eqn 4.10 adjusting a single parameter in the fit namely $\delta = 0.07$. Remember however, that here we deal here with a system with 30 rows confined between two boundaries, rather than a true $1d$ system.

For the structured walls, the structure factor exhibits the sharp Bragg peaks expected for a crystal.¹

The reduction of the order in the case of flat walls, is also seen directly when one superimpose the positions from 1000 configurations of the particles (fig. 4.2 plot a). Again we want to stress here that, despite the shape of $S(q)$, in the case of flat walls, the system is *not like fluid*. In a fluid, one would see, in a snapshot of a single configuration, lots of dislocations and superimposing a large number of such snapshots a uniform density distribution results which is not the case here. We will show in the next chapter that locally here a crystalline structure is still present and that this lack of order concerns the positional LRO in the y direction only, however: the orientational LRO due to the strong confinement in layers parallel to the walls is rather well developed, and even better for the planar walls rather than the structured walls, the order in the x direction, orthogonal to the walls, is also enhanced by the confinement. The analogy to $1d$ harmonic chains in the case of flat walls suggests that for $T = 0$ the range of positional LRO gets gradually very large, but true LRO only occurs for $T = 0$. (Note that also Ising

¹Note that for ordering *commensurate* with the corrugation potential the statement of N. D. Mermin in [39], that crystal in $d = 2$ have only orientational LRO and no positional LRO does not apply here. This situation is reminiscent of the behaviour of thin films adsorbed on substrates where true LRO commensurate with the substrate corrugation potential can occur [45]

model strips of finite width have a transition only at $T = 0$ for any finite value of D , but there the correlation length below the critical temperature T_c of the $2d$ model is much larger, of order $D \exp(\text{constant} \times D)$. Thus the system may be viewed as a kind of two-dimensional smectic phase, a phase with orientational long range order but positional long range order in one direction only. It would be wrong to interpret the destabilization of crystalline two-dimensional long range order by flat structureless walls as surface-induced melting. If surface-induced melting occurred, we would find lots of dislocations near the boundaries, which is not the case here. In fact, we have used the algorithm of [28] to check the formation of dislocation pairs from a local coordination. Apart from the rows adjacent to the walls, the coordination number of each particle in a triangular structure is 6, while dislocations show up via a 5-fold or 7-fold coordination, and at the walls the coordination number of each particle in a triangular structure is 4, dislocations showing up via 3-fold or 5-fold coordination. We have found that at $T = 1$ the average density of dislocations is 10^{-5} , and this explains why no dislocation pair is seen in typical snapshot pictures such as fig 4.2a.

Taking in mind these results and reconsidering again the elastic constants of fig 3.7, we can say that the fact that confinement by planar structureless walls turns a colloidal $2d$ crystal into a kind of smectic phase [46] (or strongly modulated fluid, respectively) also shows up when one examines these “bulk” properties of the strip (the elastic constants). While for structured walls one reaches the behavior of the bulk rapidly, this clearly does not happen, for planar walls, in the case of $C_{33}(n)$. Again we point out here that the question how for the elastic constants the thermodynamic limit is approached is intriguing. The planar boundary provides an elastic distortion of long range [7] to the crystal, and our results imply that in $d = 2$ this distortion disturbs the positional LRO.

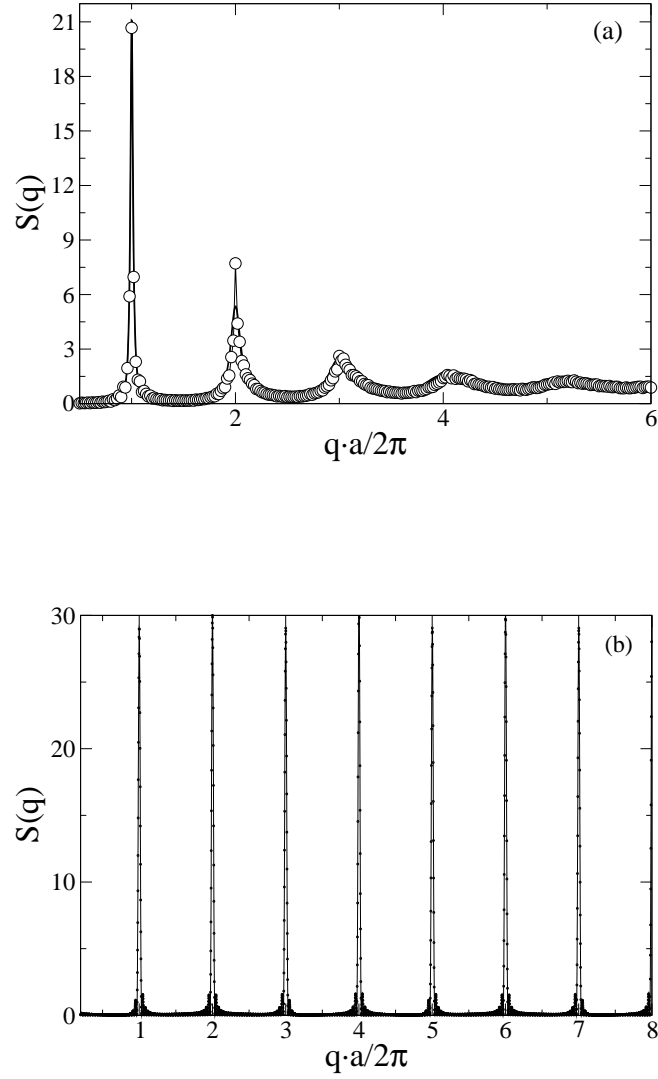


Figure 4.1: 1d static structure factor $S(q)$ plotted versus $qa/2\pi$ (a being the distance between the lattice axes in the y -direction parallel to the boundaries), for planar walls (a) and for structured walls (b). In case (a) a fit to $S(q)$ for a harmonic chain according to the eqn. 4.10 also included (straight line) while the disks are the simulations data. All data are for system of 900 particles, that is 30×30 lattices. the wave vector \mathbf{q} is oriented along the y -direction.

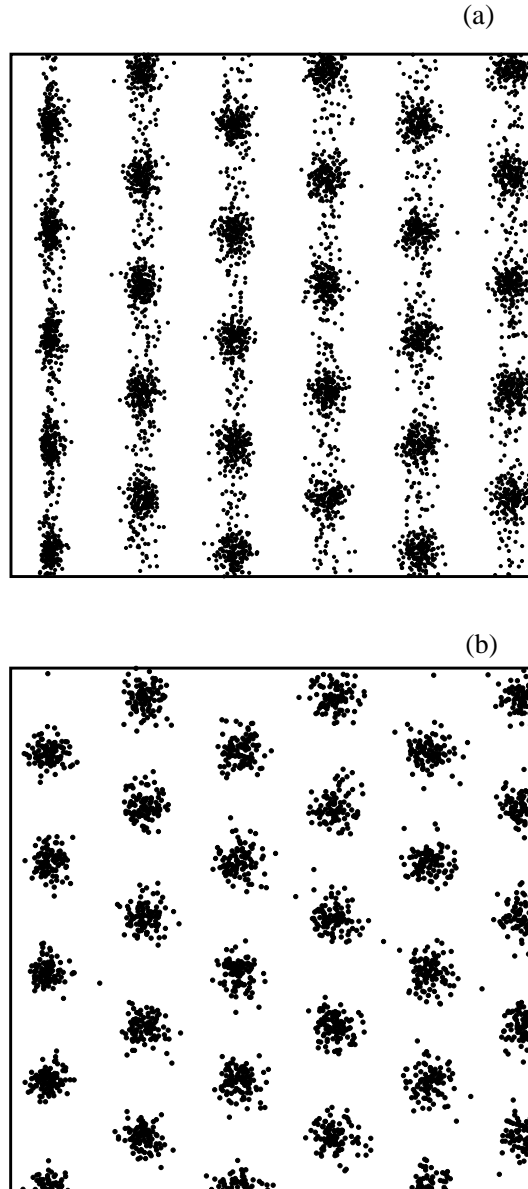


Figure 4.2: Particle configurations corresponding to the structure factors in fig. 4.1. Again plot (a) shows the case of flat walls and plot (b) the case of structured walls. 8 layers adjacent to the wall on the left are shown: 1000 configurations out of a run lasting 10^6 Monte Carlo steps are superimposed. note the prominent anisotropy of the density peaks in the case (a)

4.4 Displacement correlation function: the case of the harmonic lattice in the bulk

In order to help understanding the lack of positional LRO in the case of flat structureless walls, we now evaluate analytically the displacement correlation function

$$B(y) = \langle [u_y(y) - u_y(o)] \rangle, \quad (4.15)$$

where u_y is the displacement away from a reference lattice in the direction parallel to the walls and the angular brackets signify ensemble averaging.

We start from the continuum approximation for a two dimensional elastic solid that has a triangular structure [34]

$$\mathcal{H}_{el} = \frac{1}{2} \int \frac{dQ_x}{2\pi} \int \frac{dQ_y}{2\pi} [(\lambda + 2\mu - P) Q^2 u_L^2 + (\mu - P) Q^2 u_T^2]. \quad (4.16)$$

Here the integration is extended over the first Brillouin zone, λ and μ are the well-known Lamé coefficients, and P is the hydrostatic pressure (see for example eqn. 1.25). The Fourier transform $\mathbf{u}(\mathbf{Q})$, of the displacement vector $\mathbf{u}(l)$ has been decomposed into longitudinal (L) and transverse (T) components. So

$$\mathbf{u}(l) = \frac{1}{\sqrt{N}} \sum_{\mathbf{Q}} \mathbf{u}(\mathbf{Q}) \exp [i\mathbf{Q} \cdot \mathbf{r}_l],$$

and

$$u_L(\mathbf{Q}) = \hat{\mathbf{Q}} \cdot \mathbf{u}(\mathbf{Q}), \quad \mathbf{u}_T(\mathbf{Q}) = \mathbf{u}(\mathbf{Q}) - \hat{\mathbf{Q}} u_L(\mathbf{Q}), \quad \hat{\mathbf{Q}} \equiv \frac{\mathbf{Q}}{|\mathbf{Q}|}.$$

We wish to calculate from the elastic Hamiltonian 4.16 the displacement correlation function, in the more general case we have

$$B(\mathbf{r}) \equiv \langle [\mathbf{u}(\mathbf{r}) - \mathbf{u}(o)]^2 \rangle = \frac{2}{N} \sum_{\mathbf{Q}} \langle |\mathbf{u}(\mathbf{Q})|^2 \rangle [1 - \cos(\mathbf{Q} \cdot \mathbf{r})]. \quad (4.17)$$

Note that $B(\mathbf{r})$ also controls the static structure factor $S(\mathbf{q})$ (eqn.4.3).

Using the equipartition theorem one readily shows from eqn. 4.16 that [34]

$$\langle u_\alpha(\mathbf{Q}) u_\beta(-\mathbf{Q}) \rangle = \frac{k_B T}{\lambda + 2\mu - P} \frac{\hat{Q}_\alpha \hat{Q}_\beta}{Q^2} + \frac{k_B T}{\mu - P} \frac{(\delta_{\alpha\beta} - \hat{Q}_\alpha \hat{Q}_\beta)}{Q^2}, \quad (4.18)$$

where α and β denote Cartesian components. Here we shall focus on the $B(y)$ in eqn. 4.15 that is the displacements correlation function of y -components and consider also a distance \mathbf{r} along the y -direction, to find

$$B(y) = \langle [u_y(na_0) - u_y(o)]^2 \rangle = \frac{2}{N} \sum_{Q_x} \sum_{Q_y} \langle u_y(\mathbf{Q}) u_y(-\mathbf{Q}) \rangle [1 - \cos(Q_y na_0)], \quad (4.19)$$

where the values Q_x and Q_y over which the sums are extended are determined by the geometry of the considered crystal, and the boundary conditions chosen. We here consider a lattice of size D in the x -direction and size L in the y -direction, and choose periodic boundary conditions. It is convenient to measure the lengths in the y -direction in units of the lattice spacing $a_o \equiv 1$ (fig. 5.1) and in the x -direction in units of $d \equiv a_0\sqrt{3}/2$, the distance between the rows. Then

$$Q_x/\pi = -1, -1 + \frac{2}{D}, -1 + \frac{4}{D}, \dots, 1 - \frac{2}{D}, \quad (4.20)$$

$$Q_y/\pi = -1, -1 + \frac{2}{L}, -1 + \frac{4}{L}, \dots, 1 - \frac{4}{L}, \quad (4.21)$$

i.e. the Brillouin zone is appropriately discretized (there are L/a_0 discrete values Q_y , etc.), but the center of the Brillouin zone (the point $Q_x = Q_y = 0$) has to be omitted from the summation, since it would yield in eqn. 4.19 a uniform displacement of the whole lattice.

In the next section we will discuss a quantitative comparison of eqn. 4.19 to simulation results. It is preferable to evaluate eqns. 4.19-4.21 numerically. Here we rather discuss an approximate evaluation of eqn. 4.19 which explains the behaviour of the displacements correlation qualitatively.

Considering the limit where both $1 \ll n \ll D$ and $1 \ll n \ll L$ we can approximate the summations by integrals, to obtain ($N = LD$)

$$\begin{aligned} \langle [u_y(n) - u_y(o)]^2 \rangle &\approx 2 \int_{-\pi}^{\pi} \frac{dQ_x}{2\pi} \int_{-\pi}^{\pi} \frac{dQ_y}{2\pi} \frac{1 - \cos(Q_y n)}{Q_x^2 + Q_y^2} \cdot \\ &\cdot \left[\frac{Q_y^2}{Q_x^2 + Q_y^2} \frac{k_B T}{\lambda + 2\mu - P} + \right. \\ &\left. + \frac{Q_x^2}{Q_x^2 + Q_y^2} \frac{k_B T}{\mu - P} \right]. \end{aligned} \quad (4.22)$$

One can show that for the considered limit the integral has, as expected,

a logarithmic variation in n , similar to the simpler integral², where g is a constant,

$$\begin{aligned} I &= \frac{2k_B T}{g} \int_{-\pi}^{\pi} \frac{dQ_x}{2\pi} \int_{\pi}^{\pi} \frac{dQ_y}{2\pi} \frac{1 - \cos(Q_y n)}{Q_x^2 + Q_y^2} \\ &= \frac{k_B T}{2g} \int_{-\pi}^{\pi} \frac{dQ_x}{2\pi Q_x} [1 - \exp(Q_x n)] \approx \frac{k_B T}{2\pi g} \ln n. \end{aligned} \quad (4.23)$$

This logarithmic divergence of the correlation function of the displacements is responsible for the fact that in two-dimensional crystals the delta function singularities of $S(\mathbf{q})$ at the Bragg spots are replaced by power law singularities, as it's well known [40, 47].

On the other hand, a different result is obtained if we consider a very elongated system, $D \ll n \ll L$. Then it is still appropriate to transform $(1/L) \sum_{Q_y}(\dots)$ into $\int dQ_y/2\pi(\dots)$ but keep the sum over Q_x discrete. This yields to an expression of the type

$$\langle [u_y(n) - u_y(o)]^2 \rangle \approx \frac{2k_B T}{g} \frac{1}{D} \sum_{Q_x} \int_{\pi}^{\pi} \frac{dQ_y}{2\pi} \frac{1 - \cos(Q_y n)}{Q_x^2 + Q_y^2}. \quad (4.24)$$

It is easy to see that the dominating term in eqn. 4.24 comes from a single term in the sum, namely the term with $Q_x = 0$,

$$\langle [u_y(n) - u_y(o)]^2 \rangle \approx \frac{2k_B T}{g} \frac{1}{D} \int_{-\pi}^{\pi} \frac{dQ_y}{2\pi} \frac{1 - \cos(Q_y n)}{Q_y^2}.$$

Transforming the integration from Q_y to $z = Q_y n$ and using [35] $\int_{-\infty}^{\infty} dz (1 - \cos z)/z^2 = \pi$, a linear increase of the displacements correlation results,

$$\langle [u_y(n) - u_y(o)]^2 \rangle \approx \pi \frac{2k_B T}{g} \frac{n}{D}, \quad D \leq n \leq L. \quad (4.25)$$

Comparison of eqn. 4.9 and 4.25 shows that in this limit a crossover to quasi uni-dimensional behaviour has occurred. Equating eqns. 4.23 and 4.25 we can estimate the location of the crossover

$$n_{\text{cross}} \sim D \ln n_{\text{cross}} \sim D \ln D. \quad (4.26)$$

²Here the formula 3.7237 of [35] is used $\int_{-\infty}^{\infty} (x^2 + c^2)^{-1} \{1 - \cos[a(b-x)]\} dx = \pi [1 - \exp(ac) \cos(ab)/c]$.

Defining again the positional correlation length ξ from the condition of the mean square displacement correlation reaches a finite fraction of the square of the lattice spacing, we find a result analogous to eqn. 4.12

$$\xi \approx D \frac{g}{2\pi k_B T} : \quad (4.27)$$

thus ξ diverges in both the limits $D \rightarrow \infty$ and $T \rightarrow 0$. For the eqn. 4.27 there is an analogous result for the two-dimensional XY model, we will discuss these and other analogies in the next chapter.

In the bulk case ($D \rightarrow \infty$) there still is no positional long range order, of course, since logarithmic variation (eqns 4.6 and 4.25) of the mean square displacement correlation has taken over. It is well known that this fact imply also implies that the peak heights of the structure factors in the reciprocal lattice points are not proportional to N , but scale with a sublinear power of N

$$S(\mathbf{G}) \propto N^{1-\text{const}k_B T/g}, \quad (4.28)$$

where the constant in the exponent in eqn. 4.28 can be calculated analytically from the harmonic theory [40, 47, 48]. The consequence of eqn. 4.28 is that at the thermodynamic limit, there is no positional order, while, at low T orientational order is present [39]. We shall return on that in the next chapter.

4.5 Results from the simulations and comparison with the theory

We have evaluated the displacement correlation function $\langle [u_y(n) - u_y(o)]^2 \rangle$, using both the theory of the previous section (eqns. 4.18 and 4.19), with the elastic constants of the bulk crystal as an input and the sum in eqn. 4.19 numerically computed, and directly from the simulations (figs. 4.3 - 4.5). Fig. 4.3 shows that for large enough L the linear relation in eqn. 4.25 is in fact reproduced, in the limit $D \ll n \ll L$. However, when n becomes of the order $n \approx 2D$ or smaller, deviations set in (due to the crossover towards the logarithmic behaviour, eqn. 4.23), while for $n \approx L/4$ deviations set in due to the symmetry of the periodic boundary conditions that limit the linear increase implied by eqn. 4.25. In order to test for the initial logarithmic increase of $B(y) = \langle [u_y(n) - u_y(o)]^2 \rangle$ with y , the data for $D = 20$, $L = 500$

of fig. 4.3 are replotted on linear-log scales in fig. 4.4, and data from a direct Monte Carlo simulation of this system are included. One can see that the harmonic theory and the Monte Carlo results are in quantitative agreement, with no adjustable parameters. A similar agreement has also been found in studies of the low temperature phase of the XY model [50, 51] which can be considered a simpler reference system for our problem. From this work [50, 51] it is also clear that this agreement breaks down near the Kosterlitz-Thouless transition [52] (due to vortex pair formation the spin wave stiffness of the XY model gets renormalized), and similarly we expect that the agreement seen in fig. 4.4 gets worse when the melting transition is approached: we expect that the elastic constants get renormalized due to dislocation-pair formation [47, 48, 53, 55, 56, 57]. Although it would be very interesting to study our model at temperatures closer to the melting transition, we have not attempted to do this due to the enormous difficulties of obtaining well equilibrated simulation data. Already at $T = 1$ for $y > 50$ fig. 4.4 displays huge statistical errors, in spite of a run that lasted for many weeks at a Pentium 4 processor. Therefore it is likely that there is no systematic discrepancy between the harmonic theory and the Monte Carlo results even for $y = L/2 = 250$. Anyway one can see that for $y > 40$ the increase of $B(y)$ with y is stronger than the initial logarithmic behaviour. However from fig. 4.3 it is clear that the linear behaviour according to eqn. 4.25 cannot really be seen, because the effects due to the periodic boundary conditions start rather early.

Fig.4.5 compares now results for the harmonic theory (eqns.4.18 - 4.19) with Monte Carlo results for the case $D = 20$, $L = 100$, including also data for a system with planar walls, for the layers closest to the walls. In this case there seems to be some systematic discrepancy between the Monte Carlo data and the harmonic theory, but the general trend is similar. We have seen before that the periodic boundary conditions start to be felt at $n \approx L/4$ already, no trace of $B(y)$ increasing with y stronger than logarithmic is seen in this case. An interesting feature however, is the faster increase of the displacements correlation function of particles adjacent to a wall, for a system of the same linear dimensions ($D = 20$, $L = 100$) but with two planar walls along the y -axis rather than periodic boundary conditions. Unfortunately the mild curvature of the data in fig 4.5 (due to the periodic boundary conditions in the y -direction which are strongly felt for $y > 25$) prevents

us from making precise statements about the relation between the slope in the relations $B(y) \propto \ln y$ for a two dimensional crystal surface adjacent to a flat wall, and in the bulk respectively. This comparison is of interest since similar calculations can be done in the XY model (they will be discussed in chap. 5). From those calculations one would expect that the slope of the relation $B(y) \propto \ln y$ for a row adjacent to the wall is twice as larger as the slope in the bulk.

Figs. 4.3 - 4.5 emphasize the aspect that a crystal in two dimensions is a critical system, as far as positional long range order is concerned. The instability of this order, evidenced by the growth of the displacement correlation function with distance, is enhanced by flat walls boundary conditions, similar to an XY model with free surfaces. This enhancement of fluctuations at the free surface (or flat wall, respectively) is felt over very large distances in the x -direction, where also an anomalous enhancement of the fluctuations exists. Presumably, these long range effects of free surfaces are responsible for the difference between $C_{33}(n)$ for thin strips of n layers bounded by flat walls, and the corresponding systems with periodic boundary conditions in all directions.

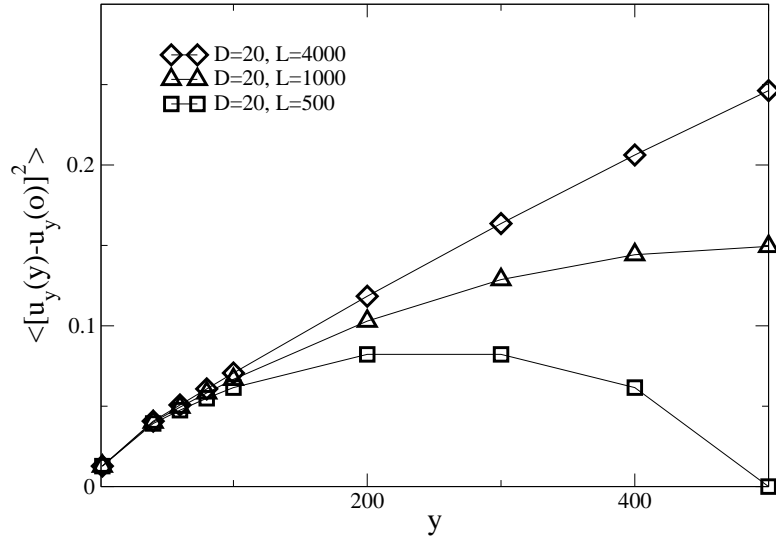


Figure 4.3: Displacement correlation function $B(y) = \langle [u_y(n) - u_y(o)]^2 \rangle$ plotted vs. y , calculated according to eqns. 4.18 - 4.21 for $L \times D$ systems with $D = 20$ and $L = 500, 1000, 4000$, as indicated in the figure. Periodic boundary conditions are used in both x and y directions. As input parameters, the Lamé coefficients $\lambda = 42$, $\mu = 41$ and the hydrostatic pressure $P = 17.4$ (all these parameters are quoted in units of $k_B T / \sigma^2$) are taken, as obtained from the Monte Carlo simulation of the model, 2.1 at $T = 1$ in the bulk. Note that $B(y)$ exhibits the symmetry $B(y) = B(L - y)$ due to the periodic boundary conditions

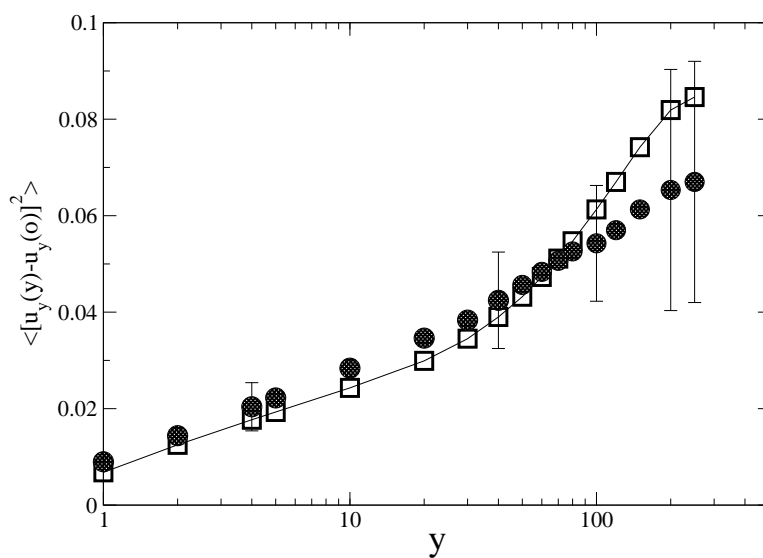


Figure 4.4: Comparison of $B(y)$ according to the harmonic theory (squares) with corresponding Monte Carlo data (full dots with error bars) for a system with linear dimensions $D = 20$, $L = 500$, and periodic boundary conditions. Note the linear scale of the ordinate, while the abscissa is logarithmic.

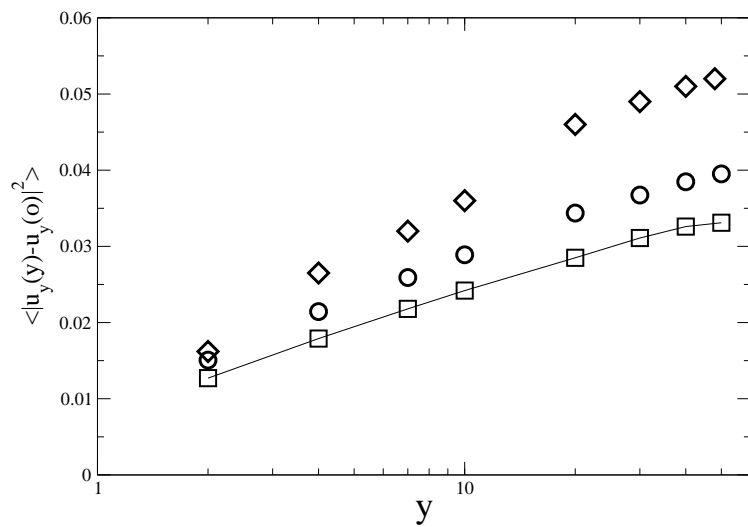


Figure 4.5: Comparison of $B(y)$ according to the harmonic theory (squares) with corresponding Monte Carlo data (open circles), for a system with linear dimensions $D = 20$, $L = 100$, and periodic boundary conditions. The diamonds show corresponding Monte Carlo data for a system with planar walls, using only displacements of particles in the rows adjacent to the walls.

Chapter 5

Confinement induced order

5.1 Order in a two-dimensional system

In the previous chapter we pointed out and studied the one-dimensional features of our systems when they appeared. However, due to the presence of a second dimension (although confined), our systems have also two-dimensional aspects. This kind of systems can be considered, so to say, in between those two dimensionalities. So now we turn our attention on the two-dimensional features of these systems.

When we want to describe ordering in $d = 2$ we must consider both positional order and bond orientational order [39, 45, 47, 48, 55, 53, 56, 57]. The average positional long range order can be studied most conveniently considering the order parameter components, see fig. 5.1

$$\Psi_{\mathbf{G}_0} = \frac{1}{N} \left| \sum_{l=1}^N \exp [i\mathbf{G}_0 \cdot \mathbf{R}_l] \right|, \quad (5.1)$$

$$\Psi_{\mathbf{G}_1} = \frac{1}{N} \left| \sum_{l=1}^N \exp [i\mathbf{G}_1 \cdot \mathbf{R}_l] \right|, \quad (5.2)$$

where \mathbf{r}_l is the position of the l 'th particle and \mathbf{G}_0 and \mathbf{G}_1 are two vectors of the reciprocal lattice. From the simulation, the full distribution function $P[\Psi_{\mathbf{G}_0}, \Psi_{\mathbf{G}_1}]$ is accessible. Note that the static structure factor in eqn. 4.1 has peaks at the reciprocal lattice spots, and the maximum values of $S(\mathbf{q})$ at these peaks positions are simply related to the second moment of the order

parameter distribution, e.g.

$$S(\mathbf{G}_0) = N\langle\Psi_{\mathbf{G}_0}^2\rangle, \quad S(\mathbf{G}_1) = N\langle\Psi_{\mathbf{G}_1}^2\rangle. \quad (5.3)$$

The local orientational order parameter $\Psi_6(k)$ is defined as [34, 39, 47, 55, 53, 56, 57], see fig. 5.1

$$\Psi_6(k) = \frac{1}{6} \sum_{j \in \text{n.n. of } k} \exp(6i\phi_{jk}), \quad (5.4)$$

where the 6 in the argument of the exponential function expresses the fact that in the ideal triangular structure the angles ϕ_{jk} 's of a considered particle can differ only by multiples of $2\pi/6$. The average orientational order parameter $\overline{\Psi}_6$ and its correlation function $g_6(\mathbf{R})$ then become

$$\overline{\Psi}_6 = \frac{1}{N} \langle |\sum_{l=1}^N \Psi_6(l)| \rangle, \quad g_6(\mathbf{R}) = \langle |\Psi_6(k)\Psi_6(k')| \rangle, \quad (5.5)$$

where $\mathbf{R} = \mathbf{R}_k - \mathbf{R}_{k'}$. Note that $g_6(\mathbf{R} \rightarrow \infty) = \overline{\Psi}_6^2$ if orientational long range order exists.

Clearly the possibility of defining such an order parameter like the orientational one as in eqns. 5.5 comes from the two-dimensional topology. However this orientational order plays a crucial role in describing the melting in $2d$.

According to the theory proposed by Halperin, Nelson and Young [47, 48, 53, 56, 57] melting in two dimensions can occur via two continuous transitions (at densities ρ_l and ρ_s) with corresponding pressures p_l and $p_s > p_l$, rather than via a single first order transition at pressure p_t (where a fluid of density ρ'_l and a solid of density ρ'_s will coexist): see fig. 5.2. Both in the fluid phase and in the hexatic phase, $\overline{\Psi}_6 = 0$, but the behaviours of $g_6(\mathbf{R})$ are different: in the fluid one finds an exponential decay, while there is a power-law decay in the hexatic phase :

$$g_6(\mathbf{R} \rightarrow \infty) \propto \exp(-r/\xi), \quad \rho < \rho_l, \quad (5.6)$$

$$g_6(\mathbf{R} \rightarrow \infty) \propto r^{-\eta}, \quad \rho_l < \rho < \rho_s, \quad (5.7)$$

and the correlation length ξ of the bond orientational order diverges as ρ_l is approached, as does the bond orientational susceptibility $\chi \equiv \int d\mathbf{R} g_6(\mathbf{R})$

[47, 48, 52, 53, 55, 56, 57]:

$$\ln \xi \propto \ln \chi \propto (\rho_l - \rho)^{-1/2}. \quad (5.8)$$

Conversely if one has a first order transition, both ξ and χ stay finite at ρ'_s and a nonzero order parameter $\overline{\Psi}_6$ has already started to increase at ρ'_l while according to the Kosterlitz, Thouless, Halperin, Nelson and Young (KTHNY) scenario, $\overline{\Psi}_6$ is nonzero for $\rho > \rho_s$ only.

The mechanism of these continuous phase transitions is the unbinding of topological defects. just as in the two-dimensional XY ferromagnet or planar rotor model where vortex-antivortex unbinding occurs [47, 48, 52, 53, 55], the transition from the solid to the hexatic phase is driven by the unbinding of dislocations pairs with oppositely oriented Burgers vectors. While a free dislocation would have an infinitely long extra half-row of atoms, such a dislocation pair at finite distance involves a finite number of atoms, so this excitation has a finite energy and can occur in the crystal in thermal equilibrium. The hexatic phase melts via disclination pair unbinding.

We conclude this section pointing out that evidence from numerical simulations and experiments for the existence of the hexatic phase is scarce.

In particular from the simulational point of view studying the KTHNY scenario, already in the bulk case, requires a lot of efforts. The reason is that in order to have statistically significant data, one requires configurations where a series of well equilibrated dislocation pairs are present, but such dislocations pairs spans on many lattice sites and involve many particles while on the other hand we want to go near the transition point and so big finite size corrections together with critical slowing down are expected.

In the sec. 2.5 we mentioned that a way of partly overcoming these problems is to artificially prevent the crystal from melting also near the transition points. From the count of the rejected moves leading to a dislocation pair, one can estimate the probability of having such a dislocation. Such a probability together with the elastic constants of the defect-free solid can be then used as an input in the renormalization group flow equations of the KTHNY theory (see [28, 29] for the case of hard disks) . In this way all the quantities of interest can be evaluated also near the critical region. However with this technique it was not possible to reach conclusive results ruling out the possibility of a weak first order phase transition preceding the KHTNY melting

scenario.

5.2 Ordering and surfaces

The effect of external walls (and/or free surfaces respectively) on phase behaviours has been studied for a long time [58, 59, 60, 61, 62, 63, 45, 49, 50, 51]. We here want to recall briefly the simplest case, a system undergoing a second-order phase transition in the bulk from a disordered state to an ordered state with one-component order parameter (e.g. an Ising ferromagnet, fig. 5.3). One must distinguish between boundary conditions at the wall providing a linear coupling to the order parameter (“surface magnetic field” H_1 in the case of a ferromagnet) and a quadratic coupling (as it occurs in ferromagnets where missing neighbors imply that the spins in the surface plane experience less exchange interactions to neighboring spins than the spins in the bulk). In both cases the range over which the order near the surface is either enhanced or reduced is of the order of the correlation length ξ_b of order parameter fluctuations in the bulk. At the critical temperature T_c of the second order transition where ξ_b has diverged to infinity, the exponential decay towards the bulk has been replaced by a power-law behavior (fig. 5.3b). Note that in fig. 5.3 we have only considered the case that the field H_1 at the surface acts in the same direction as the order parameter Ψ_b in the bulk (fig. 5.3c). The case that the field at the surface acts in the direction opposite to the order parameter in the bulk is also of great interest, it may lead to the formation of (ideally macroscopically thick) “wetting layers” [59, 60, 61, 62, 63, 45], but this phenomenon is not under consideration here.

Fig. 5.3 is not the whole story, of course, since at a phase transition it is also of interest to consider the correlation function $G(\mathbf{r}_1, \mathbf{r}_2) = \langle \Psi(\mathbf{r}_1)\Psi(\mathbf{r}_2) \rangle$ of the local order parameter $\Psi(\mathbf{r}) = \Psi(\mathbf{s}, z)$, \mathbf{s} being the set of $d - 1$ dimensional coordinates parallel to the surface. Since translational invariance is only broken in the z -direction normal to the wall, we can choose $\mathbf{s}_1 = 0$, $\mathbf{s}_2 = \mathbf{s}$, to redefine the correlation function as $G(\mathbf{r}_1, \mathbf{r}_2) \equiv g(\mathbf{s}, z_1, z_2)$. While it turns out [58, 59, 60] that the decay of g for $T > T_c$ is always given by an exponential decay, $g \propto \exp(-|\mathbf{r}_1 - \mathbf{r}_2|/\xi_b)$ and for $T \rightarrow T_c$ the decay length ξ_b does not depend on the direction of $\mathbf{r}_1 - \mathbf{r}_2$, the power law at T_c does

depend on the direction,

$$g(\mathbf{s}, z_1, z_2) \propto s^{-(d-2+\eta_{\parallel})}, \quad z_1, z_2 \text{ finite}, s \rightarrow \infty \quad (5.9)$$

$$g(\mathbf{s}, z_1, z_2) \propto |z_1 - z_2|^{-(d-2+\eta_{\perp})}, \quad s, z_1, \text{ finite}, z_2 \rightarrow \infty. \quad (5.10)$$

The exponents η_{\parallel} and η_{\perp} differ also from the exponent encountered in the bulk, $G(\mathbf{r}_1, \mathbf{r}_2) \propto |\mathbf{r}_1 - \mathbf{r}_2|^{-(d-2+\eta)}$.

All the above results apply only for a semi-infinite geometry, and it is also of interest to ask what happens when one considers instead a thin film of a large but finite thickness D . Then the correlation length can grow towards infinity only in the $d-1$ directions parallel to the confining walls. As a result, a crossover from d dimensional critical behavior to $d-1$ dimensional critical behavior sets in at a temperature near T_c when ξ_b has grown to about the distance D between the walls. At a (shifted) transition temperature $T_c(D)$, a second order transition with $d-1$ -dimensional critical behaviour occurs, if $d > 2$. In the case $d = 2$, however, $T_c(D) = 0$, since $d-1 = 1$ then coincides with the lower critical dimension. The correlation length $\xi(T)$ grows as $\xi(T) \propto (T - T_c(\infty))^{-\nu}$ (with $\nu = 1$ [64]) until $\xi(T)$ becomes of the order of D , and then a crossover sets in to a behaviour [65] $\xi(T) \propto D \exp[(\sigma/k_B T)D]$, σ being the interfacial tension between coexisting phases in $d = 2$. Note that for the XY model, however, $d = 2$ is the lower critical dimension [52, 54, 48, 66, 67], and then $\xi(T)$ grows as $\xi(T) \propto \exp[\text{const}(T - T_c(\infty))^{-1/2}]$ until $\xi(T)$ becomes of the order of D , and then a crossover sets in to [68]

$$\xi(T) = 2\Gamma(T)D/k_B T = D/[\pi\eta(T)], \quad (5.11)$$

$\Gamma(T)$ being the helicity modulus of the $d = 2$ bulk XY model, and $\eta(T)$ describes the decay of the spin-spin correlation function of the XY-model in $d = 2$ at all temperatures in the low-temperature phase (recall that $\Psi_b \equiv 0$ in this model).

As a result, subtle crossovers occur in the correlation functions in thin films near the critical point T_c of the bulk system (and below it). In an Ising system, eqn. 5.9 is expected to hold near T_c only for $s < \xi(T) \propto D$, while for $s > \xi(T)$ an exponential decay proportional to $\exp[-s/\xi(T)]$ occurs. For $T < T_c$, we have $g \approx \Psi_b^2$ for $s < \xi(T)$, while for $s > \xi(T)$ the same exponential decay occurs (but now $\xi(T)$ can be extremely large, due to the exponential dependence of $\xi(T)$ on D , as noted above). In the

XY model, however, we expect a power law decay of g with s for $s < D$ for all temperatures below T_c , and for $s > D$ an exponential decay $\exp[-\rho/\xi(T)]$ with $\xi(T)$ being given by eqn. 5.11 takes over.

We have emphasized again here the behaviour of the $d = 2$ XY model. As already shown in the previous section there are close analogies between the ordering in that model and the behaviour of positional order in $d = 2$ crystals. The analysis of the XY model will continue in the following section as well. This will help us in having a qualitative understanding of our systems.

5.3 The case of the partially confined XY model as simpler theoretical background

When we consider a confined system the behavior near the wall will again depend very much on the nature of the boundary condition provided by the wall.

With respect to positional order in the x-direction normal to the walls, both types of boundary conditions at the walls, the flat structureless walls and the structured ones, act like an ordering field does in the case of magnetic systems (fig. 5.3). Consequently, we expect that the density distribution $\rho(x)$ will be non-uniform near $x = x_{\text{wall}} = 0$ also in the fluid phase, and show a periodic modulation with a period close to $a_0\sqrt{3}/2$ which decays over a distance of order $\xi(T)$, the positional correlation length. Also with respect to the orientational order Ψ_6 , both types of walls clearly act like ordering fields, and so one expects that $\overline{\Psi}_6(x) \propto \exp[-x/\xi_6(T)]$ also in the fluid phase of a semiinfinite system. In a thin film confined between two parallel walls a finite distance apart, due to the combined effect of both walls some nonzero average order parameter $\overline{\Psi}_6(T)$ in the thin film hence will be present at all temperatures, also in the fluid phase. In the solid phase, of course, the situation will rather resemble fig. 5.3c, i.e. $\Psi_6(x) - \overline{\Psi}_6(T) \propto \exp[-x/\xi_6(T)]$, for x near the wall with $x_{\text{wall}} = 0$.

However, as we have seen in sec. 4.3 the situation is quite different with respect to the positional order in the y-direction parallel to the wall. The boundary condition provided by the structured wall also can be considered as a kind of field conjugate to the positional order, due to the commensurate corrugation of this potential in the y -direction. So for x near x_{wall} also nonzero order parameters $\Psi_{\mathbf{G}_0}(x)$, $\Psi_{\mathbf{G}_1}(x)$ will be induced due to the re-

sponse of the system to these local ordering fields, and this crystalline local order will decay towards zero proportional to $\exp[-x/\xi(T)]$, in a semi-infinite system in its fluid phase. In its crystalline phase, however, true crystalline long range order with nonzero order parameters $\Psi_{\mathbf{G}_0}$, $\Psi_{\mathbf{G}_1}$ does not exist, as noted in sec. 4.2, and we rather expect a power law decay of the surface-induced crystalline order, similar to the case of fig. 5.3b. The situation is rather analogous to the two-dimensional XY model for temperatures below the Kosterlitz-Thouless transition [52, 54, 66, 67, 69, 70] in a local surface magnetic field H_1 [49, 50, 51]. In fact, at low temperatures the Hamiltonian of the XY model can be reduced to a harmonic form (J is the exchange constant) and (for $H_1 = 0$)

$$\mathcal{H}_{XY} = -J \sum_{\langle l,j \rangle} \cos(\theta_l - \theta_j) \approx \frac{1}{2} J \sum_{\langle l,j \rangle} (\theta_l - \theta_j)^2, \quad (5.12)$$

where an unimportant constant was omitted. The spin-spin correlation function in this spin-wave regime can then be written (cfr. the analogy with the displacement correlation function)

$$\langle \mathbf{S}_0 \cdot \mathbf{S}_{\mathbf{r}} \rangle = \langle \cos(\theta_0 - \theta_{\mathbf{r}}) \rangle = \exp\left[-\frac{1}{2} \langle (\theta_0 - \theta_{\mathbf{r}})^2 \rangle\right]. \quad (5.13)$$

Thus one finds in the bulk that [52, 54, 48, 66, 67]

$$\langle (\theta_0 - \theta_{\mathbf{r}})^2 \rangle \approx \frac{k_B T}{2\pi J} \ln(\pi r/a_0), \quad (5.14)$$

and hence the spin-spin correlation function exhibits the well known power law decay

$$\langle \cos(\theta_0 - \theta_{\mathbf{r}}) \rangle \approx \left(\frac{\pi r}{a_0}\right)^{-k_B T/(2\pi J)}. \quad (5.15)$$

Surface effects on the decay of correlations of a two-dimensional Gaussian model have been analyzed by Cardy [71]. In the framework of a continuum approximation, the harmonic Hamiltonian eqn. 5.12 becomes

$$\mathcal{H}_{XY} = \frac{1}{2} J \int_{x>0} [\nabla\theta(\mathbf{r})]^2 dx dy, \quad \mathbf{r} = (x, y) \quad (5.16)$$

where a free surface at $x = 0$ is assumed for an otherwise semi infinite system. Due to the free surface, translational invariance of the correlation function $\langle e^{i\theta(\mathbf{r}_1)} e^{-i\theta(\mathbf{r}_2)} \rangle$ of the order parameter $e^{i\theta(\mathbf{r})}$ is broken, but due to

the Gaussian character of the Hamiltonian, eqn. 5.16, we still have

$$\begin{aligned}\langle e^{i\theta(\mathbf{r}_1)} e^{-i\theta(\mathbf{r}_2)} \rangle &= \exp \left\{ -\frac{1}{2} \langle [\theta(\mathbf{r}_1) - \theta(\mathbf{r}_2)]^2 \rangle \right\} = \\ &= \exp \left[G(\mathbf{r}_1, \mathbf{r}_2) - \frac{1}{2} G(\mathbf{r}_1, \mathbf{r}_1) - \frac{1}{2} G(\mathbf{r}_2, \mathbf{r}_2) \right],\end{aligned}\quad (5.17)$$

where $G(\mathbf{r}_1, \mathbf{r}_2) = \langle \theta(\mathbf{r}_1) \theta(\mathbf{r}_2) \rangle$. In the continuum, a free surface with no surface fields can be described by a Von Neumann boundary condition

$$\left. \frac{\partial G(\mathbf{r}_1, \mathbf{r}_2)}{\partial x_1} \right|_{x_1=0} = 0, \quad (5.18)$$

and this condition can be automatically realized by writing

$$G(\mathbf{r}_1, \mathbf{r}_2) = G_\infty(\mathbf{r}_1 - \mathbf{r}_2) + G_\infty(\mathbf{r}_1 - \mathbf{r}'_2),$$

where $G_\infty(\mathbf{r}) = G_\infty(\mathbf{r}_1, \mathbf{r}_2 = \mathbf{r}_1 + \mathbf{r})$ for the fully translationally invariant infinite plane, and \mathbf{r}'_2 is the mirror image of \mathbf{r}_2 with the surface being the symmetry axis (the line $x = 0$). Since $G_\infty(\mathbf{r})$ is (apart from constants) the correlation given in eqn. 5.14, one finds [71]

$$\langle e^{i\theta(\mathbf{r}_1)} e^{-i\theta(\mathbf{r}_2)} \rangle \propto \left[\frac{|\mathbf{r}_1 - \mathbf{r}'_1| |\mathbf{r}_2 - \mathbf{r}'_2|}{|\mathbf{r}_1 - \mathbf{r}_2|^2 |\mathbf{r}_1 - \mathbf{r}'_2|^2} \right], \quad (5.19)$$

with

$$\eta = \frac{k_B T}{2\pi J}. \quad (5.20)$$

If both sites $\mathbf{r}_1, \mathbf{r}_2$ are in the bulk, far away from the surface, we have $|\mathbf{r}_1| \rightarrow \infty, |\mathbf{r}_2| \rightarrow \infty$, and then $|\mathbf{r}_1 - \mathbf{r}'_1| \approx |\mathbf{r}_2 - \mathbf{r}'_2| \approx |\mathbf{r}_1 - \mathbf{r}'_2|$, for any large but finite $|\mathbf{r}_1 - \mathbf{r}_2|$. Then eqn. 5.19 reduces to eqn. 5.15, as it should be.

If site 1 is close to the surface, $\mathbf{r}_1 = (a_0, y)$, we have $|\mathbf{r}_1 - \mathbf{r}'_1| = 2a_0$, while $|\mathbf{r}_2 - \mathbf{r}'_2| = 2x$ if the site $\mathbf{r}_2 = (x, y)$ is deep in the bulk. Then

$$\langle e^{i\theta(\mathbf{r}_1)} e^{-i\theta(\mathbf{r}_2)} \rangle \approx \left[\frac{4a_0 x}{x^4} \right]^{\eta/2} \propto x^{-3\eta/2} \implies \eta_\perp = \frac{3\eta}{2}. \quad (5.21)$$

The result $\eta_\perp = 3\eta/2 = 3k_B T / (4\pi J)$ does not seem to be discussed in the literature [51, 71], while the case that both \mathbf{r}_1 and \mathbf{r}_2 are near the surface has been again analyzed. Then $\mathbf{r}_1 = (a_0, y_1)$ and $\mathbf{r}_2 = (a_0, y_1 + y)$, and eqn. 5.19

implies [71]

$$\langle e^{i\theta(\mathbf{r}_1)} e^{-i\theta(\mathbf{r}_2)} \rangle \approx \left[\frac{4a_0^2}{y^4} \right]^{\eta/2} \propto y^{-2\eta} \implies \eta_{\parallel} = 2\eta. \quad (5.22)$$

Since the low temperature phase of the XY model can be interpreted as a line of critical points, we expect a scaling relation [58, 59] to hold,

$$\eta_{\parallel} = 2\eta_{\perp} - \eta, \quad (5.23)$$

and this relation is indeed satisfied by eqns. 5.21 and 5.22. Based on numerical data, Berche [51] concluded that the relation $\eta_{\parallel} = 2\eta$ holds also outside of the spin wave regime, at all temperatures up to the Kosterlitz-Thouless (KT) transition temperature, where $\eta = 1/4$ [70] and hence $\eta_{\parallel} = 1/2$. Eqn. 5.21 then implies $\eta_{\perp} = 3/8$ at the KT transition.

If now a surface magnetic field is applied, a response of a spin at a site \mathbf{r} deep in the bulk is created. This response decays towards zero according to [58, 59]

$$\langle |\mathbf{S}(\mathbf{r})| \rangle = \langle |\exp[i\theta(\mathbf{r})]| \rangle \propto x^{-\eta/2}, \text{ for } d = 2, \quad (5.24)$$

i.e. the same exponent η that controls also the decay of correlations in the bulk controls also the order parameter profile. The correlation function between spins which are both at the surface exhibit then a finite range, however. From the scaling approach to surface critical phenomena [58, 59] one can predict

$$\langle \mathbf{S}_0 \cdot \mathbf{S}_{\mathbf{r}} \rangle - \langle \mathbf{S}_0 \rangle \cdot \langle \mathbf{S}_{\mathbf{r}} \rangle \propto \exp(-y/\xi_{\parallel}), \quad (5.25)$$

with

$$\xi_{\parallel} \propto H_1^{-(1+\eta/2-\eta_{\perp})} = H_1^{-(1-\eta)} \quad (5.26)$$

where in the last step eqn. 5.21 was used. At the KT transition, the exponent describing the divergence of ξ_{\parallel} as $H_1 \rightarrow 0$ becomes $1 - \eta = 3/4$.

Redirecting attention to the harmonic solid, studied in the previous chapter, we emphasize that the case of the planar wall does not involve any "surface field", as far as positional order in the y-direction parallel to the wall is concerned. Since the comparison between eqns. 4.23, 5.14 shows that the quantity $k_B T / (2\pi g)$ plays the same role as the exponent η in the XY model, we conclude that the positional correlations between displacements between

two particles in the surface increase as

$$\langle [u_y(n) - u_y(0)]^2 \rangle \propto \eta_{\parallel} \ln n, \quad (5.27)$$

while the mean square correlation between a particle near the wall and another particle deep in the bulk should behave as

$$\langle [u_y(n) - u_y(0)]^2 \rangle \propto \eta_{\perp} \ln n. \quad (5.28)$$

We suggest that the scaling relation, eqn. 5.23, between the exponents η , η_{\parallel} and η_{\perp} can be carried over to the present case as well.

Finally we have to mention also that according to the KTHNY theory of melting one should also consider in addition to the fluid phase and to the crystalline phase also the hexatic phase.

However although it would be very interesting to study how wall effects show up in the KTHNY scenario of melting, this problem shall not be addressed here, since, as we discussed in sec. 5.1, it still would require a prohibitively large computational effort.

5.4 Order in two-dimensional confined crystals: numerical results

We present here the results coming out from our numerical simulations regarding the order induced by the confinement in our systems (see secs. 2.1 and 2.2) : we looked both at the orientational order and at the positional order (layering) in the x -direction.

Before doing a quantitative analysis we present in fig. 5.4, just in the spirit of fig. 4.2, a series of about 1000 superimposed snapshot pictures of the instantaneous positions of the particles. These plots give a good qualitative insight into the effect of the confining walls on the order of the two dimensional solid. In this case we are at $T = 1.6$ i.e. far above the melting transition of the bulk solid (at the chosen density, $T_{\text{melting}} \cong 1.35$). We can see the density modulation (layering) induced by the walls and the tendency towards the fluid phase as x moves to the values of the center of the box, such a phase, being homogeneous, yields a uniform grey pattern in the bulk. However near the walls we recognize the non uniform density distri-

bution, the density is enhanced in layers parallel to the walls and depleted in between. The effect of the different types of confinement, is visible in the first rows near the wall: while for the case of the flat walls the patterns are strongly elongated and so homogeneous in the y -direction, this does not happen in the case of the structured walls where we see close to the wall, local ordering also in the y -direction. So as already pointed out in the previous chapter we can see already from the snapshot pictures that the walls affect the positional order in the y -direction in different manner, while the mean-square displacement of the particles away from the lattice positions of the ideal crystal structure is uniformly smaller for the particles close to a structured wall, there is a pronounced anisotropy of fluctuations close to a planar wall.

We have studied the layering phenomena in the strips by recording the average density profiles in x -direction (figs. 5.5, 5.6 and 5.7). Since $\rho(x)$ exhibits the symmetry $\rho(x) = \rho(D - x)$, only the left half of the strip is shown. For low temperatures, such as $T = 1$, we see that the layering effect [enhancement of $\rho(x)$ around the ideal positions of the lattice rows] is visible over a few layers only (five layers in the case of $T = 1$), and then the bulk behavior is reached. Approaching the melting transition from the opposite side, however, we see a somewhat larger range over which layering can be observed. While for $T = 1.8$ (and higher) for $10 \leq x \leq 20$ the density is uniform in the thin strips and agrees with the density in the bulk, irrespective of the boundary conditions at the wall, already for $T = 1.6$ a weak density modulation is still left even in the center of the strip. Thus the increasing range of the layering effect as one approaches the melting temperature T_{melting} from above reflects the existence of an increasing correlation length ξ of positional order. As is well known, ξ remains finite at T_{melting} if the transition is first order, while ξ should diverge to infinity at the transition from the hexatic phase to the crystal, if the KTHNY scenario of two-dimensional melting applies [52, 54, 48, 55, 53, 47, 56, 57]. In principle, one could try to use the layering phenomenon due to walls to extract information on ξ . In practice, this is rather difficult in the transition region since the finite strip width D causes important finite size effects. This is demonstrated in fig. 5.7(top), where data for $T = 1.4$ are shown: Using data only for $n_x = 30$ well-defined ordering in a layered structure is enforced over the entire strip, while the bulk at $T = 1.4$ clearly has melted, and the bulk

density distribution already is uniform. A comparison with corresponding data for $n_x = 60$ (fig. 5.7, bottom) shows, however, that now the strip is disordered in its center, and also the amount of layering near the walls is systematically smaller than was found for $n_x = 30$. As a consequence, a reliable estimation of ξ for T near T_{melting} would require a systematic variation of the strip width $D = n_x a \sqrt{3}/2$ over a wide range, in order to be able to extrapolate the results towards $D \rightarrow \infty$. As already pointed out, the huge computer resources required to do this have prevented us from carrying out such a systematic study of two-dimensional melting via surface effects. A naive fit of the density differences $\rho(x_{\text{max}}) - \rho$ at the maxima positions x_{max} in the range $3 \leq 27$ to a function like

$$f(x) \propto \exp(-x/\xi) + \exp[(D-x)/\xi], \quad (5.29)$$

yields the data shown in fig 5.8. In principle, we expect that ξ should not depend on the type of boundary condition at the wall: only the prefactor of the above function should. This expectation is borne out for $T = 2$ and $T = 1.8$, within the statistical errors. while for $T \leq 1.6$ the results for the case of structured walls are slightly but systematically larger. Presumably this effect is due to a nonlinear response of the density distribution $\rho(x)$ to the perturbing “field” created by the walls, which is expected for x close to both walls.

This problem can be avoided by restricting the fit to the inner region of the strip, where the density oscillations around the average density are small enough (figs. 5.5, 5.6 and 5.7) so that such nonlinear effects are negligible, but then the problem is that due to the statistical noise of the data the statistical errors of ξ become much larger.

We now turn to the behaviour of the local orientational order parameter $\langle |\Psi_6(x)|^2 \rangle$, fig. 5.9. As expected on theoretical grounds (see the discussion of sec. 5.2), we see that both boundary conditions enhance the orientational order near the walls in a similar manner. While for $T < T_{\text{melting}}$ a clearly developed flat plateau is observed for $10 \leq x \leq 20$, for $T > T_{\text{melting}}$ the residual order parameter near the center of the film is not constant over an extended region of x . Thus, the fact that $\langle |\Psi_6(x)|^2 \rangle$ is still nonzero everywhere in the thin strip even at temperatures far above T_{melting} again is clearly a finite-size effect! Consequently, plotting $\langle |\Psi_6(x = D/2)|^2 \rangle$ vs. T

(fig. 5.10 top) the melting transition does not show a clear vanishing of this mean square order parameter, but near $T = T_{\text{melting}}$ there is a mild inflection point in the curves, and for $T > T_{\text{melting}}$ one finds the “finite size tails” well known from simulation studies of other phase transitions, too [72, 73].

Again one can associate a correlation length ξ (which should be twice the correlation length ξ_6 defined in sec. 5.2, since we deal with the order parameter square), fitting the data again to a function of the type $A\{\exp(-x/\xi) + \exp[(D-x)/\xi]\}$, where A is an amplitude factor depending on the type of boundary condition. Fig. 5.11 shows that this correlation length also is very small at high temperatures, and increases slightly faster than the positional correlation length does (fig. 5.8).

The last thing we want to show here is an analysis of the orientational correlation function $g_6(\mathbf{r})$ {eqn. 5.5}. However, while this correlation function is translationally invariant in the bulk, in a system with walls such a translational invariance holds in y direction only. We here hence restrict attention to the behavior of the decay of this correlation in y -direction for different distances x of both sites from the wall,

$$g_6(x, y) = \langle \Psi_6(x, 0) \Psi_6(x, y) \rangle. \quad (5.30)$$

Figs. 5.12 and 5.13 give a global view of this function for three temperatures. One can clearly see that near the walls there is very little y -dependence at all temperatures, due to the high degree of orientational order enforced at the walls. In the center of the strip, there is again little variation at low temperatures $T = 1$, where the system everywhere is well ordered, and at high temperatures $T = 1.8$, where the system in the center is almost disordered. In contrast, close to the transition (e.g. for $T = 1.4$) a slow variation of $g(x, y)$ with both x and y is observed. Due to the residual order which occurs in $g(x, y)$ for large distances, apart from the limiting case of very large D and correspondingly large enough x in the middle of the strip, we have not succeeded in a convincing quantitatively reliable analysis of the functional variation of $g(x, y)$. This problem hence must be left to future work.

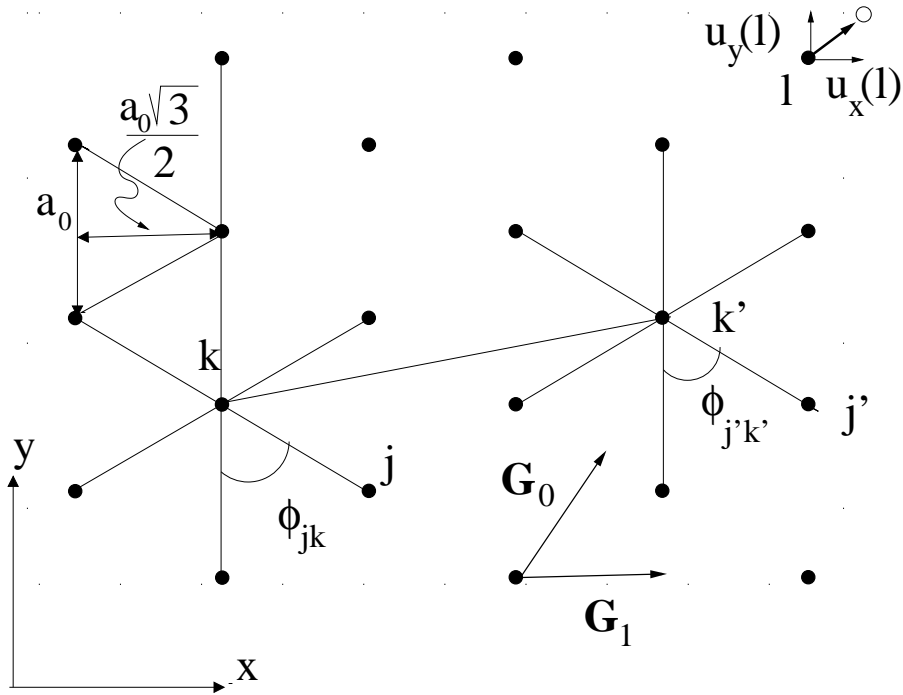


Figure 5.1: Geometry of the triangular lattice: the y -axis is oriented along a nearest neighbour direction, the x -axis perpendicular to it. The lattice spacing is denoted as a_0 , and hence neighbouring rows of particles along the x -axis are at distance $a_0\sqrt{3}/2$. The angle between a bond connecting particles k and j and a reference direction (the y -direction in the figure) is denoted as ϕ_{jk} . The basic vectors of the reciprocal lattice are denoted as \mathbf{G}_0 and \mathbf{G}_1 . The displacement $\mathbf{u}(l)$ of the l 'th particle from its ideal lattice position is decomposed in Cartesian coordinates $u_x(l)$ and $u_y(l)$.

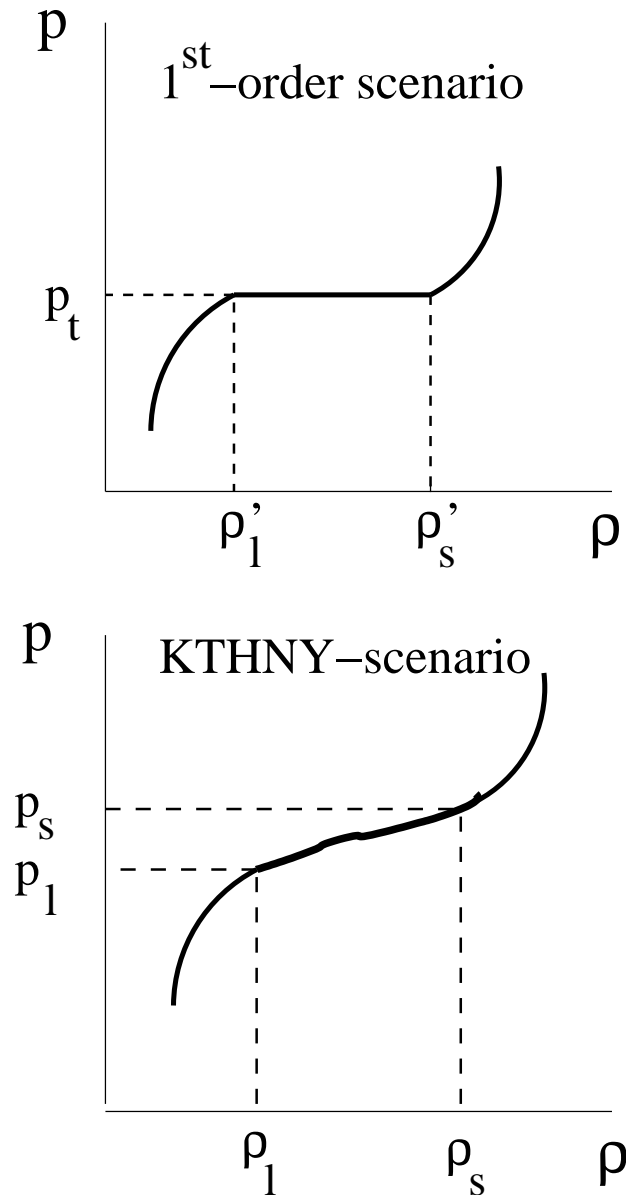


Figure 5.2: Qualitative isotherms where the pressure p is plotted versus density ρ , for the case of a first order transition (upper part) and according to the KTHNY theory (lower part) [29]. Note that in the case of soft disks one can equivalently consider the variation of the pressure with temperature rather than density

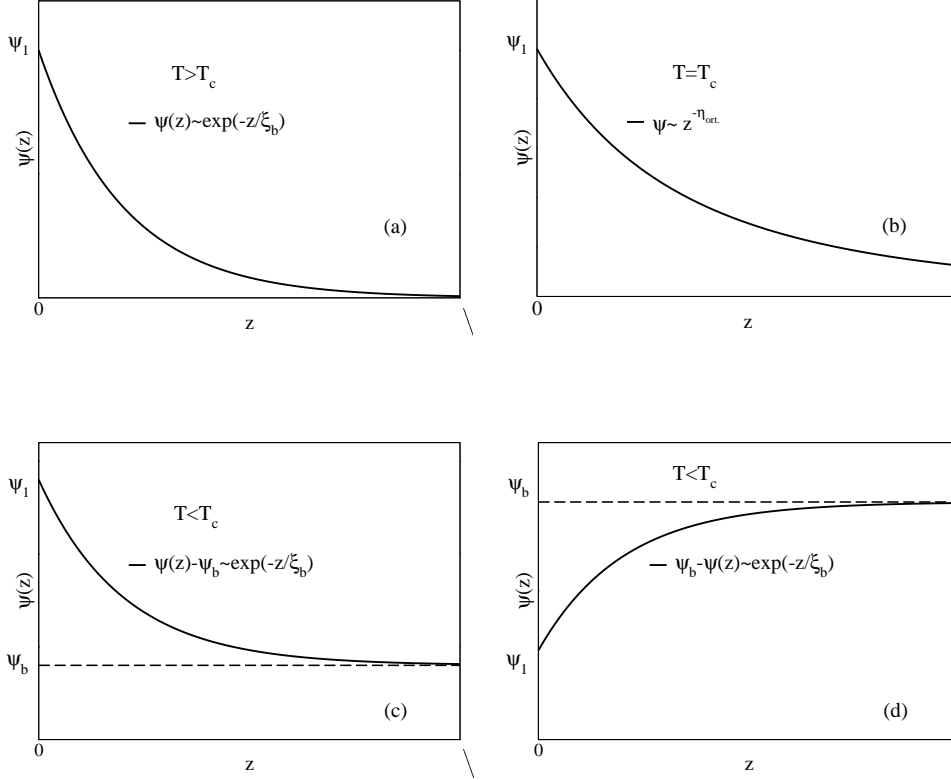


Figure 5.3: Schematic variation of the local order parameter $\Psi(z)$ as a function of the distance z from a wall (or free surface respectively) that is located at $z = 0$. the second order phase transition from the disordered phase (where $\Psi_b > 0$) occurs at T_c in the bulk. In cases (a)-(c) it is assumed that at the wall at $z = 0$ a local surface field $H(z) = H_1\delta(z)$ conjugate to the order parameter $\Psi(z)$ acts. As a result, there exists not only a local order parameter Ψ_1 right at the surface, but surface-induced order occurs in a region of a width of order ξ_b , the order-parameter correlation length in the bulk, both for $T > T_c$ and for $T < T_c$. This surface induced order decays to zero for $T > T_c$ and to Ψ_b for $T < T_c$. Right at $T = T_c$ the order decays also to zero, but much more slowly namely according to a power law, with an exponent that has been denoted as $\eta_{\text{ort.}} = \eta/2$ here. In case (d) it is assumed that the surface is “neutral”, no sign of the order parameter is preferred, and so the surface couples only to the order parameter square: the most frequent case then is that the ordering tendency at the surface is reduced (e.g. by the “missing neighbor effect”). Then $\Psi_1 < \Psi_b$ for $T < T_c$, and $\Psi(z)$ relaxes towards Ψ_b from below. The range over which Ψ_b and $\Psi(z)$ appreciably differ is again of the order of ξ_b .

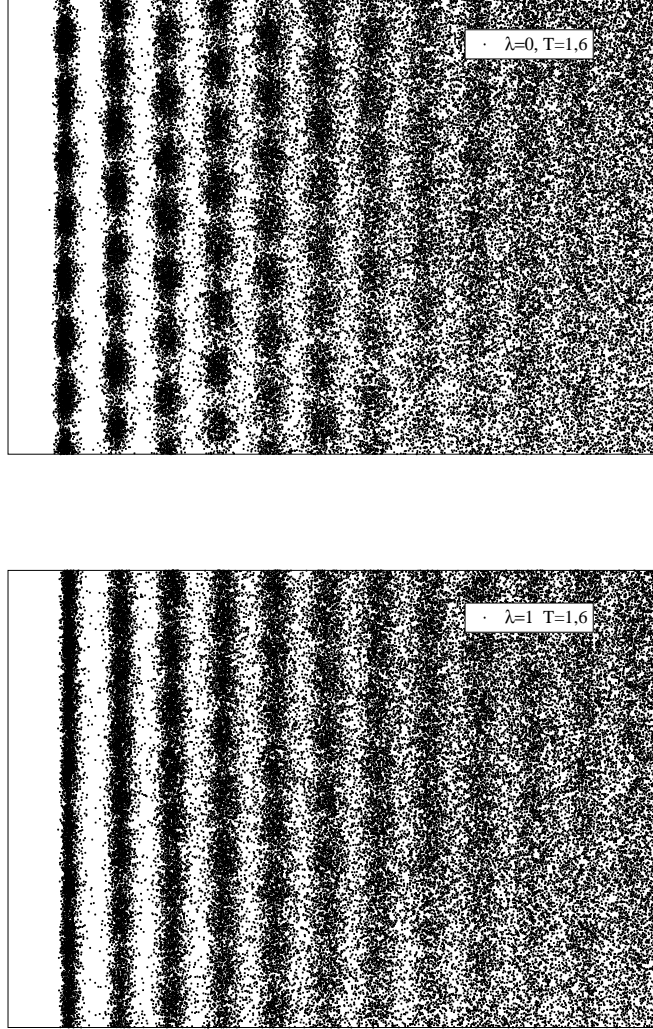


Figure 5.4: Configurations of the particles in the first 9 rows adjacent to the left wall at $T = 1.6$, for the structured wall (top) and the planar wall (bottom). 1000 configurations of a run lasting 10^6 Monte Carlo steps (MCS) per particle are superimposed, fixing the center of mass of the mobile particles in each configuration in the same position. The linear dimensions were $L_y = 30$ and $n_x = 30$, with periodic boundary conditions in the y -direction. We have supposed to write the wall potential as

$$V_{\text{wall}} = \lambda V_{\text{planar}} + (1 - \lambda) V_{\text{structured}}. \quad (5.31)$$

So $\lambda = 0$ means structured walls while $\lambda = 1$ means planar walls

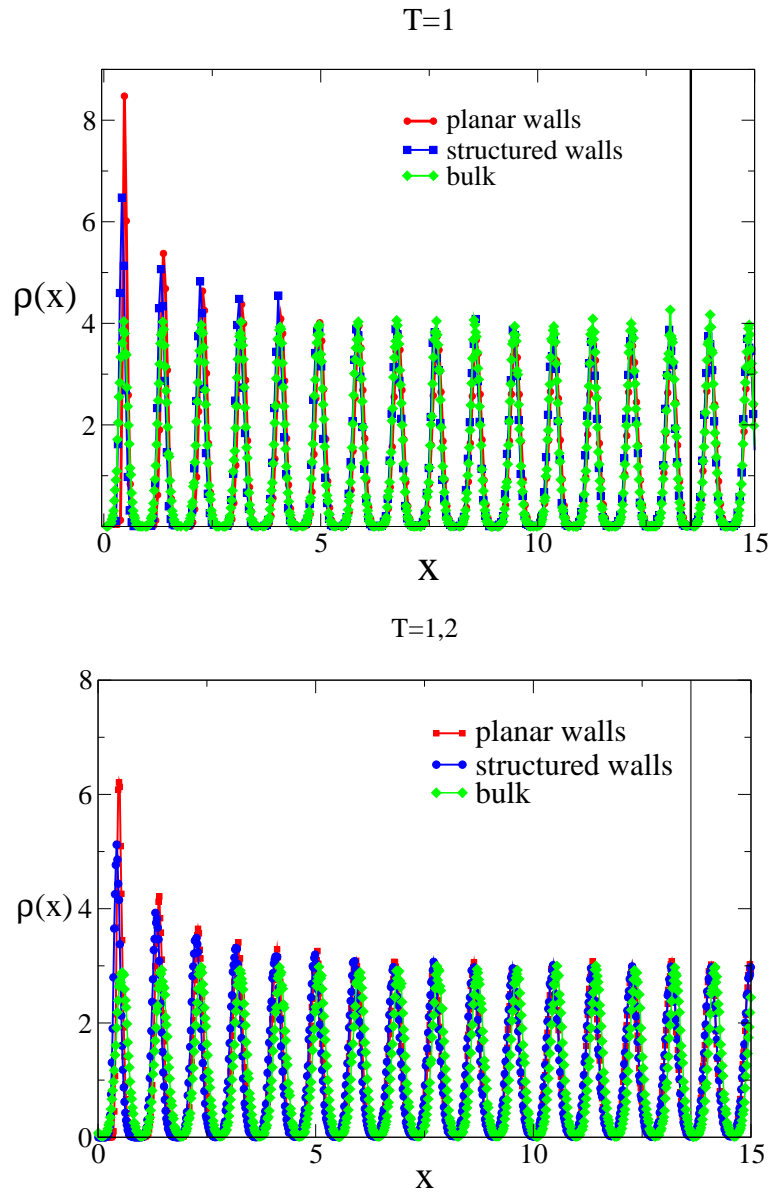


Figure 5.5: Density distribution $\rho(x)$ plotted vs x for $n_x = 30$ and temperatures: $T = 1.0$ (top) and $T = 1.2$ (bottom). The black vertical line, marks the center of the strip.

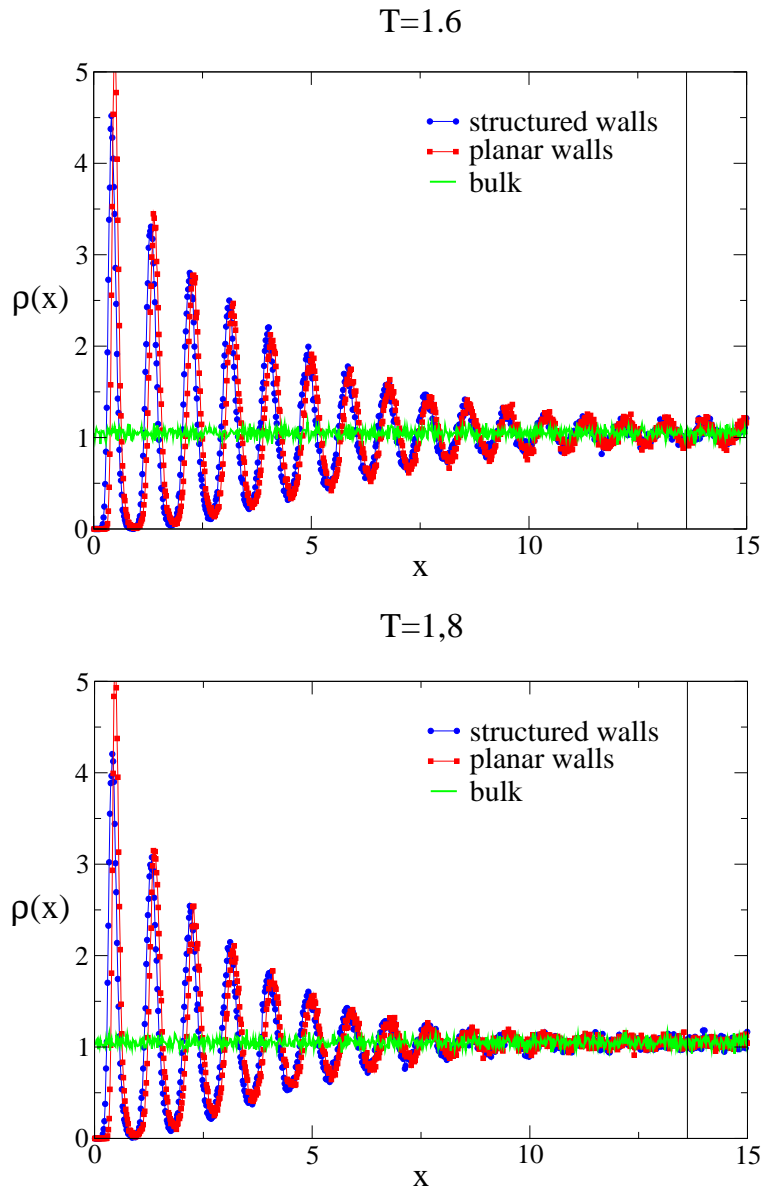


Figure 5.6: Density distribution $\rho(x)$ plotted vs x for $n_x = 30$ and temperatures: $T = 1.6$ (top) and $T = 1.8$ (bottom).

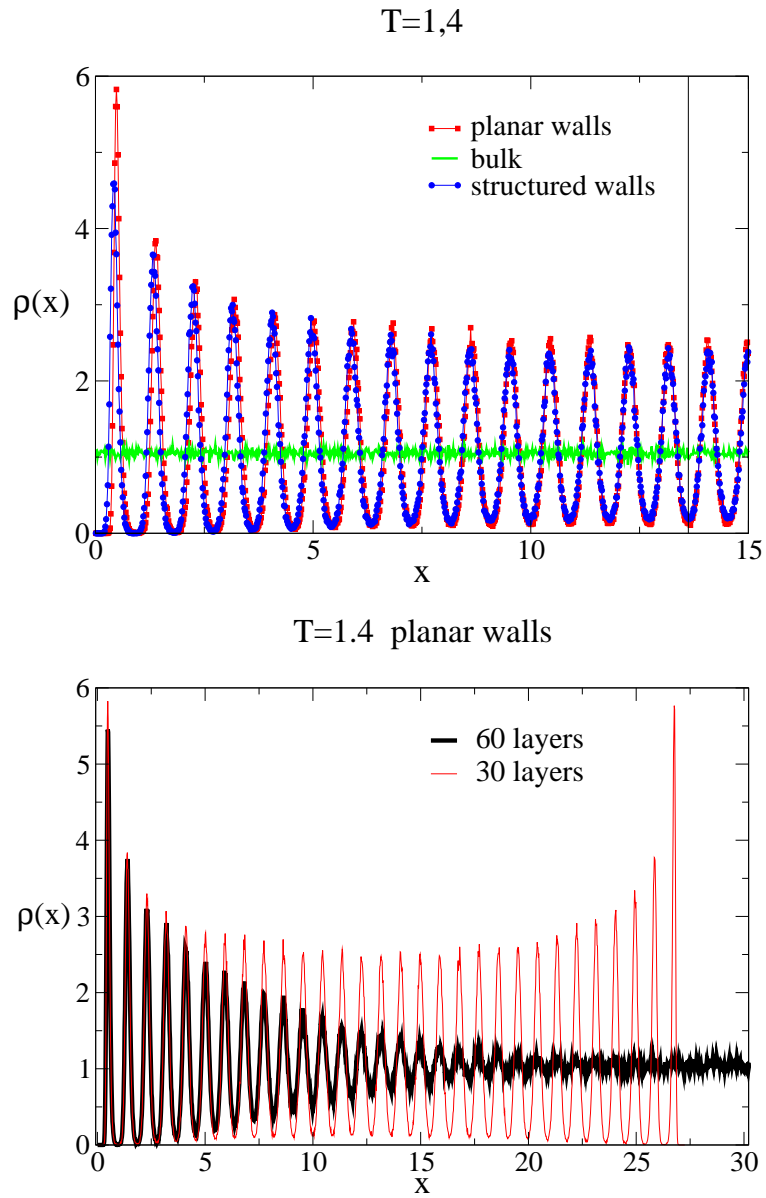


Figure 5.7: Top: same as figs. 5.5 and 5.6 but for $T = 1.4$. Bottom: density distribution $\rho(x)$ vs x for $T = 1.4$ and planar walls in the case of $n_x = 30$ (red line) and $n_x = 60$ (black line), respectively.

Correlation length in the positional order decay

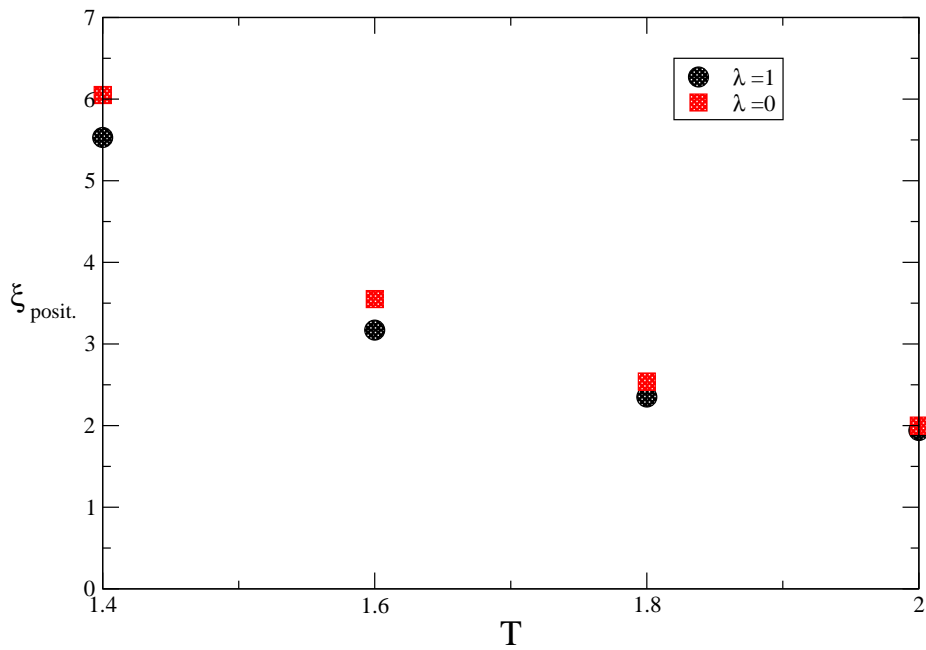


Figure 5.8: Correlation length ξ for the decay of the positional order near the walls plotted vs. temperature, for a system with $n_x = 60$, $n_y = 60$ and for the two types of boundary conditions at the walls. Circles refer to the planar wall and squares to the structured wall boundary condition, respectively (see fig. 5.4).

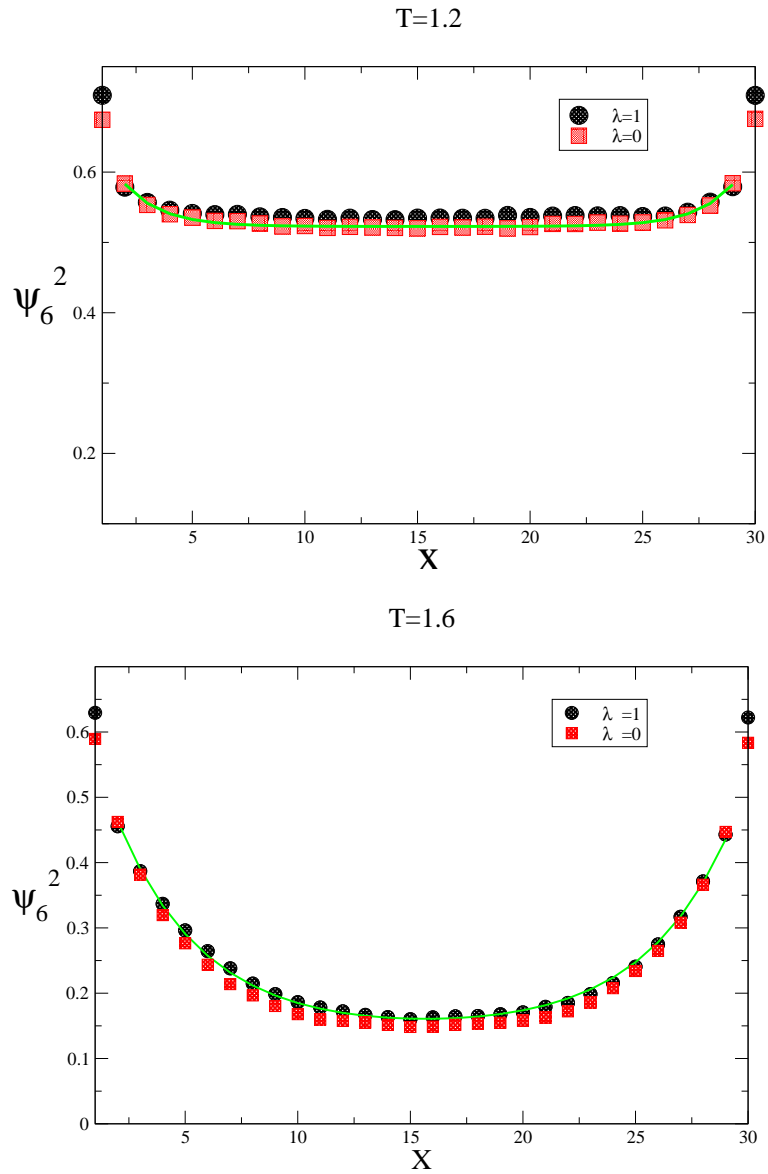


Figure 5.9: Plot of the local orientational order parameter square $\langle |\Psi_6(x)|^2 \rangle$ versus x , for $n_x = n_y = 30$ and two temperatures, $T = 1.2$ (top) and 1.6 (bottom). Circles refer to the planar wall and squares to the structured wall boundary condition, respectively. The green lines are fit according to the eqn. 5.29

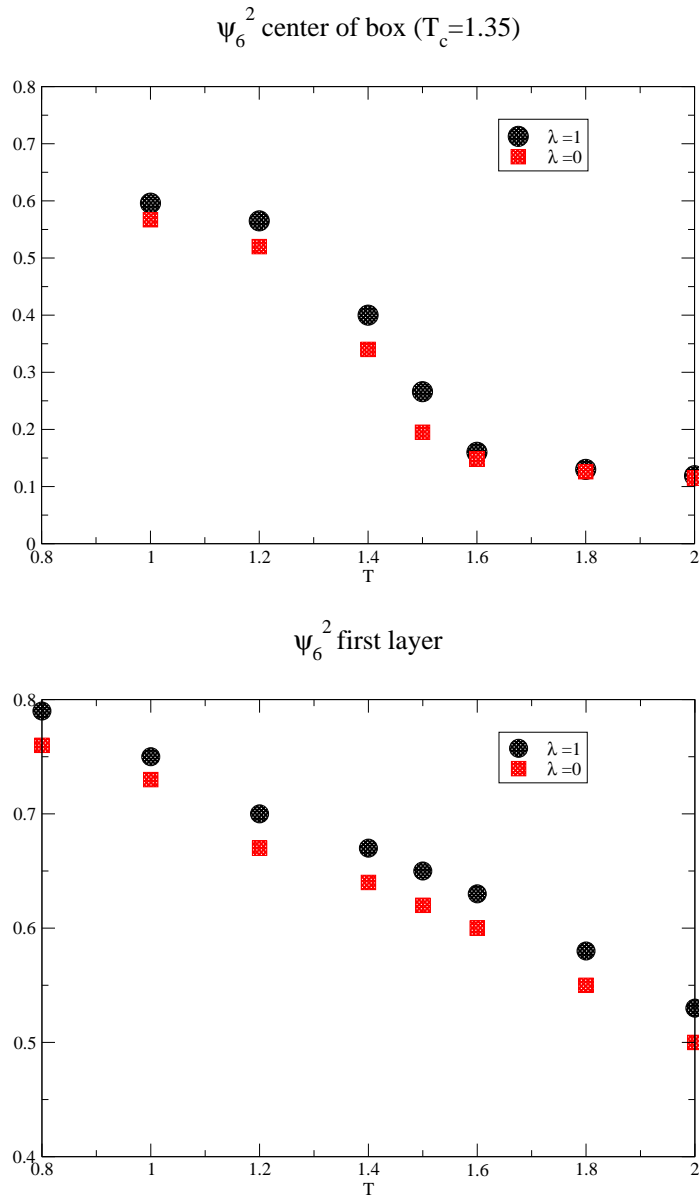


Figure 5.10: Mean square order parameter in the center of the strip (top, T_c is the melting temperature of the bulk) and near the walls (bottom) plotted vs. temperature. Circles refer to the planar wall and squares to the structured wall boundary condition, respectively. All data refer to $n_x = n_y = 30$.

Correlation length for ψ_6^2 ; $T > T_{c \text{ bulk}}$

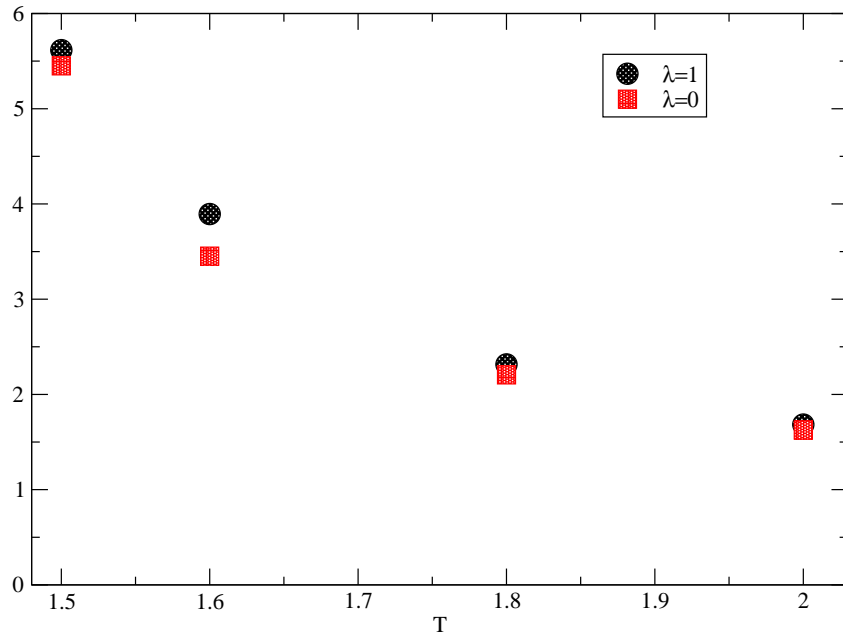


Figure 5.11: Correlation length extracted from the decay of the local orientational order parameter square with distance (fig.5.9) plotted vs. temperature. Circles refer to the planar wall and squares to the structured wall boundary condition, respectively. All data refer to $n_x = n_y = 30$.

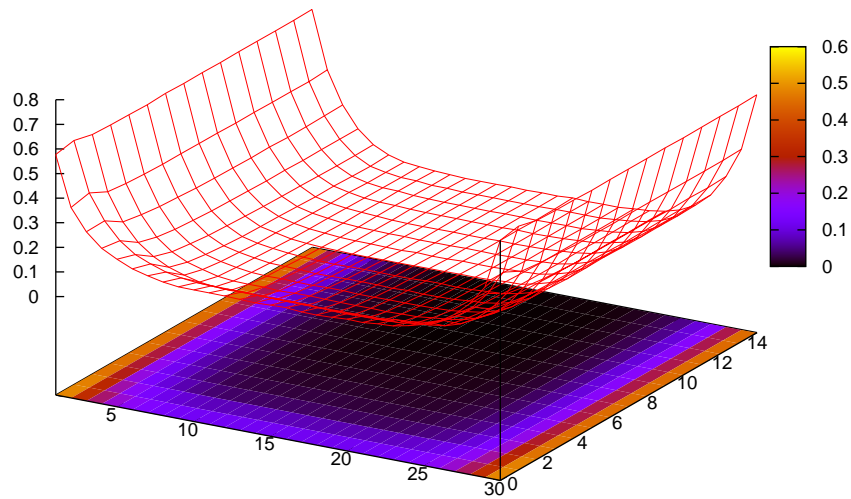
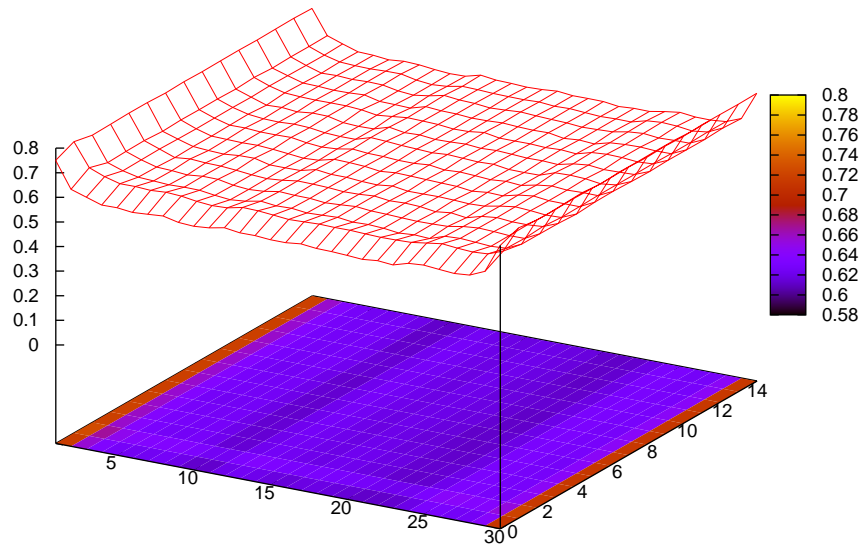


Figure 5.12: Correlation function $g_6(x, y)$ for $n_x = n_y = 30$ and $T = 1$ (top) or 1.8 (bottom), respectively. In the projection the numerical values of this function according to a colour scale are indicated. Here the x -axis runs from 0 to 30 while the y -axis runs from 0 to 15.

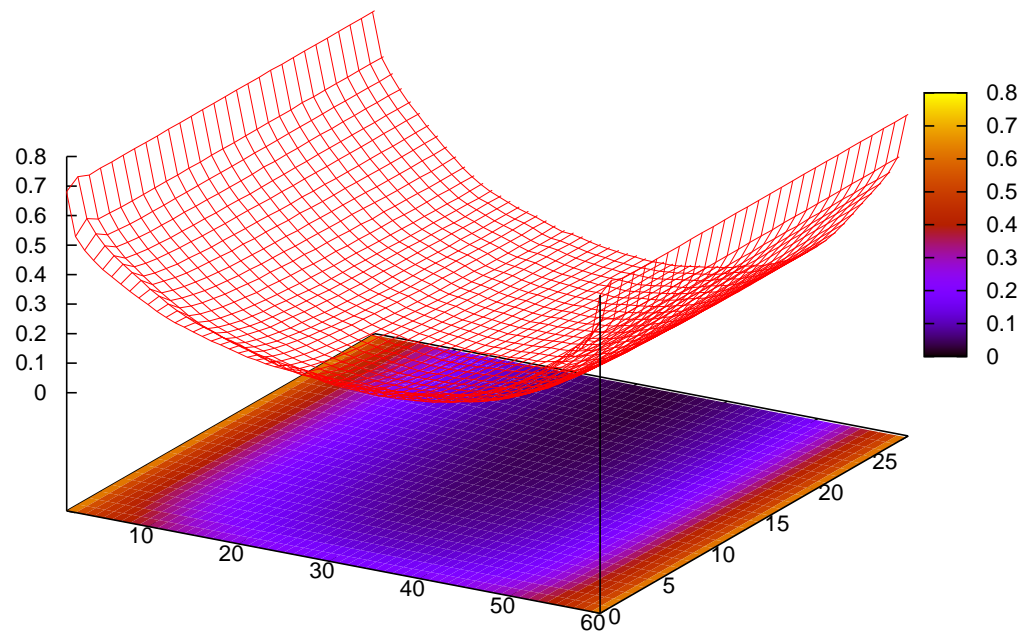


Figure 5.13: Correlation function $g_6(x, y)$, as in fig. 5.12. Here $T = 1.4$, $n_x = n_y = 60$, the x -axis runs from 0 to 60 and the y -axis runs from 0 to 30.

Conclusions

We can now summarize the main findings coming out from this work.

In this thesis we dealt with two-dimensional model colloidal crystals in a confined geometry. We used an idealized description both for the colloid colloid interactions and for the walls. This allowed us to overcome numerical problems in the simulations and, to reach within a reasonable CPU time, results and conclusions we believe they can be qualitative valid for real systems as well.

The first part of the work was devoted to the study of the elastic behaviour for a model colloidal crystal in confined geometry,

After the first introductory chapter with some reminders about elasticity theory, in chapter 2 we introduced two kinds of confinement: the flat walls and the structured walls. The wall potential in the flat walls case can be viewed as the $1/r^{12}$ potential integrated along the y direction and the x direction ($x < x_{\text{left wall}}$ and $x > x_{\text{right wall}}$) while the structured wall potential, as mentioned in chapter 2 can resemble a situation in which in a colloidal crystal a wall is formed “freezing” a one or two rows of particles to their equilibrium position with, for example, laser optical tweezers.

Clearly the wall potentials brought distortions in the triangular bulk lattice. This was true in particular for the case of the flat walls, sometimes, like in the case of the hard flat walls, for the same chosen width of the strip, the crystal melted.

We studied these distortions and chose parameters like the width of the strip and the coupling constant in the wall potential ϵ_{wall} to get in the strip an equilibrium lattice as near as possible to the usual triangular lattice.

In the second part of chapter 2 we presented the methods used for the computation of the elastic constants. We considered both the fluctuation of the stress tensor and the local strain tensor: then we proposed some easy

generalization for the formulae, originally derived in the bulk case. This was done by taking into account the contribution to the interactions due to the wall potentials and by considering, for the crystal in a strip geometry, in the elastic free energy a less symmetric but more adequate expression than the bulk one.

In chapter 3 we used the methods of the previous chapter to compute the elastic constants. For our systems the results given by the two methods agree within the numerical error. Only exception was the value of C_{33} in the case of the flat walls, here it was not possible to have an estimate of this value with the strain fluctuation method. This failure was caused from the high shear fluctuations present in the whole simulation strip in those conditions. One of the key hypothesis for the method to work, namely almost zero or very small strain fluctuations in the whole strip, was clearly not fulfilled and the expected shape for the compliance curve coming out from the block analysis, was not recovered.

While for almost all the confined elastic constants with both types of walls we did not find large differences with the bulk case, the behaviour of C_{33} in the case of the flat walls was dramatically different from the bulk, and hence the most interesting one. For every strip width we tried C_{33} drops to about half the value of the bulk case. We can say that when flat walls are present the crystal in between can be easily sheared along the direction of the wall.

In chapter 4 we investigated further the behaviour of our confined crystals focusing on the mean square displacements.

We saw that while in the structured case we have a normal crystal both in the unconfined y direction and the confined x direction, in the case of flat walls, due to the confinement, there is a loss of long range positional order along the wall direction. We characterized the behaviour of the crystal in the flat wall case, considering one-dimensional harmonic formulae and applying them to the system: in particular the structure factor $S(q)$ per row along the y direction was considered. The good agreement found with the fitting to the $1d$ harmonic expression shows that indeed as long as we look at the displacements from lattice equilibrium positions along the wall direction, the behaviour of the crystal confined between flat walls, is one-dimensional rather than two-dimensional. Also plots of the instantaneous configurations in the flat wall case, show clearly, in contrast with the structured walls case,

lack of positional order in the wall direction: the system presents series of smectic strips parallel to the walls rather than a crystal like picture.

In the second part of chapter 4 we focused more quantitatively on the crossover between one-dimensional behaviour and two-dimensional behaviour for the displacements correlation function in a strip geometry $D \times L$. We considered for simplicity a triangular lattice in the “bulk” case, that is, periodic boundary conditions in both directions (rather than two walls as boundaries in the x -direction plus periodic boundary conditions in the y -direction) and a geometry where D , the extension of the lattice in x was lower or equal than L , the extension of the lattice in y . We could prove that when $D \approx L$ the displacements correlation function $B(y) = \langle [u_y(y) - u_y(0)]^2 \rangle$ has a two-dimensional behaviour proportional to $\ln y$ while when we consider $D \ll L$ then the behaviour of $B(y)$ is proportional to y i.e. one-dimensional. Knowing, from previous simulations of the bulk system, the Lamé coefficients for our system we could verify in a numerical way the analytic formulae obtained, also in the case of very big strips. Moreover we could show that the presence of flat walls enhanced significantly $B(y)$ with respect to the bulk case as expected from the behaviour of $S(q)$.

In chapter 5 we focused on the order inside the strip induced by the confinement. Here we observed with both types of walls pretty similar behaviours.

We considered first the positional order in the x direction, that is, the strong modulation in the density induced by the walls perpendicular to them, and estimated the correlation length associated with it.

Then we focused on the orientational order described by the order parameter $\overline{\Psi}_6(x)$. Also in this case, at a sufficiently high temperature and sufficiently large strips we found high orientational order at the walls which decreases, with a typical correlation length, when we moved to the center of the strips. In this case however high finite size corrections are present: also at high temperature and for wide strips at the center of the strip the orientational order parameter was significantly non zero as it should be in the fluid phase. This was caused by the still too small system sizes considered and also by the strong layering induced by the walls.

Finally we want to sketch some further research lines coming out from this work:

as already mentioned in chapter 4 it would be very interesting to under-

stand, in the case of flat walls for large enough strip width D , how the bulk behaviour, for example in the case of $C_{33}(D)$ or of $B(y)$, is reached. the problem is that we expect D to be very large, and so, far beyond the values accessible with normal computational power.

Another interesting problem would be the study of the KTHNY-scenario of melting in presence of walls. Again here CPU time issues make this problem very difficult as we saw in chapter 5.

An easier problem (from the computational point of view) would be the study of the strips in an “incommensurate” situation, that is relaxing the condition 2.4 to a more realistic expression

$$D = \frac{\sqrt{3}}{2}a(n + \Delta),$$

where Δ can be any number (clearly not too large). We started to study partially our confined systems with the condition written above and some preliminary data and results are shown in the appendix A.

One could consider to extend the study of the effects of the walls to three dimensional colloidal crystals or to two dimensional colloidal binary crystals as well; for these systems at the moment results for the bulk case are available [74, 75].

Appendix A

Varying the distance between the walls

We want to present here some results obtained in geometrical configurations where the distance between the walls does not exactly match the distance of the lattice sites in the bulk.

Throughout the whole thesis the condition in eqn. 2.5 held with in most of the simulations n equal to 30 or 60 and $a \approx 1.049$. Now, as anticipated in the conclusions, we consider the case

$$D = \frac{\sqrt{3}}{2}a(n + \Delta), \quad (\text{A.1})$$

where Δ in principle can be any number. To be clearer, in the simulations we will present we just change the distance in the x direction according to eqn. A.1 with $n = 30$, while we keep constant the length of the simulation box in the y direction, so the dimensions of the box are

$$L_x = D = \frac{\sqrt{3}}{2}a(30 + \Delta), \quad L_y = 30 \cdot a, \quad (\text{A.2})$$

and the temperature considered is $T = 1$.

The case Δ positive is the least interesting one, here the situation looks very similar to the commensurate case at high T , i.e. increasing Δ the system will show layers near the walls and will start to melt at the center of the strip like in figs. 5.4 and 5.6.

Clearly when we consider negative value for Δ the situation changes.

The crystal, has now less space to relax in the x direction, will be somehow frustrated and so internal stresses together with deformations of the bulk lattice will be present at the equilibrium, this is shown in fig. A.1 where we considered the probability distribution of the order parameter $\Psi_{\mathbf{G}_0}$ defined in eqn. 5.2, in the case of structured walls, we see that the larger is $|\Delta|$ the more the lattice is different from the bulk triangular lattice; the vector \mathbf{G}_0 (fig. 5.1) is not a reciprocal vector of the deformed lattice anymore.

Maybe more interesting is to consider the distribution of the order parameter $\Psi_{\mathbf{G}_1}$. The reciprocal lattice \mathbf{G}_1 is directed along x , orthogonal to the walls and it gives a measure of the number of layers in the strip. In fig. A.2 the distribution of $\Psi_{\mathbf{G}_1}$ for different values of Δ is plotted. Here we can see that increasing $|\Delta|$ this order parameter has a value very close to 1 for $\Delta = -1$, $\Psi_{\mathbf{G}_1}$ then decreases to an intermediate value for $\Delta = 1.5$ and to almost 0 for $\Delta = -2$; when $|\Delta|$ is sufficiently large the system rearranges its structure changing the number of layers from the initial 30 to 29. Deformations and changes of the number of layers in the strip can be shown looking at the superimposed configurations as well. In fig. A.3 is plotted the intermediate case $\Delta = -1.5$: we can clearly see two regions in the strip where misfits appear. In fig. A.4 the case $\Delta = -2$ is considered and one can see by counting, that the number of layers at the equilibrium decreased. In fig. A.5, following Chaudhuri and Sengupta [76], we plotted the stress $\sigma = \sigma_{yy} - \sigma_{xx}$ versus $|\Delta|$ which can be considered proportional to a geometrical strain ϵ measured respect to the ideal bulk triangular lattice: $\epsilon = (a - a_x)/a = |\Delta|/n$. After the initial increase, we see that the system starts its internal rearrangement inside the strip as $|\Delta|$ reaches 1.5.

Looking now briefly at the case of the flat walls, we find here the same behaviour of the structured case, namely increasing Δ , deformations start appearing and eventually we have a change in the number of layers, but in contrast with the structured case we never observe intermediate states like the case $\Delta = -1.5$. So for example looking at $P(\Psi_{\mathbf{G}_1})$ we can observe a two peaked curve like the one in fig. A.6, that is the system during the Monte Carlo simulation can suddenly have its structural change. The mechanism of the transition is similar to the system with structured wall as it is shown in fig. A.7 where the configurations during the jump of $\Psi_{\mathbf{G}_1}$ are shown but this jump is very fast, (hundreds of Monte Carlo cycles, see fig. A.6). Clearly the free energy landscapes for the strip in the two cases are different. Like

for the results of C_{33} this is a signature of the different elastic behaviour induced on the strip by the two types of confinement.

Finally we conclude mentioning that analogous structural changes were observed by Chaudhuri and Sengupta in two-dimensional hard disk channels confined by hard walls [76]

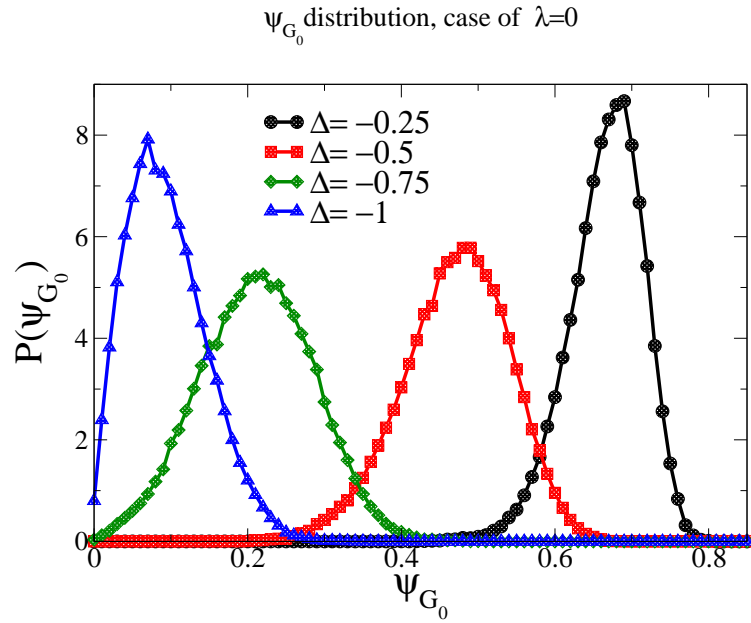


Figure A.1: Probability distribution for the order parameter Ψ_{G_0} (see eqn. 5.1 and fig. 5.1) in the case of structured wall and for different values of Δ .

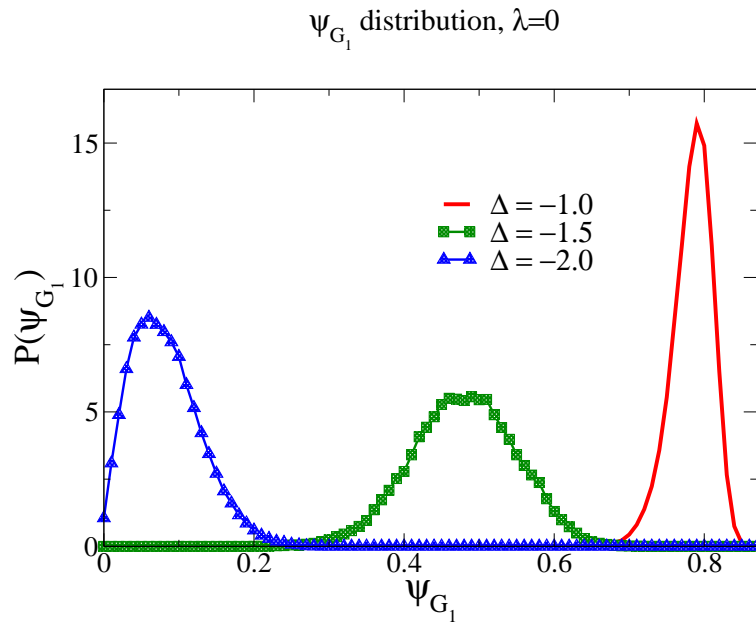


Figure A.2: Probability distribution of the order parameter Ψ_{G_1} (see eqn. 5.2 and fig. 5.1) in the case of structured walls for different values of Δ .

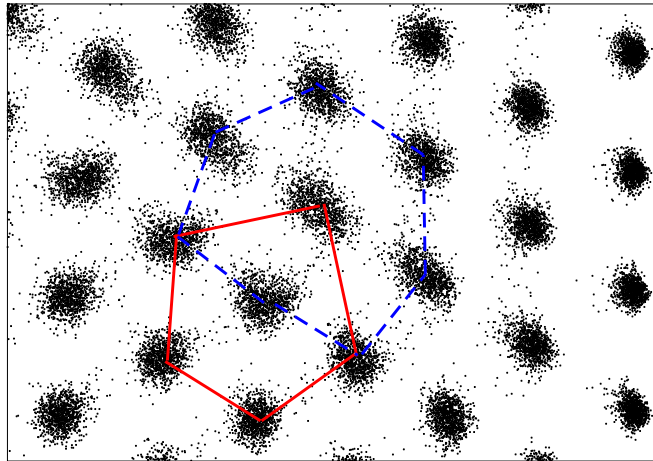
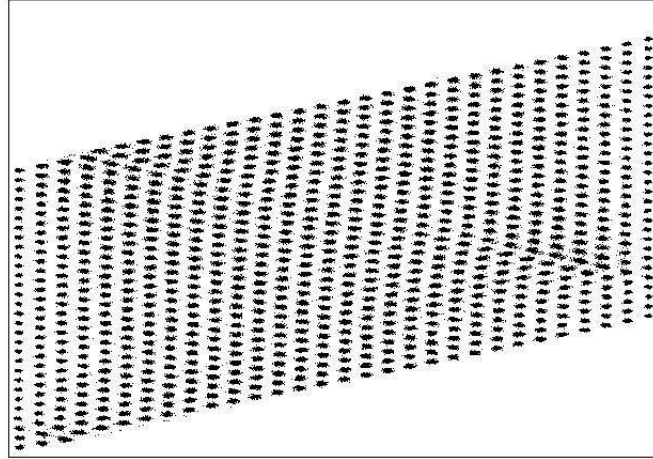


Figure A.3: Superimposed configurations in the case of structured walls with $\Delta = -1.5$. Top: the whole simulation box is showed. Bottom: a close up showing the core of one of the two dislocations, the sites with 5 nearest neighbours and the one with 7 are highlighted. The figures are obtained like in figs. 4.2 and 5.4.

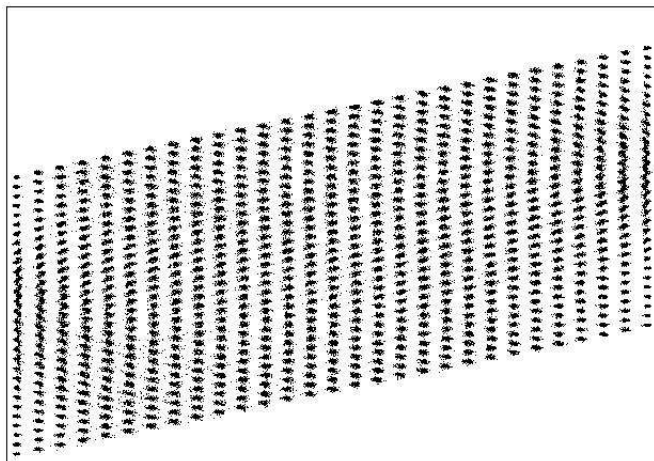


Figure A.4: Superimposed configurations in the case of structured walls and $\Delta = -2$, counting the number of layers from left to right, 29 layers are present although we started the simulations with the usual 30. Here in order to have a smaller file only 100 configurations are plotted.

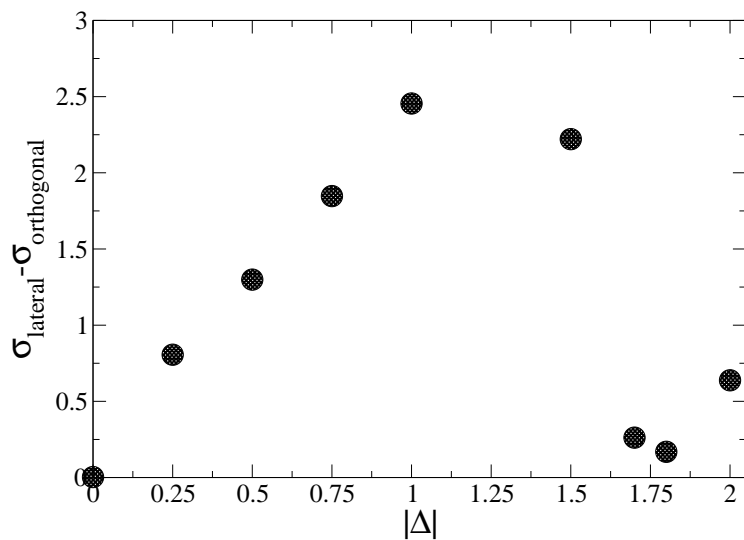


Figure A.5: Measure of the internal stress inside the strip versus $|\Delta|$ in the case of the structured wall.

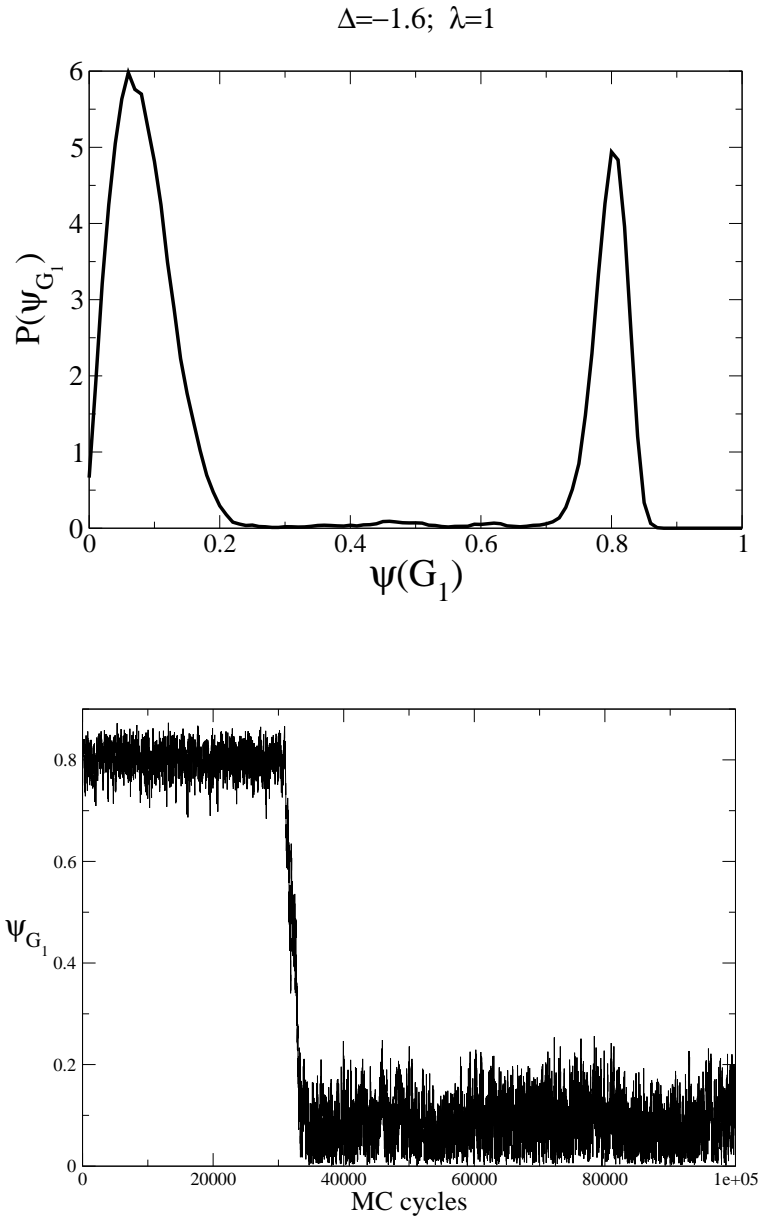


Figure A.6: Case of the flat walls with $\Delta = -1.6$. Top: distribution of the order parameter Ψ_{G_1} Bottom: evolution of Ψ_{G_1} during the Monte Carlo simulations.

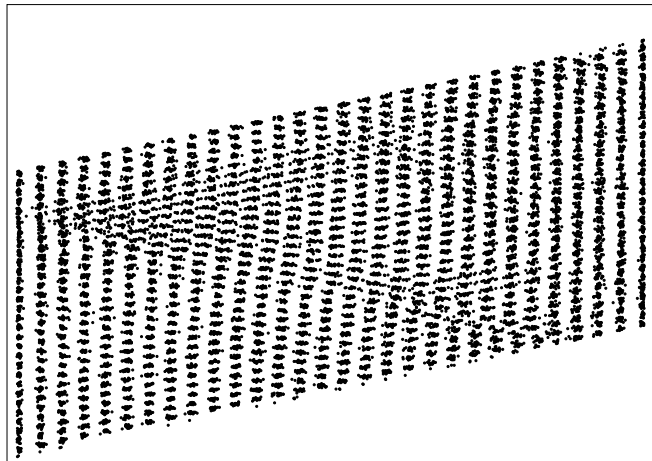


Figure A.7: Superimposed configuration in the case of flat walls and $\Delta = -1.6$; the configurations are taken only during the jump of Ψ_{G_1} (see previous figure).

Bibliography

- [1] L. D. Landau, E. M. Lifshits *Teoria dell'Elasticità*, Editori Riuniti 1999
- [2] D. C. Wallace *Phys. Rev.* **162**, 776, 1968
- [3] J.H. Weiner *Statistical Mechanics of Elasticity*, Dover 2002
- [4] C. Truesdell, R. A. Toupin in *Handbuch der Physik* edited by S. Flügge, Springer Verlag, Berlin 1960, Vol III/1
- [5] J.C. Ericksson, *Surf. Sci.* **14**, 221, 1969
- [6] R. Shuttleworth, *Proc. R. Soc, London* **163**, 644, 1950
- [7] P. Müller, A. Saúl *Surf. Sci. Rep.* **54**, 157, 2004
- [8] K. Zahn et al., *Phys. Rev. Lett.* **82**, 2781, 1999
- [9] K. Zahn, G. Maret *Phys. Rev. Lett.* **85**, 3656, 2000
- [10] K Zhan et al. *Phys Rev Lett.* **90**, 155506, 2003
- [11] W.C. Poon and P.N. Pusey, in *Observation, prediction and simulation of phase transitions in complex fluids*, edited by M Baus et al., Kluwer Dordrecht, 1995 pp. 3; H. N. W. Lekkerker et al., *ibid.*, pp 53
- [12] T. Palberg, *Curr. Opin. Coll. Interface Sci.* **2**, 697, 1997
- [13] H. Löwen, *J. Phys.: Condens. Matter* **13**, R415, 2001
- [14] H. Löwen, C.N. Likos, eds., *Colloidal Dispersion in External Fields* Special issue of *J. Phys. : Condes. Matter* **16**, 38, 2004
- [15] B. V. Derjaguin, L.D. Landau, *Acta Physicochimica URSS*, **14**, 633, 1941

- [16] E. J. Verwey, J. T. G. Overbeek, *Theory of the Stability of Lyophobic Colloids*, Elsevier, 1948
- [17] K. Bagchi, H.C. Andersen, W. Swope *Phys. Rev. E* **53**, 9794, 1996
- [18] P. Glassom, V. Dotsenko, P. Fozooni, M. J. Lea, W. Biley, G. Papa-georgiou, S.E. Andresen, A. Kristensen, *Phys. Rev. Lett.* **87**, 176802, 2001
- [19] Y.-L. Lai, Lin I, *Phys. Rev. E* **64**, 015601, 2001; L.W. Teng, P.S. Tu, Lin I, *Phys. Rev. Lett.* **90**, 245004, 2003
- [20] J. H. Chu, Lin I, *Phys Rev. Lett.* **72**, 4009, 1994
- [21] R. Haghgooe P.S. Doyle, *Phys Rev. E* **70**, 061408, 2004
- [22] R. Haghgooe P.S. Doyle, *Phys Rev. E* **72**, 011405, 2005
- [23] M. Parrinello, A. Rahman, *J. Chem. Phys.* **76**, 2662, 1982; A. A. Gusev, M.M. Zehnder U.W. Suter, *Phys. Rev. B* **54**, 1, 1996
- [24] D. R. Squire, A. C. Holt, W. G. Hoover, *Physica* **42**, 388, 1969
- [25] O. Farago, Y. Kantor *Phys. Rev. E* **61**, 2478, 2000
- [26] F. Varnik, J. Baschnagel, K. Binder *J. Phys. Chem.* **113**, 4444, 2000
- [27] S. Sengupta, P. Nielaba, M. Rao, K. Binder *Phys. Rev. E* **61**, 1072, 2000
- [28] S. Sengupta, P. Nielaba, K. Binder *Phys. Rev. E* **61**, 6294, 2000
- [29] K. Binder, S. Sengupta, P. Nielaba *J.Phys.: Condens. Matter* **14**, 2323, 2002
- [30] K. Binder *Z. Phys. B: Condens. Matter* **43**, 119, 1981
- [31] M Rovere, D. W. Heerman, K. Binder *Europhys. Lett.* **6**, 585, 1988; *J. Phys. Condens. Matt.* **2**, 7009, 1990
- [32] M. Rovere, P. Nielaba, K. Binder *Z. Phys. B: Condens. Matt.* **90**, 215, 1993

- [33] J. Lebowitz, J. K. Percus, L. Verlet, *Phys. Rev.* **153**, 250, 1967; K.W. Krathy, *Phys. Rev. A* **31**, 945, 1985; J. J. Salacuse, A. R. Denton, P. A. Egelstaff, *Phys. Rev. E* **53**, 2382, 1996
- [34] P. M. Chaikin, T.C. Lubensky, *Principles of Condensed Matter Physics*, Cambridge University Press, 1995
- [35] I. S. Gradshteyn, I.M. Ryzhik, *Table of Integrals, Series and Products*, Academic Press, 1980
- [36] N. W. Ashcroft, N. D. Mermin, *Solid State Physics*, HRW International Editions, 1981
- [37] R. E. Peierls, *Helv. Phys. Acta*, **7**, 81, 1923
- [38] L. D. Landau, *Phys. Z. Sowjet.* **11**, 26, 1937
- [39] N. D. Mermin, *Phys. Rev.* **176**, 250, 1968
- [40] B. Jancovici, *Phys. Rev. Lett.* **19**, 20, 1967
- [41] V. J. Emery, J. D. Axe *Phys. Rev. Lett.* **40**, 1507, 1978
- [42] J.D. Axe in *Ordering in Strongly-Fluctuating Condensed Matter Systems* (T. Riste ed.) Plenum Press, 1980, p. 399
- [43] J.P. Hansen, I. R. Mc Donald, *Theory of Simple Liquids*, Academic Press, London
- [44] G. Piacente, I. V. Schweigert, J. J. Betouras, F. M. Peeters *Phys. Rev. B*, **69**, 045324, 2004
- [45] K. Binder in *Cohesion and Structure at Surfaces*, ed by D. G. Pettifor, Elsevier, 1995, p. 121
- [46] S. Ostlund, B. I. Halperin *Phys. Rev. B*, **23**, 335, 1981
- [47] D. R. Nelson, B. Halperin, *Phys. Rev. B*, **19**, 2457, 1979
- [48] D. R. Nelson, in *Phase Transitions and Critical Phenomena, Vol. 7*, (C. Domb and J. L. Lebowitz eds.) Academic Press, 1983
- [49] B. Berche , *Phys. Lett. A* **302**, 336, 2002

- [50] B. Berche, A. I. Farinas Sanchez, V. Paredes, *Europhys. Lett.* **60**, 539, 2002
- [51] B. Berche, *J. Phys. A: Math. Gen.* **36**, 585, 2003
- [52] J. M. Kosterlitz, D. J. Thouless, *J. Phys. C* **6**, 1181, 1973
- [53] A. P. Young *Phys Rev. B* **19**, 1855, 1979
- [54] A. P. Young, in *Strongly Fluctuating Condensed Matter Systems* (T. Riste, ed.) Plenum Press, 1980, p. 271
- [55] B. I. Halperin, D. R. Nelson, *Phys. Rev. Lett.* **41**, 121, 1978
- [56] K. J. Strandburg, *Rev. Mod. Phys.* **60**, 161, 1988
- [57] H. Kleinert, *Gauge fields in Condensed Matter*, World Scientific, 1989
- [58] K. Binder, P. C. Hohenberg, *Phys. Rev. B* **6**, 3461, 1972; *ibid B* **9**, 2194, 1974
- [59] K. Binder, in *Phase Transition and Critical Phenomena, Vol. 8* (C. Domb and J. L. Lebowitz eds), Academic Press, 1983, p. 1
- [60] H. W. Diehl, in *Phase Transition and Critical Phenomena, Vol. 10* (C. Domb and J. L. Lebowitz eds), Academic Press, 1986, p. 75
- [61] D. E. Sullivan, M. M. Telo da Gama, in *Fluid Interfacial Phenomena* (C. A. Croxton, ed.), Wiley, 1986, p. 45
- [62] S. Dietrich, in *Phase Transition and Critical Phenomena, Vol. 12* (C. Domb and J. L. Lebowitz eds), Academic Press, 1988, p. 1
- [63] G. Forgacs, R. Lipowsky, T. M Nieuwenhuizen, in *Phase Transition and Critical Phenomena, Vol. 14* (C. Domb and J. L. Lebowitz eds), Academic Press, 1991, p. 135
- [64] R. J. Baxter, *Exactly Solved Models in Statistical Mechanics*, Academic Press, London, 1982
- [65] M. E. Fisher, *J. Phys. Soc. Japan Suppl.* **26**, 87, 1969
- [66] B. Nienhuis, in *Phase Transition and Critical Phenomena, Vol. 11* (C. Domb and J. L. Lebowitz eds), Academic Press, 1987, p 1

- [67] J. L. Cardy, in *Phase Transition and Critical Phenomena, Vol. 11* (C. Domb and J. L. Lebowitz eds), Academic Press, 1987, p 55
- [68] M. E. Fisher, V. P. Privman, *Phys. Rev. B* **32**, 447, 1985
- [69] J. M. Kosterlitz, *J. Phys. C: Solid State Phys.* **7**, 1046, 1974
- [70] H. W. J. Blöte and B. Nienhuis, *J. Phys. A: Math. Gen.* **22**, 1415, 1989
- [71] J. L. Cardy, *Nucl. Phys. B* **240**, 514, 1984
- [72] K. Binder, D. W. Heermann, *Monte Carlo Simulation in Statistical Physics. An Introduction*, 4th ed. Springer, 2002
- [73] D. P. Landau, K. Binder, *A Guide to Monte Carlo Simulation in Statistical Physics*, 2nd ed. Cambridge University Press, 2005
- [74] K. Franzrahe, *Phd thesis*, University of Konstanz
- [75] P. Henseler, *Phd thesis*, University of Konstanz
- [76] D. Chaudhuri, S. Sengupta, *Phys. Rev. Lett.* **93**, 115702, 2004

Curriculum Vitae

Name: Andrea Ricci
Date of Birth: 17 July 1966
Place of Birth: Rome, Italy
Nationality: Italian

1979-1984 Secondary school education, Liceo Scientifico Statale
"Marcello Malpighi", Rome

1984-1990 Physics Studies at the University of Rome "La Sapienza"

1990-1997 Working experience as office clerk and employee in Non Gov.

Organizations

1992 Civil service at A.N.F.F.A.S. in Rome (NGO: support to people
with psychic disease and their families)

1997-2002 Physics Studies at the University of Rome "La Sapienza"

May 2002 Laura (M. Sci.) in Physics under the supervision of Prof.
Giovanni Ciccotti at the University of Rome "La Sapienza"

Since October 2002 Ph D under the supervision of Prof. Kurt
Binder in the Condensed Matter Theory Group at the Institute for Physics
of the University of Mainz